Alma Mater Studiorum · University of Bologna

School of Science
Department of Physics and Astronomy
Master Degree in Physics

Exploring brain network features in Borderline Personality Disorder: a graph-based analysis of MR images

Supervisor:
Prof. Claudia Testa

Co-supervisor:
Dr. Stefania Evangelisti

Submitted by:
Giovanni Sighinolfi

Academic Year 2019/2020

Abstract

A network approach to the modelling and the analysis of functional and structural Magnetic Resonance (MR) images is an increasingly popular technique, because of the solidity of the mathematical theory at its basis, the graph theory, which allows to explore a wide range of network properties. For this work, both Functional Connectivity (FC) and Structural Covariance (SC) networks were constructed.
The cohort of participants to this study was composed of 27 subjects affected by the Borderline Personality Disorder (BPD), a mental disorder causing behavioral and emotional dysregulation, and a matching group of 28 healthy controls.
Brain networks were analyzed using the methods provided by graph theory, both at global and nodal level, by exploring their topological and organizational properties mainly in terms of centrality, efficiency in information transfer and modularity. The outcomes obtained from such measures, in patients and controls separately, were compared in order to find statistically significant differences between the two groups, that may be characteristic of the disease. Additionally, the outcomes of the topological quantities were correlated with a series of clinical scores, evaluating the neuro-psychological condition of the subjects.
The results show significant differences between patients and controls mostly in the FC networks and especially located in the limbic system of the brain, which indeed has a fundamental role in emotion regulation. Node-specific variations tend to involve the amygdala, the caudal anterior cingulate cortex, the entorhinal cortex and the temporal pole. Such evident results were not retrieved from the SC networks, though they still supported a greater variability within the limbic system.
Therefore, the analysis of brain graphs allowed to achieve the detection of topological alterations in a young psychiatric population, which would be interesting to monitor in time.

Contents

Introduction **7**

1 The basics of fMRI **9**
1.1 The BOLD signal . . . 9
1.2 fMRI acquisition . . . 11
1.3 Analysis of rs-fMR images . . . 13

2 Graph theory in fMRI **15**
2.1 Definition of nodes . . . 15
2.2 Definition of edges . . . 16
2.3 Properties of brain graphs . . . 17

3 Borderline Personality Disorder **19**
3.1 Clinical characteristics . . . 19

4 Materials and methods **21**
4.1 Subjects . . . 21
4.2 MRI acquisition . . . 22
4.3 Data pre-processing . . . 23
4.3.1 fMRI data . . . 23
4.3.2 Structural MRI data . . . 24
4.4 Networks construction . . . 26
4.4.1 Functional networks . . . 26
4.4.2 Structural covariance networks . . . 30
4.5 Network properties . . . 32
4.5.1 Global properties . . . 32
4.5.2 Local properties . . . 33
4.6 Comparison between patients and controls . . . 35
4.6.1 Permutation tests . . . 36
4.6.2 Analysis of altered connectivity . . . 37
4.7 Correlations with the clinical scores . . . 38

5 Results **39**
5.1 Comparison with the random networks . . . 39
5.2 Comparison between patients and controls . . . 43
5.2.1 Functional Connectivity networks . . . 43
5.2.2 Structural covariance networks . . . 76
5.3 Correlation with the clinical scores . . . 90
5.3.1 All subjects . . . 91

5.3.2 Patients and controls separately 102

6 Discussion **117**
6.1 Comparison with the random networks 117
6.2 Comparison between patients and controls 117
6.2.1 FC networks 118
6.2.2 SC networks 121
6.3 Correlation with the clinical scores 121

7 Conclusions **123**

References **125**

Appendices **131**

A Tables **133**

B Codes **141**
B.1 Harmonic characteristic path length 141
B.2 Within-module strength 141

Introduction

Magnetic Resonance Imaging (MRI) is nowadays an acknowledged, solid and reliable imaging technique, which aims at investigating the properties and the characteristics of the brain, both from a structural and a functional point of view. In the latter case, we talk about functional Magnetic Resonance Imaging (fMRI), which can provide an indirect measure of the temporal evolution of the activity of the brain. This field of research has further developed when it was found that the activity measured by fMRI is not only present during a stimulation of specific brain areas, but also when the individual is at rest: the functional MRI under such conditions has acquired a specific name, i.e. resting-state fMRI (rs-fMRI).
Both stimuli-based and rs-fMRI have gained, in years, growing popularity in exploring the features of the brain, in particular in subjects affected by neuro-psychological or psychiatric diseases, as they are expected to show alterations in this sense.
Several methods have been developed to analyze the fMRI data: translating the 4D images into networks, whose nodes represent brain regions and whose links describe the connectivity relating these nodes, besides being an intuitive solution for modelling the brain, is one of the most popular approaches to this issue. The reason is that it can rely on the findings of a solid and widely developed mathematical theory, i.e. the graph theory.
In particular, this work uses both functional and structural images to retrieve Functional Connectivity (FC) and Structural Covariance (SC) networks, respectively. The topological and organizational characteristics of such networks are then explored by exploiting the methods provided by the graph theory.

The Borderline Personality Disorder is a mental disorder characterized by a general instability in the context of emotion regulation, which translates into complex interpersonal relationships, an unstable sense of self, volatile emotions and impulsive behaviors, which are frequently related to intense anger and self-harm episodes. Since the limbic system has a fundamental role within the brain in behavior and emotion regulation, considering the symptoms just described, it can be expected that such system presents relevant alterations from a functional and/or a structural point of view in individuals affected by this disease with respect to healthy subjects. Therefore, it is of interest to investigate the properties of the brain of individuals suffering from this mental disorder and to compare them with the ones of a matching group of healthy controls, looking for differences that may characterize the disease. Using a network approach to analyze the graphs derived from functional and structural MR images, as it is done in this work, is indeed a viable method to achieve this.

Besides the present introduction, this thesis is divided into seven chapters. The first two consist of a brief recall of the principles at the basis of the techniques used for this study, i.e. the fMRI and the graph theory, respectively; the third chapter describes the general characteristics of the borderline personality disorder; in chapter 4, the data available for the analysis, including a description of the cohort of subjects, and the methods used to perform it are explained; chapter 5 reports all the results obtained from the analysis, which are then discussed in chapter 6; finally, chapter 7 collects the conclusions that were retrieved from this study, the limitations that influenced it and the possible future developments.

Chapter 1

The basics of fMRI

Functional Magnetic Resonance Imaging (fMRI) is a branch of MRI which studies the activity of the brain, rather than its structure. This task can be achieved by performing an indirect measure of the neuronal activation, since the latter is associated to an hemodynamic response, which consist of an increase of the blood flow, volume and oxygenation in correspondence of the area that was activated. The combination of such effects gives rise to the Blood Oxygenation Level Dependent (BOLD) signal, which is responsible of the changes in the transverse relaxation of the MR signal, at the basis of the fMRI measurements.
Nowadays, the fMRI acquisitions are distinguished into two macro-categories: task-based and resting-state (rs). The first consist of measuring the activity of the brain while a certain task involving sensory-motor or cognitive processes are administered to the subject: in this case it is evident that the activation of certain dedicated areas in particular would be observed. Nevertheless, it was first found by Biswal et al. in 1995 [1] that the brain activity is still present even when the subject is at rest, i.e. lying down without doing or thinking about anything specific (thus the term 'resting-state'). It was later verified by further studies that the activity of the brain in such conditions was indeed organized in specific structures and networks, which made this topic particularly interesting.
For deepening the topics of Nuclear Magnetic Resonance (NMR), MRI and fMRI, refer for example to [2], [3], [4] and [5].

1.1 The BOLD signal

Physiological origin
The neuronal activity, which basically consists of information transfer within the brain, requires energy to be performed: the latter is provided by adenosine triphosphate (ATP), a molecule which carry out this function for almost every biological process in the human body. The production of ATP can be achieved through the aerobic glycolysis, a metabolic process that converts the glucose into pyruvate in the presence of oxygen, releasing two molecules of ATP and nicotinamide adenine dinucleotide (NADH). The metabolic pathway is followed by the pyruvate decarboxylation and the Krebs cycle, whose products are used in the oxidative phosphorylation to produce additional ATP, for a total of 36 molecules in the entire process. Nonetheless, the brain does not store neither glucose nor oxygen supplies, which are therefore provided to neurons through blood: the first

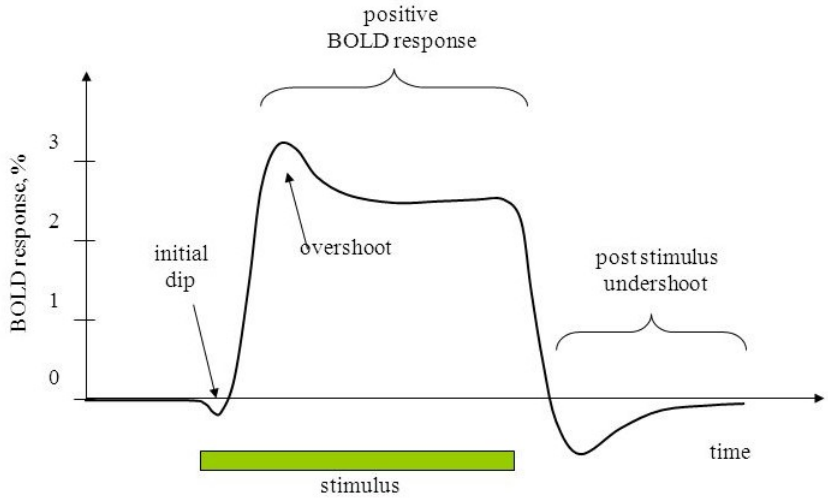

Figure 1.1: Representation of the BOLD signal percentage variation in presence of a stimulus. Image from [6].

is carried by plasma, while the second by red cells. As a consequence, when a specific region requires energy and ATP, the cerebral blood flow in correspondence of that area increases and, together with that, a higher cerebral metabolic rate of O_2, used for the glycolysis, and an increment in cerebral blood volume occur. The combination of such elements gives rise to the BOLD signal, whose percentage variation in presence of a stimulus is sketched in Fig. 1.1. Note that the percentage variation is quite small, even at its maximum ($\sim$5%): obtaining a good contrast in functional images is indeed a task of fMRI.

Relevance for MRI

As mentioned, the oxygen is transported by the red blood cells, and in particular by the hemoglobin (Hb), a protein composed by four subunits, each made of a polypeptide structure bound to an heme group, which consist of a Fe^{2+} ion that can bound molecular oxygen, O_2: if it does, the hemoglobin is also called oxyhemoglobin (HbO_2) and it is diamagnetic, if it does not it is also called deoxyhemoglobin and it is paramagnetic.
When such materials are immersed into a magnetic field, in a diamagnetic one, a magnetic moment is induced in atoms, causing small distortions of the field; in a paramagnetic one, instead, atoms already have a net magnetic moment, thus more distortion of the external field emerge in this case. Because of the high field dishomogeneities that are generated, the transverse relaxation time T_2^*, which is the characteristic time of the decay of the transverse magnetization in Nuclear Magnetic Resonance (NMR), becomes shorter and the signal decreases faster: thanks to this, the different ratio of oxy/deoxyhemoglobin in brain regions that are active allows to build a contrast within the images. In particular, in active conditions the oxygen request increases and so does the ratio of HbO_2 in blood: as a consequence the MR signal presents a slower decay, and is therefore higher, with respect to the rest condition, where the ratio of Hb is higher, causing larger dishomogeneities and faster decay. Fig. 1.2 describes this situation.

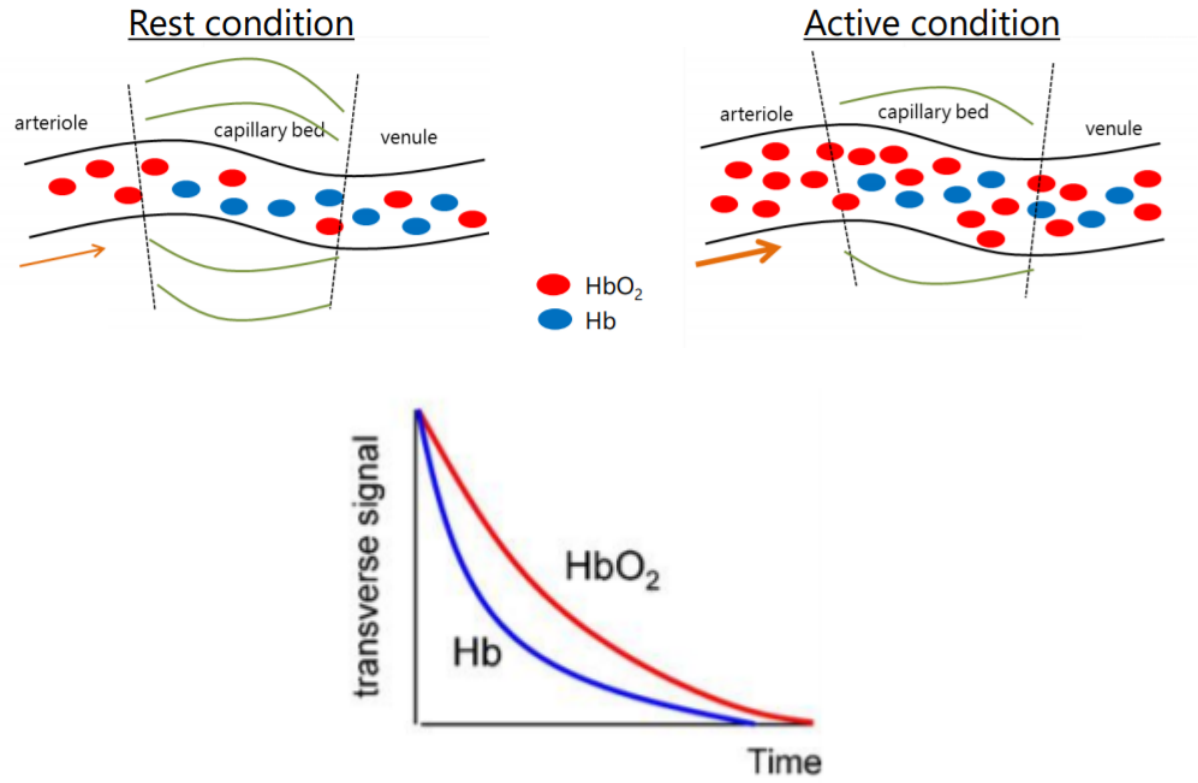

Figure 1.2: In active conditions, the ratio of HbO_2 in blood increases and, as a consequence, the MR signal decays more slowly.

1.2 fMRI acquisition

The fMRI acquisition sequence needs to be fast, since the hemodynamic response changes in the order of seconds. Therefore, the most common choice for this task is the Gradient Echo (GE) Echo Planar Imaging (EPI), as it is a fast T_2^*-weighted method that can acquire whole brain data in few seconds.

The GE-EPI sequence

A GE sequence consist of a manipulation of the Free Induction Decay (FID) signal, which is the basic signal generated by the relaxation of the transverse magnetization after a perturbation, and is described by a characteristic time of decay T_2^*. The first step is to apply a radio-frequency (RF) pulse to tilt the magnetization from the equilibrium, i.e. aligned to the external magnetic field. Then, a dephasing gradient field is applied on a slice of the brain, selected by another specific gradient, in order to cause a linear change in the magnetic field and consequently alter the resonant frequencies across the selection. As a result the dephasing, and thus the decay of the signal, is accelerated. A rephasing gradient is then applied with the same strength but opposite polarity with respect to the dephasing gradient, in order to recover the phase dissipation previously generated: this causes the echo phenomenon. One advantage of the GE sequence is that it allows to achieve the echo in short times, therefore allowing to set the Echo Time (TE), i.e. the time needed to reach an echo starting from the RF pulse, at small values. The shorter TE allows also to use shorter repetition times (TR), i.e. the time that must pass before repeating the RF pulse: this increases the T_1 weighting and, more importantly, allows to repeat the pulse sequence more quickly and shorten the acquisition time.

A diagram of this sequence can be seen in Fig. 1.3.

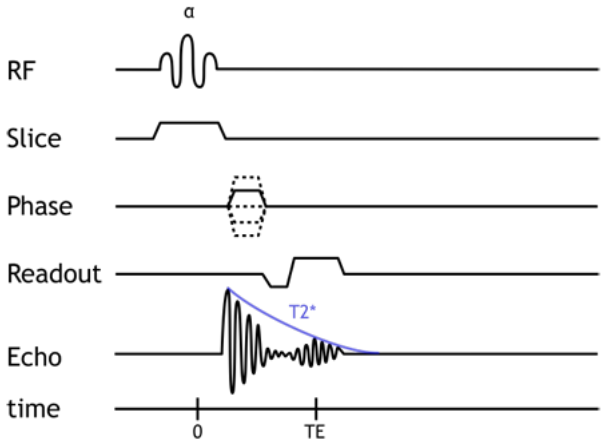

Figure 1.3: Temporal diagram of the GE sequence. The echo can be achieved within a short TE.

The EPI sequence utilizes rapidly switching gradients to acquire the entire k-space, i.e. the space where MR images are generated, within one gradient echo. To achieve this, multiple gradient echoes are formed within the original one. By using varying gradient strengths, we obtain successive phase encoding steps and thus cover the full k-space matrix within that gradient echo. Alternating the frequency-encoding gradient lets us move back and forth across the frequency-encoding direction with each phase encoding step, and the alternation is what creates the gradient echoes.
The diagram of the GE-EPI sequence is reported in Fig. 1.4. The main advantages of the GE-EPI sequence are that it is sensible to magnetic susceptibility variations and it is a very fast acquisition method. As a trade-off, the resulting images will have low contrast and Signal to Noise Ratio (SNR), so that distortions may be generated.

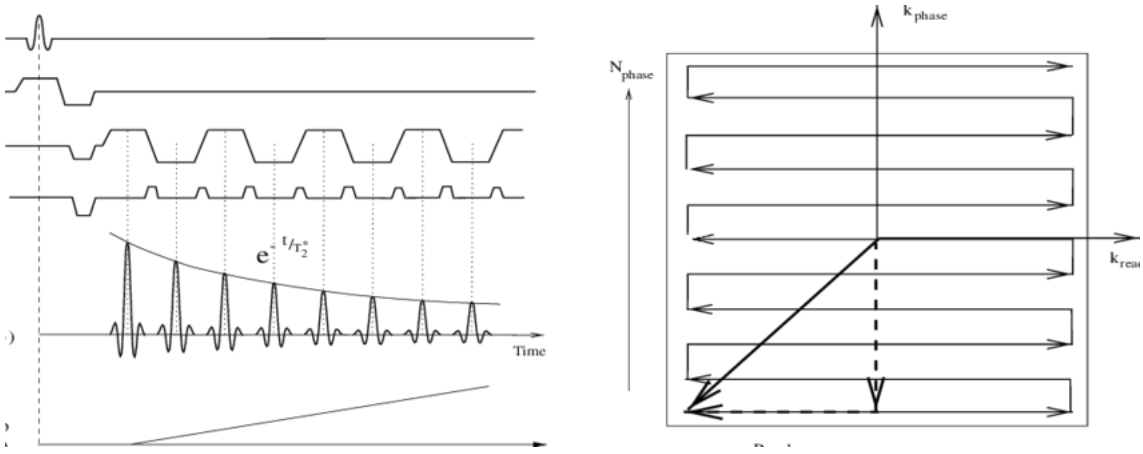

Figure 1.4: Temporal diagram of the GE-EPI sequence and the corresponding imaging procedure in the k-space. The alternation of the frequency-encoding gradient allows to cover the entire k-space within one GE sequence. Image from [7].

Note that in fMRI we are not interested in the acquisition of one single brain volume, but rather in a series, in order to obtain the evolution of the BOLD signal in time. This implies that, for each subject, we may want to image a sequence of N volumes, so that the total acquisition time is TR×N and TR, which in this case is the repetition time

needed for the acquisition of one full volume, represents the temporal resolution of this technique.

Additional aspects of the acquisition
A last important aspect of the rs-fMRI acquisition is the instruction of the subjects, who should lie still with their eyes closed, trying not to think about anything specific and without sleeping: this is crucial to minimize the sensory or cognitive inputs that they may receive. It is also important that they minimize the body movement during the acquisition, which is one the main sources of artifacts in such images, together with the physiological noises of the cardiac and respiratory cycles. The temporal evolution of the BOLD signal of the activated areas at resting state is typically characterized by fluctuations in the 0.01-0.1 Hz range.

1.3 Analysis of rs-fMR images

After a standardized pre-processing procedure, which is described in section 4.3.1, the rs-fMR images can be analyzed and investigated with various methods, developed in the past years. In this section the most common ones are briefly described; for a full and exhaustive review of such techniques, refer to [8].

Seed-based functional connectivity
In seed-based functional connectivity analysis, the activity of an a-priori selected Region Of Interest (ROI), or "seed region", is correlated to the activity in all the other voxels or predefined regions in the brain. In particular, the activity is quantified as the temporal evolution of the BOLD signal, which, in the following, will also be referred to simply as "time series". How ROIs can be defined, how time series can be extracted and how the correlation can be quantified will be deepened in chapter 2, as these elements are in common with the network approach, which was used for this study.
Even though the statistics and the results of such technique are quite straightforward, a major drawback is that it requires an a-priori selection of the seed region. As a consequence, this kind of approach is mostly used to study the properties of regions that are already acknowledged to be altered in the subjects or that belong to one of the typical networks of activation observed in the human brain, such as the Default Mode Network (DMN).

Independent Component Analysis
Supposing that the brain is organized into a number of functionally discrete networks, Independent Component Analysis (ICA) is a technique that aims to separate the brain functional patterns into distinct components with minimal a-priori assumptions. In particular, the hypothesis of ICA is that fMRI data consist of a mix of independent signals from a number of spatially distributed sources, and decomposes the data into several such independent components, in order to obtain a maximally independent decomposition.
In the case that a set of subjects, and not a single individual, is under study, a variation of this technique is the group-ICA, which tries to perform a unique decomposition across the entire set of participants, rather than for each one separately. Various methods can be used to achieve this task properly.
The main advantage of this technique is that it is data-driven and thus it does not

require a prior selection of ROIs; nonetheless, it is necessary to require a specific number of components to identify, which can only be an empirical choice. Moreover, also the selection of the meaningful components among the ones automatically identified by ICA, especially to distinguish signal from noise, remains a problem, as a manual identification is suggested.

Clustering
The operation of clustering consist in partitioning the data into a subset of groups, called clusters, so that the ones within a cluster are more similar to each other than they are to those assigned to other clusters. Applied to fMRI, this technique consist of partitioning the brain into subsets of voxels or regions that are functionally connected with one other, or that exhibit similar patterns of functional connectivity with the rest of the brain. Several different methods can be used in this sense.
As ICA, also clustering is data-driven and it also presents a similar issue: in most cases, the user must establish the number of clusters to find within the data, which is an arbitrary choice.

Pattern classification
Multi-Variate Pattern Analysis (MVPA) takes into account multi-voxel patterns of brain activity or connectivity, to be assigned to separate classes with pattern classification algorithms (such as neural networks or support vector machines), basing on automatically or manually chosen features of the data. The classification is then performed by the algorithm through a training subset of the data, where the classifier can learn the relationship between the features and the classes; a testing data set is then used to verify the performances of the technique. As a disadvantage, this method is very sensible to the choice of the features for the classifier.

Graph theory
The application of graph theory to fMRI is based on the idea that ROIs, or even single voxels, can be seen as nodes connected to each other through a set of links, which can be defined in different ways, basing on a specific definition of connectivity between the ROIs.
The greatest advantage of this approach, beside the intuitiveness of viewing the brain as a set of nodes connected to each other, is that it allows to exploit the solid findings of graph theory to investigate intrinsic properties of the functional connectivity of the brain. The most relevant issue, nonetheless, is the need to arbitrarily define the nodes and the links within the network.
This approach is more deeply explored in chapter 2, as it is the one used in this work.

Local methods
Local methods consist of approaches that address the local activity of a voxel: the most relevant examples are the amplitude of low frequency fluctuations (ALFF), which calculates the voxelwise magnitude of specific frequency bands in the frequency domain, and regional homogeneity (ReHo), which is computed only from the direct neighborhood of single voxels.
These are both easily implemented, straightforward techniques which can be used to characterize spontaneous local brain activity of the voxels.

Chapter 2

Graph theory in fMRI

A graph consists of a set of nodes connected by edges (links): the nodes represent physical or topological objects of interest and the edges identify connections that exist among them, which can be defined in multiple ways, not only from a conceptual point of view (meaning which kind of connection we look for), but also mathematically. A network, in fact, can be weighted or unweighted, whether we decide to assign a weight to a link or we are simply interested in its existence, and it can be directed or undirected, whether the relation occurs only in one sense or not.
Applying this concept to the brain, the aim is to construct a model of the latter that can represent the structural or functional links between ROIs. Various types of brain networks can be built: here we focus on the ones of interest for fMRI, but the concepts can be generalized also to the other cases.
For a complete overview of brain networks definition and analysis, refer to [9], [10], [11], [12] and [13].

2.1 Definition of nodes

The choice of how to define nodes for brain networks is the first fundamental step to take in their construction, and several different approaches have been developed in years.

Dimension of nodes
In cellular systems the most intuitive approach is to define nodes as neurons, connected by synapses as links, since they tend to have simple nervous systems. Such technique would clearly not be viable for a human brain, where there are billions of neurons, not only because of the computational difficulty of dealing with such numbers, but also because the GE-EPI sequences do not allow such high spatial resolutions. For similar reasons, also considering each voxel of the images as a separate node is a method not typically used: even though they indeed carry physiological information, since they are associated to the time series of the BOLD signal, they would be too numerous to perform an efficient study. Moreover, other aspects should be considered, such as the fact that the interpretation of their role in the network is not straightforward, since they are not associated to a specific role within the brain.
For these reasons, the most common approach is to group voxels into larger nodes, basing on a certain criterion: in particular, the two main options are to define them

basing on a template of the brain, which already subdivides the latter into a set of anatomical or functional ROIs, or to drive a parcellation directly from the data, basing on certain properties. A first advantage of such choices, common to both cases, is that these definitions are less affected by noise and artifacts since the time series of each voxel belonging to the node are averaged into a single one, associated to the ROI. On the other hand, an issue is that each node would have a different size: the values obtained by averaging across many voxels in larger regions will be less noisy than the ones estimated by averaging across smaller regions, leading to a bias in favor of stronger statistical associations between larger areas [14].

Template and data-driven approaches
Choosing a reference template, being it anatomical (such as the FreeSurfer atlas [15] or the Automated Anatomical Labelling, AAL [16]) or functional (such as the POWER atlas [17]), has two meaningful advantages: firstly, the nodes are associated to a specific role within the brain, which is useful in terms of interpretation of the results; secondly, this choice allows the comparison of outcomes between studies that used the same or similar templates. Nevertheless, it must also be noted that networks constructed with different parcellation schemes may lead to significantly different results [18]. In particular, also the number of nodes can considerably change the outcomes.
Data-driven parcellations can be obtained, for example through a group-ICA of the fMRI data across the subjects under study, in order to find maximally independent spatial and temporal components. Approaches of this type are typically found to provide more consistent and reliable results (see for example [19]), but they do not have the advantages explained for the template case: they do not allow an inter-study comparisons and the interpretation of the nodes identified within the brain is not as straightforward, since voxels that anatomically belong to different structures or are located in different functional regions may be grouped within the same node.
The considerations just described led to choosing the template approach for this study, in particular using the FreeSurfer atlas [15], which is one the most common choices among the various possibilities.

2.2 Definition of edges

Choosing the statistical association
The crucial issue in the definition of edges in fMRI brain networks is the choice of the statistical association between the nodal time series to use. A first distinction to make is between functional associations and effective associations: the first measures the extent to which two processes behave similarly over time; the second measures the extent to which one process can be predicted or explained by the other. As a consequence, the association matrix generated by estimating the functional connectivity between each pair of nodes will be symmetric, whereas the association matrix generated by an effective connectivity analysis does not need to be. The greatest part of analysis of rs-fMRI with the network approach studies functional connectivity, which is used also for this study, thus this section will focus on it.

Functional connectivity matrices
The most common choice for computing functional connectivity is to evaluate the full or

the partial Pearson's correlation among the time series of nodes, but other approaches are available, such as the wavelet correlation. The first is the most used method for constructing brain networks, even though it does not distinguish if two parcels are directly or indirectly connected. To mitigate this issue, the partial correlation is sometimes used, as it evaluates the correlation between the time series of two nodes after having adjusted for the time series of all the other ROIs, which nonetheless becomes problematic when there are not considerably more time points than parcels. For these reasons, in this work we used the full Pearson's correlation, even if also a Tikhonov-regularized partial correlation approach was attempted, and finally discarded, as described in section 4.4.1.

Weight of links

Recalling that functional connectivity matrices are undirected by construction, another choice to take is between weighted and binarized networks: in the first case, the links maintain as weight the value of correlation calculated through the method of functional association chosen; in the second case, the edges having a weight above a certain threshold are set equal to 1, whereas the others are set to 0. In this study, the weighted networks are chosen, as it is reported in literature that they provide more reliable results [20], since they retain more topological information than the binarized ones, which, for this work, were simply built as a check of the main case, as described in section 4.4.1.

Thresholding

A last comment about the definition of edges should be on the density at which a brain network should be evaluated, which is defined as

$$k = \frac{\epsilon_\tau}{\frac{N(N-1)}{2}} \tag{2.1}$$

where ϵ_τ is the number of edges generated by the thresholding at a certain value of τ, and $\frac{N(N-1)}{2}$ is the maximum number of edges that could exist in a network of N nodes. When k is maximum, all the links within the network are preserved, but, as it decreases, those that have progressively lower weights are cut from the graph (set equal to 0), and only the most solid ones remain. As it is described in [10], the properties of a network do change as a function of the density: to face this issue, there are two possible solutions: one is to use an optimization algorithm to find a unique threshold to adopt for studying the network (for example, by controlling the probability of type I error - false positives - on multiple hypothesis testing of each element in the association matrix); the second, which is much more common, and is used also for this work, is to analyze the networks over a range of densities, instead of a single one. The complex or nonrandom topology of brain graphs is typically clearest in relatively low-cost networks, i.e., those with connection densities less than about 0.5.

2.3 Properties of brain graphs

The graph theory gives access to a wide range of possible measures that can be carried out on brain networks. In this section, the general properties that are exhibited and

characterize all kinds of brain networks are described, while the specific measures performed for the analysis in this study are listed in section 4.5.

- *Degree/strength - degree/strength distribution*: brain networks typically show heterogeneous degree/strength distributions, such as broad-scale or fat-tailed probability distributions of the degree/strength of single nodes, indicating the likely presence of network hubs, i.e. highly connected nodes that have a crucial role within the graph.
  The degree of a node is the number of edges connecting it to the rest of the network; the distribution of degrees over all nodes in the network can be described as a degree (probability) distribution. The strength is the analogous of the degree for weighted networks, i.e. it is the sum of the weights of the links that connect a node to its neighbors.
- *Small-worldness*: it indicates a balance between network segregation and integration. It is a combination of high global and local efficiency of information transfer between nodes, which implies short characteristic path length (the average length of the path to go from any node to any other) and high clustering coefficient (proportional to the number of triangles of connectivity that a node forms with its neighbors).
- *Modularity*: it indicates that the network is likely to be decomposed into smaller subsystems that maximize their intra-connections, while minimizing the interconnections among them.

At last, it is important to underline that the brain network measures should be compared to the ones of random networks, in order to have a point of reference to judge the non-randomness of the same metrics measured in the neuroimaging data. Moreover, it is essential that the random networks to be compared have the same number of nodes and edges of the brain graph, so that the testing can be reliable.

Chapter 3

Borderline Personality Disorder

The aim of this work is to investigate the properties that characterize the brain networks of a set of subjects affected by the Borderline Personality Disorder (BPD) and compare them to those of a group of healthy controls (HC), in order to find significant variations that may discriminate the two different conditions.
Details on the composition of the cohort of participants to the study are reported in section 4.1, whereas in this chapter the general attributes of the disease are briefly described.
For extended literature on the characterization of BPD, refer for example to [21], [22] and [23].

3.1 Clinical characteristics

Diagnosis and symptoms
According to the psychiatric classification system in the fourth edition of the Diagnostic and Statistical Manual of Mental Disorders (DSM-IV) [24], used also to perform the diagnosis of the subjects of this study, BPD is characterized by a pattern of instability in interpersonal relationships, an unstable sense of self, intense and volatile emotions, and impulsive behaviors, which make the patients difficult to treat. Moreover, BPD subjects tend to exhibit suicidal and self-injury tendencies, which are some of the most indicative factors to perform the diagnosis.

Comorbities
BPD is frequently associated with various comorbities, among which mood disorders, anxiety disorders, and disorders associated with substance misuse [25], because of the common symptoms that they show. Nevertheless, a criterion of exclusion of the candidates from this study was the presence of such comorbities.

Course of the disease
BPD has a good prognosis with respect to other personality disorders: high rates of remission were reported in both short-term and long term follow-up studies [26]. In particular, impulsive symptoms (such as suicide and self-injury efforts) are the least prevalent and consistent with age and treatment, whereas affective features (anger, anxiety, depression) and interpersonal features are the most stable. Nonetheless, note that

the participants to the study were not under pharmacological treatment before or at the moment of the neuroimaging acquisition.

Causes
A combination of biological (temperamental in particular) and psycho-social factors, such as adverse childhood events, are the most probable causes of the development of such condition [27], even though genetic factors may contribute [28].

Epidemiology
The prevalence, defined as the proportion of a particular population found to be affected by a medical condition at a specific time, within the general population was found to be comprised between 1-2% in recent years [23].
Most patients with BPD in clinical settings are females, even though general surveys do not support a higher prevalence among subjects of this sex: such disproportion, which is exhibited also by our cohort of participants, might be related to the fact that female subjects affected by this disease are more inclined to seek for clinical help [22].

Neuroimaging findings
Previous neuroimaging results from PET and fMRI report functional dysfunctions predominantly within the frontolimbic system in BPD [29]. The regions particularly involved in this sense are the amygdala [30], the anterior cingulate cortex [31] and other orbitofrontal areas. A recent study of rs-fMRI with a network approach by Xu et al. [32] report generally increased functional connectivity in BPDs with respect to HCs, especially among the limbic regions.
Also from a structural point of view, the amygdala shows volumetric aberrations, together with hippocampus [33], supporting the findings from the functional perspective.

Chapter 4

Materials and methods

4.1 Subjects

The cohort of subjects participating to the present study was composed by a total of 55 young individuals, among which 27 were affected by BPD and 28 were age- and sex-matched HCs. The presence of neuro-psychological comorbities and the assumptions of medical treatments was a criterion of exclusion from the study.
The condition of BPD was diagnosed through a Structured Clinical Diagnostic Interview for DSM-IV Axis II (SCID-II) [24], which consists of an interview that provides a categorical assessment of personality disorder, in accord with the criterion given by DSM-IV. The BPD patients' ages range between 18.9 and 30.3 years, with mean 24.1±3.5 years, whereas those of the controls range between 19.5 and 29.5 years, with mean 24.9±2.8 years; the subjects are predominantly females: only 6 subjects per group were males.
All the participants to the study were subjected to a psychiatric and neuro-psychological evaluation based on a set of clinical scales for the assessment of their condition. In this context, the following five scales were selected for the subsequent analysis:

- the Barratt Impulsiveness Scale-11 (BIS-11, in the following indicated as BIS), to assess the personality/behavioral construct of impulsiveness [34].
- the Difficulties in Emotion Regulation Scale (DERS), used to identify emotional regulation issues [35].
- the Anger Rumination Scale (ARS), which measures "the tendency to focus on angry moods, recall past anger episodes, and think over the causes and consequences of anger episodes" [36].
- the Self-Harm Inventory (SHI), for identifying self-destructive behaviors [37].
- the Ruminative Response Scale (RRS), which measures the depressive rumination [38].

Moreover, two additional scores, evaluated for BPD patients only, were considered in this study:

- the Beck's Depression Inventory (BDI), for measuring the severity of depression [39].

- the Work and Social Adjustment Scale (WSAS), to assess functional impairment in the social context [40].

All these scales are defined so that the severity of the condition increases with the scores. Tab. 4.1 summarizes the average demographic and clinical information of the subjects of this study.

	BPD	**HC**
# Females/Males	21/6	22/6
Age (years)	24.1±3.5	24.9±2.8
BIS	74.6±10.6	52.9±8.8
DERS	121.8±14.0	65.0±17.7
ARS	34.2±7.8	21.6±7.0
SHI	8.1±4.0	0.8±1.3
RRS	63.0±9.0	39.3±12.0
BDI	25.5±8.5	-
WSAS	20.6±9.7	-

Table 4.1: Summary table of the demographic information and clinical scores of BPD patients and healthy controls.

4.2 MRI acquisition

The resting-state functional MR images were acquired with a 1.5 T GE Signa HDx 15 scanner equipped with an 8-channel head coil, following a standardized MR protocol: all the subjects were instructed to lie still with their eyes closed without falling asleep, trying not to think about anything specific, during a 9 min rs-fMRI acquisition. The sequence used for the acquisition was a Gradient Echo EchoPlanar Imaging (GE-EPI), which is a fast sequence commonly chosen for rs-fMRI to trade off with the long acquisition times. The repetition time was set to TR = 3 s, so that a total of 180 volumes were imaged, with spatial resolution equal to 1.875 mm × 1.875 mm × 4 mm. The Echo time was TE = 40 ms and 34 pure axial slices were acquired for each repetition. For two subjects, one patient and one control, an inferior number of volumes was acquired (139 and 146 respectively), because of the excessive movement of the individuals during some repetitions, which could not be corrected in the pre-processing steps, see section 4.3.1. Since the difference with the standard 180 volumes was acceptable, they were nonetheless included in the subsequent analysis.
As a result, the rs-fMRI acquisition of one subject is composed by a stack of N whole-brain volumes, where N is the total number of repetitions. Each voxel in each brain volume is characterized by a value, which is the intensity of the BOLD signal at that repetition and the sequence of values of a single voxel for each repetition constitutes the time series vector, which is the temporal evolution of the BOLD signal during the acquisition.
The MR protocol also included a 3D high-resolution volumetric T1-weighted structural brain image (FSPGR, fast spoiled gradient-echo, pure axial slices, TR/TE = 12.3 ms/5.2 ms, FOV = 25.6 cm, nv = 256, 1 mm isotropic). An example of a raw fMR and T1-weighted images is reported in Fig. 4.1.

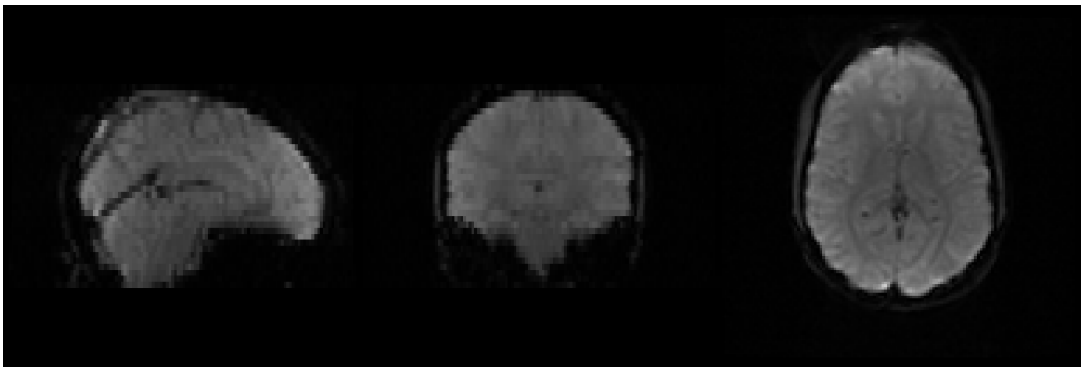

(a) Single slice of a single volume in a raw rs-fMR image.

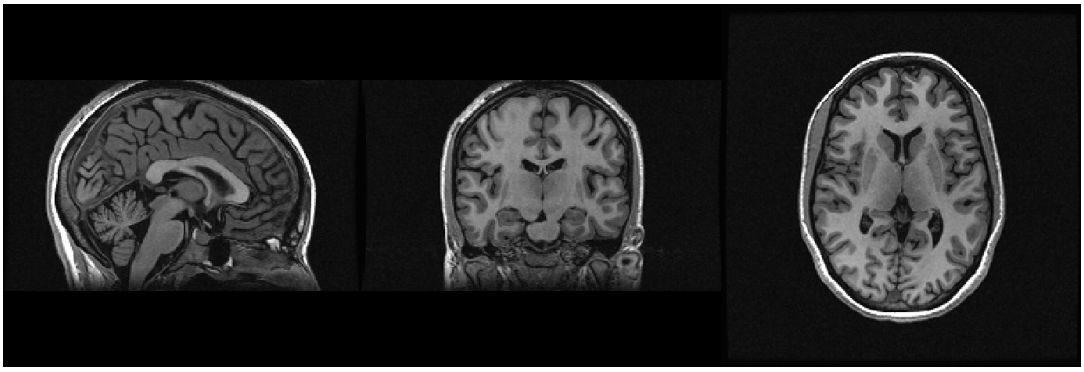

(b) Single slice of a raw structural T1-weighted image.

Figure 4.1: Example of raw rs-fMR and T1-weighted images of an healthy subject.

4.3 Data pre-processing

The pre-processing of the raw data, both functional and structural, was performed prior to the thesis work, but the main steps are briefly described here.

4.3.1 fMRI data

The functional MR images were pre-processed in order to remove elements of confusion, with the instruments of FSL [41], a commonly used software which provides analysis tools for brain fMRI, MRI and DTI data.
The pipeline of pre-processing started with a quality evaluation by naked eye of the images, checking for visible artifacts or movements of the patients during the acquisition, and was followed by six standardized steps, repeated separately for each subject:

- *Motion correction*: aligns all the volumes of an fMRI acquisition to a reference volume, typically the central one, to correct for the possible movement of the patient during the imaging procedure. Movement in resting state images that exceeded 1 mm of displacement or 2° of rotation in any direction were excluded from the data. Since all the volumes to be aligned belong to the same individual, the registration could be linear and was performed with MCFLIRT [42].

- *Brain extraction*: this is fundamental to isolate the brain, brain stem and cerebellum from the skull, which is useless to the purposes of fMRI (BET tool [43]).

- *Spatial smoothing*: a Gaussian spatial smoothing allows to make assumptions of

normality. In this case, an amplitude of 5 mm was chosen, which makes a good trade off, considering that the slices of the volumes are 4 mm thick.

- *Intensity normalization*: brings the intensities to a common scale across subjects.
- *Temporal high-pass filter*: removes drift effects of the BOLD signal across volumes. The filter, as it is common for fMRI, was set at 100 sec (0.01 Hz), which is the longest scale time that we consider to observe meaningful variation.
  The spatial smoothing, the intensity normalization and the high pass filtering were carried out with the FEAT tool [44].
- *Physiological noise correction*: the respiratory and cardiac cycles can affect the data, not only because they can likely cause body and head movement, but also because the frequency of the cardiac cycle in particular is in the range of frequencies where we expect to observe meaningful data. This operation was accomplished with the MELODIC tool [45], which performs an ICA of the series of functional brain volumes of the subject, in order to find an optimal decomposition into different spatial and temporal components. These components were then manually labeled by an expert as signal or noise, basing on their spatial, temporal and spectral properties [46].

The components classified as signal at the end of the sixth pre-processing step constitute the filtered and clean rs-fMR images, from which the mean time series of the brain regions could be retrieved, as it is explained in subsection 4.4.1. An example of such images can be seen in Fig. 4.2.

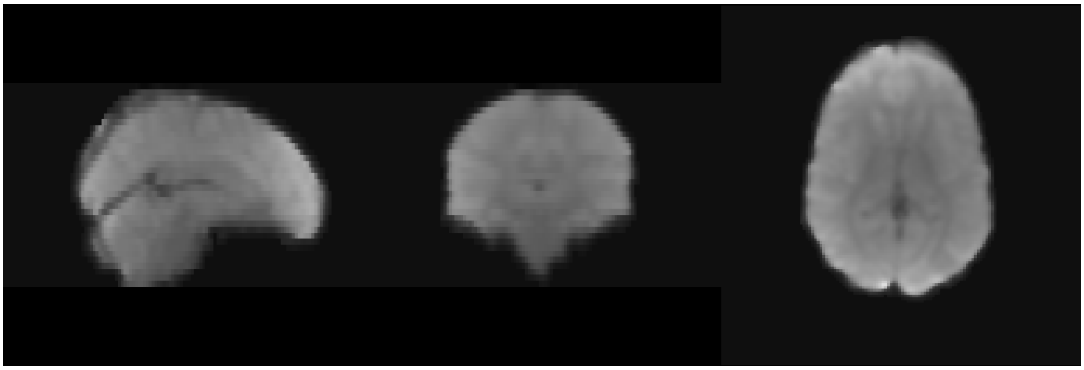

Figure 4.2: Example of a single slice of a single volume of the filtered and clean fMRI of an healthy subject. With respect to Fig. 4.1a, the results after skull and scalp removal and the spatial smoothing are visible.

4.3.2 Structural MRI data

The raw structural images were pre-processed, segmented and parcellated with FreeSurfer 5.3 [15], in order to subdivide the brain volumes into a set of 82 anatomical cortical and sub-cortical ROIs, separated between left and right hemisphere and belonging to six main systems within the brain: the frontal, the parietal, the occipital, the temporal and the limbic lobes, plus the basal ganglia. Additionally, also the cerebellum cortex and the brain stem were identified, for a total of 85 anatomical ROIs (the brain stem does not have a left and right component): each of these will represent a node in the networks.

The subdivision just described, which can be visualized in Fig. 4.3, was chosen also basing on the prior hypothesis that the limbic system is specially affected by the disease, and a parcellation that separates the lobes of the brain would definitely help in verifying this.

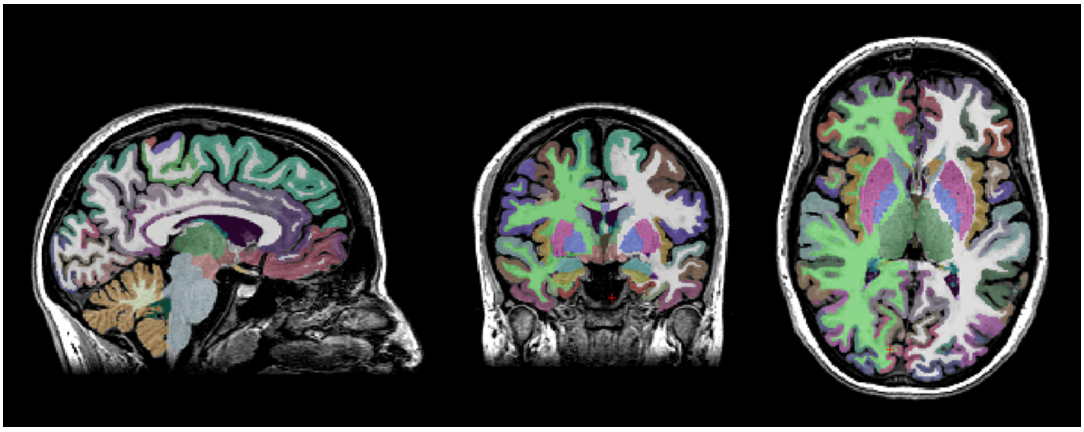

Figure 4.3: Example of the segmentation and parcellation of the cortical and subcortical regions performed by Freesurfer in an healthy control.

A complete list of the regions, the abbreviation of their names and the system they belong to can be seen in Tab. A.1, in the Appendix. Note that the limbic system was actually extended to include ROIs that, from a functional point of view, have a role in emotion regulation, even though anatomically they belong to a different lobe. A representation of the regions assigned to the limbic system can be seen in Fig. 4.4, overlaid on a T1 image. This choice was made in order to achieve a more comprehensive understanding of the role of the limbic system in BPD, which is of particular interest, as mentioned above.

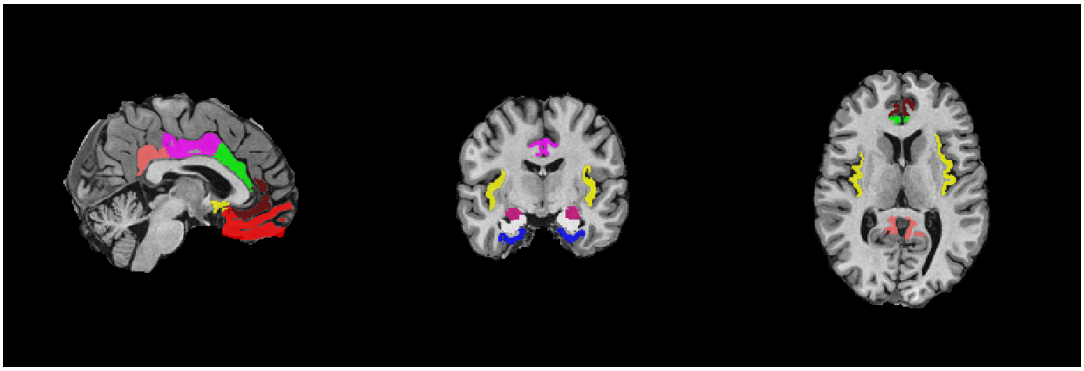

Figure 4.4: Representation of the ROIs belonging to the extended limbic system considered for this study. Referring to the abbreviations in Tab. A.1: purple=AMY, white=HIP, green=cAC, blue=ENTH, yellow=insula, pink=iC, shiny pink=PC, red=MoF, brown=rAC; ACC, LoF and PHG are not visible from this cut of the brain.

The functional images were also linearly co-registered with the FLIRT tool [47], using a Boundary Based Registration (BBR) approach, to the corresponding structural image of the subjects' brain, in order to obtain a transformation matrix between the EPI

and the T1 spaces. Additionally, the structural images of each individual were non-linearly registered to the standard Montreal Neurological Institute (MNI) brain, which constitutes a common space for group comparisons, with the FNIRT tool [48]. This last step also allowed to combine the two transformations just described into one that directly connects the EPI and the standard space.

4.4 Networks construction

4.4.1 Functional networks

Starting from the segmentation and parcellation of the structural brain volumes, a set of 85 binary masks, one for each ROI, was generated for every subject. The masks were then transformed from the T1 space, where they were originally defined by FreeSurfer, to the EPI space, exploiting the transformation matrix T1-EPI described in subsection 4.3.2. This procedure also changed the intensity values of the voxels in the ROI, since the transformation is not a simple translation, so that the final masks were not binary anymore. The new intensity value of a voxel in the EPI space was interpreted as the probability of that voxel to be part of that ROI in the new space. A visual inspection was also operated to check that the regions were correctly defined and transformed.
Since the ROIs, and not the voxels, correspond to the nodes of the network, a single time series should be associated to each of them. To achieve this, the time series of each voxel belonging to the transformed ROI within the functional filtered and clean images were averaged, using the probabilities associated to the voxels in the EPI space as weights, through the `fslmeants` utility of FSL. In this way, 55 180×85 matrices were obtained, one per subject, where each columns correspond to the mean time series associated to a specific ROI.
Starting from these matrices, the following analysis was conducted almost entirely on MATLAB R2019a.

Full networks
For each subject, a 'Functional Connectivity' (FC) network was built: in such graphs, the presence and the strength of a connection between two nodes is equal to the full Pearson's correlation coefficient between the time series associated to those nodes. This operation was repeated for each possible pair of regions in which the brain was parcellated and, as a result, 55 85×85 symmetric and weighted FC matrices were obtained. The value of each element in the matrices, which ranges between -1 and +1, describes how strongly the time series of the two regions are correlated: we assume that if the temporal evolution of the BOLD signal of the two different regions is similar, then those two ROIs are functionally connected to each other. The negative correlation values were set equal to 0, as their neuro-psychological interpretation is debated [49]. These graphs are referred to as 'full' in the following, to distinguish them from the other cases explored in this work and described in this section.
To visualize the FC matrices, refer to Fig. 4.5, where those of BPD patients and HC were averaged separately. In the image, the nodes are ordered as in Tab. A.1 and the systems they belong to are indicated below the matrices.

A frequent approach to deal with FC matrices is to binarize them; nevertheless, according to recent findings [20], maintaining a weighted network could actually improve the

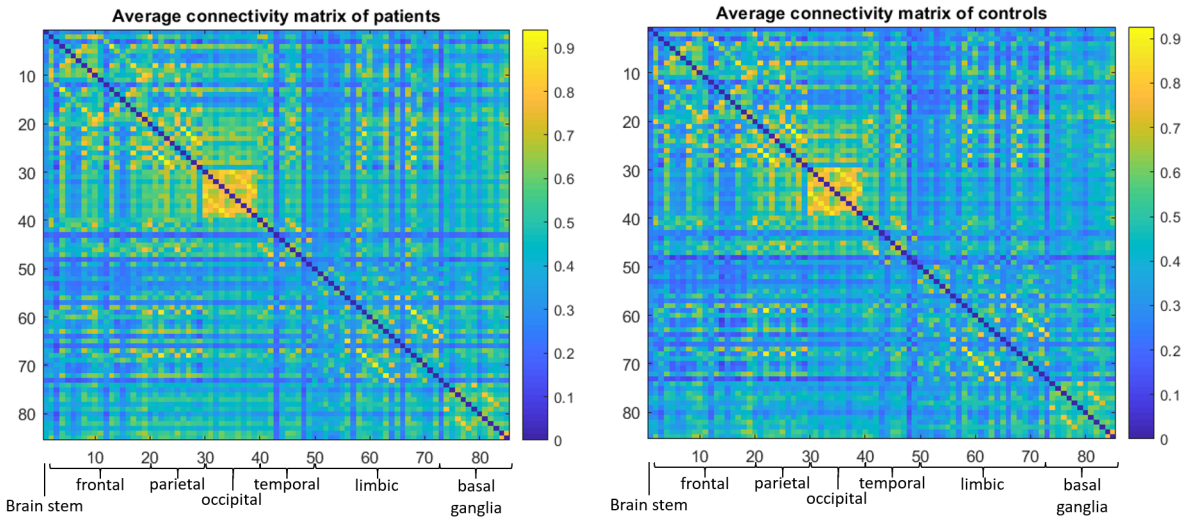

(a) Average connectivity matrix of patients. *(b) Average connectivity matrix of controls.*

Figure 4.5: Average FC matrices, calculated as the Pearson's correlation of the time series of each pair of ROIs, in patients and controls. Each column and each row correspond to a node and each element of the matrix tells how correlated the time series of the two corresponding nodes are.

stability and reliability of the results, since the network would retain more topological information; therefore it was decided to keep the weighted networks for the analysis.
For each of the 55 FC matrices, a set of 100 more matrices was generated, one for each density value from 1% to 100%, with a step of 1%. This procedure was conducted because, even in the case of weighted networks, there is not a unique density at which brain networks should be evaluated [10], so that the standard strategy is to evaluate their properties on a full set of densities, and then establish a smaller range where the measures appear to be significant. The operation was completed with the '`threshold_proportional`' function of the Brain Connectivity Toolbox (BCT) [50], which sets to 0 the links with lowest weights in the network, until the latter reaches the preset density. The reason to set to 0 the edges with the lowest weights is not only due to the fact that they are less meaningful in the network, but also because low correlation values are more likely to emerge by chance.
For each of the 55×100 FC matrices defined, a corresponding random network was also created. This was achieved via the '`randmio_und`' function of the BCT, which shuffles every edge of the original network a preset number of times (100 in this case) while preserving its degree distribution.
An overview of the process from the filtered and clean fMR images to the networks is sketched in Fig. 4.6.

Tikhonov-regularized partial correlation matrices
Recent papers, such as [19], suggest that Tikhonov-regularized partial correlation matrices may provide more reliable results than the simple Pearson's correlation ones, at least if the nodes are data-driven through a group-ICA analysis of all the subjects. This regularization approach was also attempted: firstly, the partial correlation matrices were generated, so that the correlation between each pair of time series was adjusted by all the remaining variables, i.e. the time series of the other regions; secondly, a single regu-

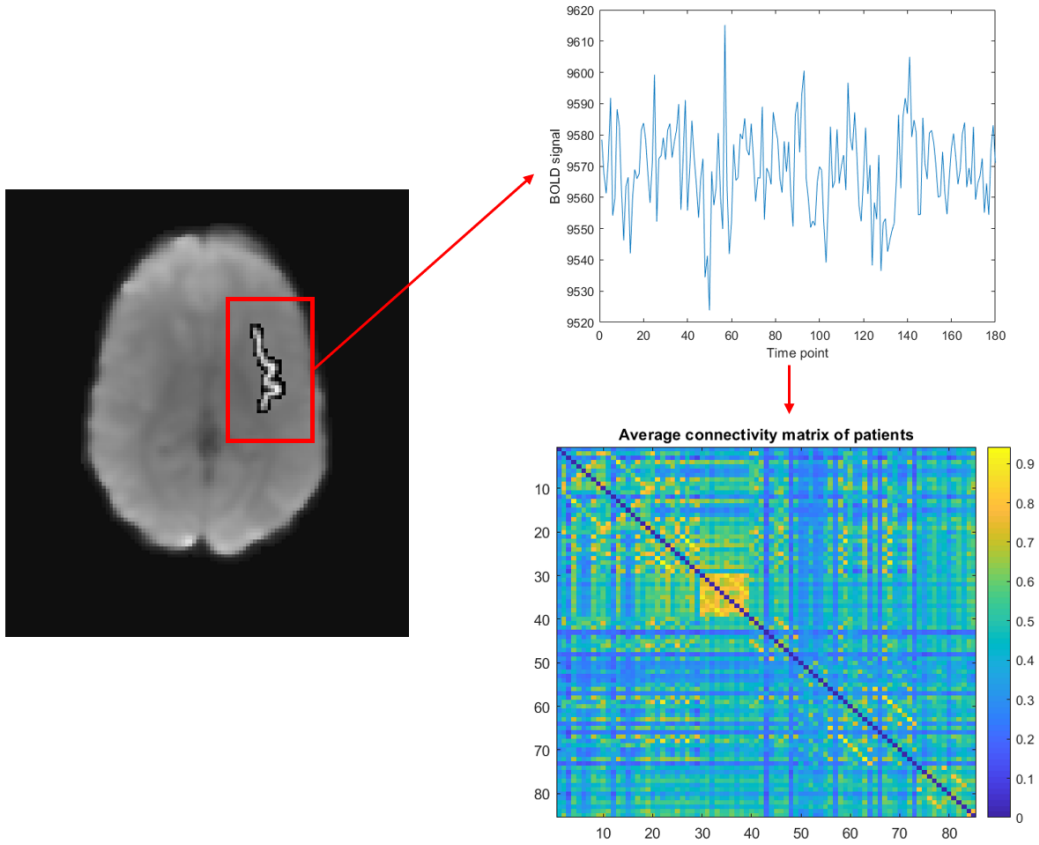

Figure 4.6: Sketch of the process followed to build the FC networks from the fMRI images: the time series of the ROIs are obtained through a weighted average of the time series of the voxels belonging to the ROI; then the time series of each pair of ROIs are correlated to construct the network.

larization coefficient α for all subjects was found by minimizing the root mean squared distance between the regularized subject precision matrices and the group average of the unregularized subject precision matrices, where the precision matrix Ω is defined as the inverse of the covariance matrix Σ and the regularized precision matrices are defined as

$$\overline{\Omega} = (\Sigma + \alpha I)^{-1}$$

I being the identity matrix. Nonetheless, this method was finally rejected because the weights of the links were generally lowered and about half of the connections were associated to negative values. Since we chose to set the latter to 0, the modular structure, which is very typical of brain networks, would have been disrupted and the connections within the network severely reduced, see Fig. 4.7: consequently all the properties that should characterize brain graphs could not be observed under such conditions and the option was therefore discarded. This issue was likely due to the small number of time points in the time series (180), in particular with respect to the number of nodes (85), which, combined with the low temporal resolution of the instrumentation used (3 s), make the partial correlations less accurate. This method is indeed suggested for configurations where the number of time points is considerably larger than the number of ROIs. A 3 T scanner could definitely improve the quality of the data, ensuring the possibility to use approaches of this kind for network construction.

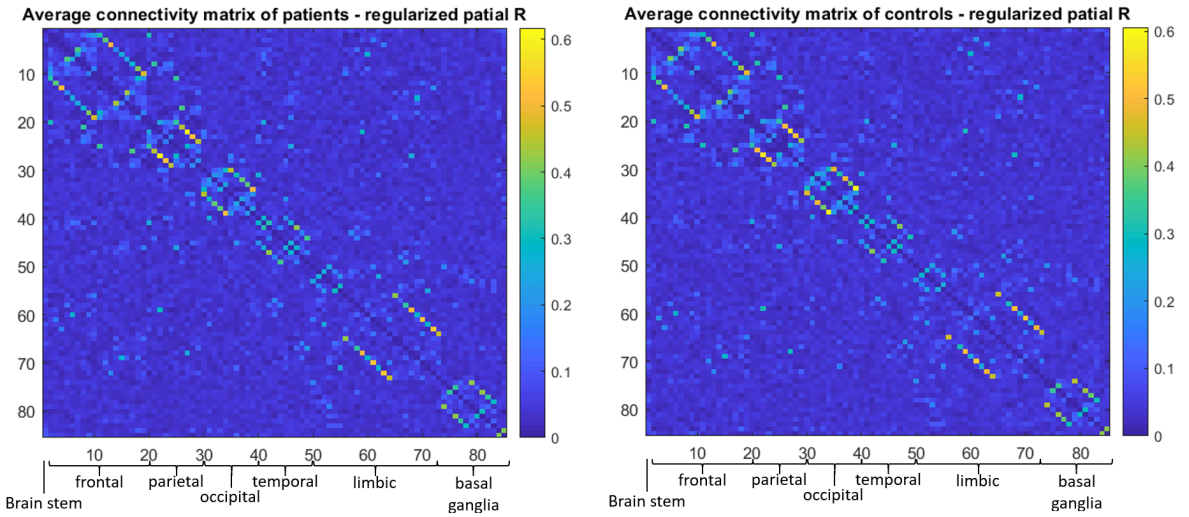

(a) Average connectivity matrix of patients with regularized partial correlation.

(b) Average connectivity matrix of controls with regularized partial correlation.

Figure 4.7: Average FC matrices, calculated as the regularized partial correlation of the time series of each pair of ROIs, of patients and controls. The modular structure typical of brain networks is disrupted.

Binarized networks

Following the network construction procedure just described, also the binarized networks were generated, only for this case of FC graph, mainly in order to have an additional check on the outcomes of the weighted graphs, as it will be clarified in chapters 5 and 6. In this case, at each density, all the weights that had passed the thresholding process were set equal to 1, regardless of the weight that they originally had: a binarized network, in fact, states simply if there exist a connection between two nodes.

Limbic and occipital subnetworks

Moreover, two smaller weighted networks were also considered for this research: one comprising only the nodes of the limbic system, since it is of particular interest for the disease under study, as mentioned above, and one comprising only the regions of the occipital lobe, which instead we expect not be affected by BPD, considering its symptoms, and which would serve as a control network, opposed to the limbic one. An image of these two system within the brain can be seen in Fig. 4.8

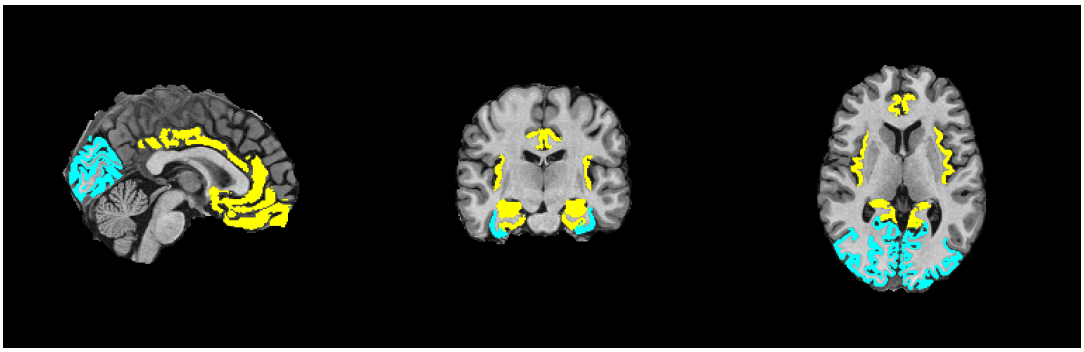

Figure 4.8: Superposition of the extended limbic (yellow) and occipital (light blue) systems, as classified in Tab. A.1, on a high-resolution structural image of the brain.

Wavelet-decomposed networks
On an additional line of study, a wavelet decomposition was applied on all the nodal time series of each subject, as previous evidences have shown that FC networks may have different properties at different frequencies [51]; moreover, different alterations in disease-related networks could emerge [52] and also noise reduction could be achieved [53]. To perform the wavelet decomposition of the time series, the Wavelet Toolbox for MATLAB was used. In particular, the Maximum Overlap Discrete Wavelet Transform (MODWT) was adopted, which can be seen as a non-downsampled version of the Discrete Wavelet Transform (DWT), achieved by adding redundancy to the DWT. It has been verified, in fact, that this choice produces less variable estimates and more stable results than the DWT method [54]. Basing on the same paper, it was decided to apply a Daubechies filter of level 6 and to subdivide the original signal into four frequency ranges: scale 1 corresponds to 0.08-0.17 Hz, scale 2 to 0.04-0.08 Hz, scale 3 to 0.02-0.04 Hz and scale 4 to 0.01-0.02 Hz. After the time series decomposition, the procedure followed for the network construction was the same as described above, repeated for each of the four frequency ranges: the networks were built by calculating the Pearson's correlation between the time series each pair of ROIs, a set of matrices was generated over the density range 1-100% and, for each of those graphs, a corresponding random network with the same degree distribution was created.

4.4.2 Structural covariance networks

Alongside the functional evaluations, also a study of structural properties with a network approach was developed, in particular by adopting the Structural Covariance (SC) networks. The basic idea to build such graphs is to determine the strength of the connection between two nodes by finding the correlations between the values of the Volumes Of Interest (VOIs, the volumes of the ROIs) across subjects, so that the sequence of the VOIs of one group constitute a series to correlate with those of the other regions; this is done for patients and controls separately.
In this case, the preparation of the data is not as straightforward as for functional networks, since the volume of a region likely has a dependence on the Total Intracranial Volume (TIV) of the subject, i.e. the volume of his/her brain, which in turn can depend on his/her age and sex: these effects must be corrected. Recent findings actually suggest that the dependence on sex might not be significant, once the volumetric data are corrected for the TIV [55]. Moreover, the age of the subjects in our cohort is expected not to be very relevant, as they are all young adults.
Different approaches are available to perform the TIV correction: basing on [55], it was decided to use the covariate regression method, which applies a multiple regression model to decompose the Volume Of Interest (VOI) value, finding in this way the dependence from each variable, that can finally be regressed out. Therefore, all the subjects were inserted into a unique multiple regression, using as variables of interest the TIV, the age, the sex, which are the nuisance regressors, and the BPD diagnosis, since we hypothesize that it affects the volumes of the regions. Therefore, the model adopted to correct the data was:

$$VOI = b_0 + b_{BPD}BPD + b_{TIV}TIV + b_{Sex}Sex + b_{Age}Age + \epsilon$$

where ϵ describes a noise, from which the TIV, the sex and the age components were regressed out, obtaining in this way a 55×85 matrix of VOI_{adj} values. Note that, even

though it was decided to regress out all the possible nuisance variables, it was indeed verified that removing only the TIV contribution would return compatible results.
To verify the efficacy of the procedure described above, the correction was repeated with another independent and validated correction method, the residuals adjustment one. In this case, we have: $VOI_{adj,res} = VOI - b(TIV - \overline{TIV})$, where b is the slope of the VOI-TIV regression line and $\overline{TIV}$ is the average TIV value of the healthy controls. Also in this case, results compatible with the ones of the covariate regression method were obtained.

Full networks
Once the adjusted values of the volumes were retrieved, it was possible to build two unique SC networks, one for the BPDs and the other for the HCs, as described at the beginning of this subsection, using as series the adjusted volumes in patients and controls separately. Analogously to the FC networks, also the structural ones were built with the Pearson's correlations. The resulting weighted and symmetric matrices are shown in Fig. 4.9.

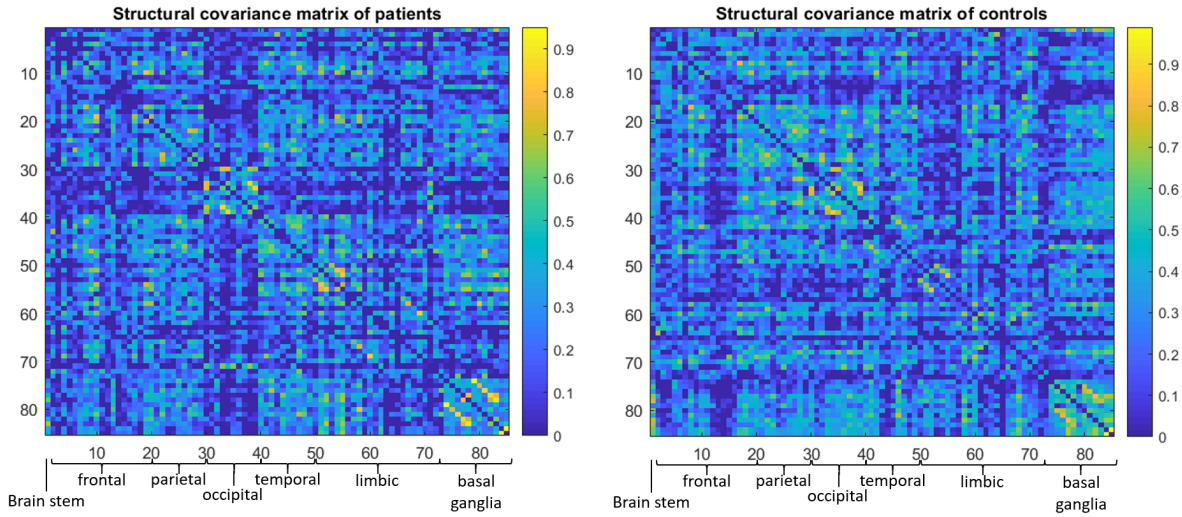

(a) Structural covariance matrix of patients. *(b) Structural covariance matrix of controls.*

Figure 4.9: Structural covariance matrices, calculated as the Pearson's correlation of the adjusted volumetric series of each pair or ROIs, of patients and controls.

Limbic and occipital subnetworks
Analogously to what was made within the FC networks, also the SC ones were analyzed in their reduced versions of the limbic and the occipital subnetworks, again seeking for significant variations in the first, which is of particular interest for this disease, with respect to the second.

Female subjects only
The same process was adopted to build networks of female subjects only, since the number of individuals of such sex clearly outnumbered males in our cohort, and, as mentioned above, sex differences may be relevant in structural evaluations. Note that, in this case, the term related to sex in the covariate regression method was not included, since it is useless.

4.5 Network properties

The properties of both the FC and the SC networks of patients and controls separately were evaluated at global and local level at every density, mostly using the functions of the Brain Connectivity Toolbox [50], except for those cases where the contrary is explicitly said.

4.5.1 Global properties

The following global properties were evaluated for each network, except for the modularity coefficient in the limbic and occipital subnetworks, as those already represent physical existing modules which should not be subdivided further:

- *Mean Connectivity*: it is the average connectivity value of a matrix and it is obtained by calculating the mean of all the Pearson's correlations coefficients inside it. It gives an hint on how strong the connections between nodes are, thus it is particularly useful for weighted networks.
- *Degree and strength distribution*: typical degree and strength (in case of weighted networks) distributions of brain graphs are broad-scale or fat-tailed, indicating the presence of hubs (highly connected nodes) among nodes.
- *Characteristic path length* (CPL): the average shortest path length between any pair of nodes; it quantifies the integration ability of a network. The classical definition can generate problems in disconnected networks (as brain graphs typically are at low densities), therefore a modified measure was used: the harmonic mean version of the original definition,

$$CPL = \frac{n(n-1)}{\sum_{i \neq j \in G} d_{ij}^{-1}} \tag{4.1}$$

  where G is the set of all nodes, n is the total number of nodes in the network and d is the weighted shortest path length between nodes i and j, which is infinite between disconnected nodes and is calculated as

$$d_{ij} = \sum_{a_{uv} \in gi \longleftrightarrow j} (w_{uv})^{-1}$$

  where a_{uv} indicate the presence of a link between nodes u and v and $gi \longleftrightarrow j$ is the shortest weighted path between i and j. With this definition, disconnected nodes do not contribute to the sum in the denominator.
  The code written to implement this measure can be found in the Appendix.
- *Global efficiency* (E_{glob}): the average inverse shortest path length between any pair of nodes in the network; it measures the efficiency of distant information transfer, similarly to the characteristic path length.

$$E_{glob} = \frac{1}{n} \sum_{i \in G} \frac{\sum_{j \neq i \in G} (d_{ij})^{-1}}{n-1} \tag{4.2}$$

- *Average local efficiency* (E_{loc}): nodal version of the global efficiency, indicates how efficiently the information is integrated among the neighbours of the node. See the formula for nodal local efficiency in the next subsection: to obtain an estimate at global level, the average of the values associated to each node is calculated.
- *Average clustering coefficient* (CC): another measure of local efficiency in information transfer, in this case proportional to the number of triangles that a node may form with its neighbours. See the formula for nodal clustering coefficient in the next subsection: to obtain an estimate at global level, the average of the values associated to each node is calculated.
- *Small-worldness* (SW): the property to exhibit simultaneously high local and global information transfer efficiency between nodes, i.e. high clustering coefficient and short characteristic path length. Quantitatively it is defined as the average clustering coefficient (normalized by the one of a corresponding random network) divided by the characteristic path length of a network (also normalized):

$$SW = \frac{CC/CC_r}{CPL/CPL_r} \tag{4.3}$$

  where CC is the clustering coefficient and CPL the characteristic path length. Note that to verify this property, it is not only needed that $SW > 1$ but also $CC/CC_r > 1$ and $CPL/CPL_r \sim 1$. Brain networks tend to exhibit this property, typically up to a density of 50%.
- *Largest Connected Component Size* (LCC): checks the dimension of the largest connected component as a function of the density.
- *Modularity coefficient* (Q): a scalar which quantifies the likeliness of the network to be partitioned into modules that maximize the ratio of intramodular to intermodular edges:

$$Q = \frac{1}{l} \sum_{i,j \in G} \left[w_{ij} - \frac{s_i s_j}{l} \right] \delta_{m_i, m_j} \tag{4.4}$$

  where l is the sum of all weights in the network, m_i is the module containing node i, and $\delta_{m_i,m_j} = 1$ if $m_i = m_j$ and 0 otherwise. The modularity was computed with the Community Louvain algorithm.

All the measures of the subjects' networks described above were compared and normalized by the results obtained with the corresponding random networks, except for the mean connectivity, the LCC size and the modularity. This is a standard procedure to retrieve outcomes which highlight differences among groups, BPD patients and healthy controls in this case, and to avoid to include properties that could emerge from a certain degree of randomness in the network configuration.

4.5.2 Local properties

At nodal level, the following measures were evaluated for all the networks, except for the module-related properties in the limbic and occipital subnetworks, for the same reason illustrated in subsection 4.5.1:

- *Composition of modules*: it was qualitatively evaluated which nodes compose the modules identified by the community algorithm in the networks, to state if it would reflect the anatomical subdivision into systems of the brain.
- *Degree and strength* (Deg, Str): the degree and strength were studied also at a local level, looking for central nodes in the networks. Respectively:

$$k_i = \sum_{j \in G} a_{ij} \tag{4.5}$$

where a_ij is equal to 1 if a link exist between nodes i and j.

$$s_i = \sum_{j \in G} w_{ij} \tag{4.6}$$

where W_{ij} is the weight of the link between nodes i and j

- *Betweenness centrality* (BC): another measure of centrality of a node in the network, based on the number of shortest paths that pass through that node to connect any other pair of nodes in the graph.

$$b_i = \frac{1}{(n-1)(n-2)} \sum_{h,j \in G, h \neq j, h \neq i, j \neq i} \frac{\rho_{hj}(i)}{\rho_{hj}} \tag{4.7}$$

where ρ_{hj} is the number of shortest path between h and j and $\rho_{hj}(i)$ is the number of shortest path between h and j that pass through i

- *Local efficiency and clustering coefficient*: the measures of local efficiency of information transfer among neighbors were not only averaged to obtain an estimate at a global levels, but they were also studied per node, to find out which are the most relevant on this side.

$$E_{loc} = \frac{1}{2} \sum_{i \in G} \frac{\sum_{j,h \in G, j \neq i} (w_{ij} w_{ih} [d_{jh}(N_i)]^{-1})^{-1/3}}{k_i(k_i - 1)} \tag{4.8}$$

$$CC = \frac{1}{n} \sum_{i \in G} \frac{\sum_{j,h \in G} (w_{ij} wihwih)^{1/3}}{k_i(k_i - 1)} \tag{4.9}$$

- *Participation coefficient* (PC): it assesses the ratio of intramodular connectivity to intermodular connectivity. Nodes with high participation coefficient are essential in linking different modules in the network. A ROI is called 'integrating' hub if its participation coefficient is at least 1 standard deviation larger than the average of PC for all nodes. Determining hubs basing on the simple degree or strength of the node, in fact, may be misleading, as this procedure may let emerge regions simply because they are part of the largest subnetwork(s) [56]. Identifying integrating hubs as those with the highest participation coefficient solves this issue.

$$PC_i = 1 - \sum_{m \in M} \left(\frac{s_i(m)}{s_i} \right)^2 \tag{4.10}$$

where M is the set of all modules in the network and $s_i(m)$ is the sum of the weight of links between i and all nodes in module m.

- *Within-module strength* (*modStr*): measures the strength of a node, considering only the connections with the nodes within the same module. This is used to evaluate the relevance of a node inside the module where it is found, and in particular the regions whose *modStr* is greater than 1 standard deviation of the average of all nodes are called 'segregating' hubs. This measure is not present in the BCT, therefore it was implemented specifically for this purpose and the code is reported in the Appendix.

$$modStr_i = \sum_{j \in M_i} w_{ij} \tag{4.11}$$

  where $M - i$ is the set of nodes within the module node i is assigned to.

The visualization of specific brain networks and of nodal properties was performed with the BrainNet Viewer software [57] for MATLAB, which is specifically designed for this purpose and therefore allows to set many visualization options within a ball-and-stick-model.

4.6 Comparison between patients and controls

As mentioned earlier, there is not a specific density at which functional or structural brain network should be studied: for this reason, we performed the measures of the networks properties over a full range of densities (1-100%). Following the same logic, also the results of the measurements should be evaluated on a set of densities, rather than a single one: to solve this issue, we integrated the results of the measures over a range of densities where they were significant, obtaining the Area Under the Curve (AUC) of the measures. The ranges varied basing on the type of networks studied and the chosen ones are reported in Tab. 4.2 for each case.

		Density range (%)
Functional	Full	5-50
	Limbic	15-50
	Occipital	30-50
	Wavelet decomposition	5-50
Structural	Full	5-30
	Limbic	15-50
	Occipital	33-55
	Females-only	5-30

Table 4.2: The range of densities over which the measures were integrated, for each network studied.

Two main measures were considered to set the upper density boundaries of assessment: the small-worldness and the LCC size. In particular, the small-worldness should have been greater than 1 and clearly different between patients and controls below the threshold; at the same time the LCC size should have been equal for BPDs and HCs and maximum (i.e. including all the nodes in the network) or very close to it at the upper boundary. As expected, in most cases this is verified up to a density of ∼50%. The lower boundary, instead, was selected as low as possible, yet trying to avoid the abrupt discontinuities in the trends of the measures that often emerge at very low densities. Such

undesired behaviors emerge especially from small networks: this is the reason why the subnetworks of the limbic system, which includes 24 nodes, and of the occipital system, which contains 10 regions, present lower bounds that continuously increase. The plots of the small-worldness and the largest connected component size as a function of density for the full FC network are shown in Fig. 4.10 to visualize an example of how the choice of ranges was taken.

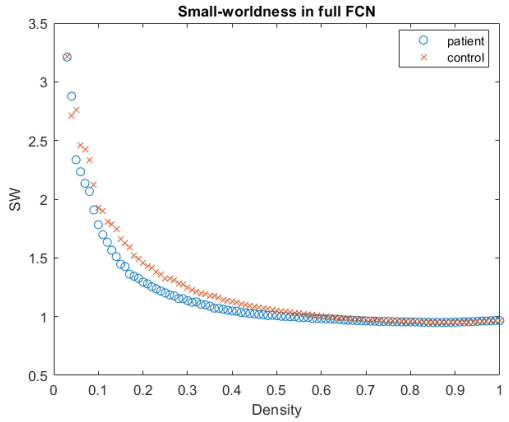

(a) Small-worldness of the full FC network as a function of density.

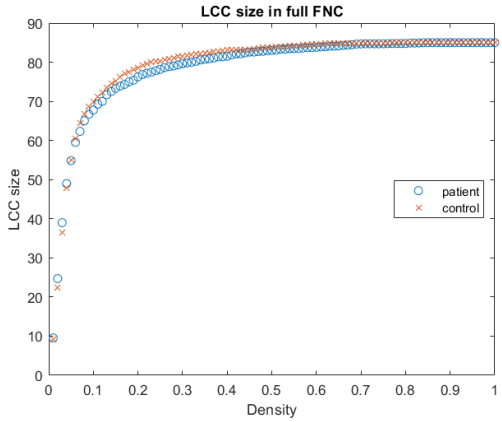

(b) LCC size of the full FC network as a function of density.

Figure 4.10: Small-worldness and LCC size of the full FC network as a function of density. The SW is greater than 1 and visibly different between patients and controls up to a density of 50%; the LCC size is almost maximum at that density, thus the choice of the upper boundary. The choice of the lower boundary was mostly based on the normalized CPL which is significantly greater than 1 at densities lower than 5%, see Fig. 5.7.

4.6.1 Permutation tests

FC networks

In order to verify whether the differences found between the AUCs of patients and controls were statistically significant or not, a permutation test was applied for each measure, using the Randomise tool from FSL [58]. For functional networks, the integrals from the 55 patients were merged into a unique vector, and the values were labelled as belonging to healthy controls or BPD patients. Randomise is based on a General Linear Model (GLM), where it is possible to specify the contrast, i.e. the comparisons that should be made (patients vs controls in this case) and a design matrix where one can add the nuisance variables to be regressed out of the model, age and sex for our data. The AUCs were then permuted 10000 times separately for each measure and, at each repetition, they were randomly subdivided into two groups, which are thus composed of patients and controls indiscriminately because of the permutation. Finally, they were averaged and subtracted one from the other, to return a difference between the two random groups. The tool counts the number of times that the difference between the averaged measures of patients and controls is lower (if positive) or higher (if negative) than the ones of the random groups. The outcome, normalized by the number of permutations is the p-Value which states if the AUC difference between patients and controls is statistically significant. A p-Value inferior to 0.05 was considered significant.
In the case of local measures, this procedure is also repeated for each node.

SC networks
Also for structural networks the significance of differences in AUC between patients and controls was estimated through permutation tests, nevertheless the implementation was complicated by the fact that there is not one network per patient, but one per group, obviously implying that there are not 55 measures which can be permuted, but only two independent ones that must be compared. Therefore, the permutation needed to be done on the original data, i.e. the adjusted VOIs, which were mixed among patients and controls for 10000 times. For each repetition, the entire procedure, from the network construction to the integral calculation was carried out and finally the difference of the measures between the randomized networks and those between patients and controls were compared and the result was stored. Once the 10000 permutations were completed, the p-Value related to each measure was calculated as described for the FC networks. Note that in this case it is not necessary to deal with the sex and the age of the subjects, since those nuisance variables were already regressed out at the beginning of the analysis.

In case of local measures, for both FC and SC networks, the 85 p-Values related to the ROIs were also corrected for multiple comparisons, with the Benjamini-Hochberg method for False Discovery Rate (FDR) [59], using the `fdr_bh` function for MATLAB [60].

4.6.2 Analysis of altered connectivity

FC networks
In FC networks, the analysis of altered connectivity was carried out with the Network-Based Statistic (NBS) [61].
NBS is a nonparametric cluster-based method that performs statistical analysis on large networks to deal with the multiple comparisons problem. In particular, it controls the Family-Wise Error Rate (FWER) while performing a mass univariate hypothesis testing at each connection of the graph, which constitute the family.
The implementation of this technique was achieved with the NBS Connectome toolbox for MATLAB, used to verify the presence of statistically significant altered functional connections in patients with respect to controls. This analysis was carried out only at the maximum density of the full FC networks, since they include all the links that may present variations. The software takes as input the FC matrices of all the subjects, properly labelled as patients or controls, and the GLM to be fitted to each edge: in particular, this includes the contrast between patients and controls and the nuisance variables of sex and age, to be regressed out. NBS Connectome at first performs a t-test at every connection in the network (mass univariate test) to identify a set of potential edges that could be significantly varied, as those that overcome a certain threshold with their t-scores. The threshold must be defined by the user and there is not a unique rule to choose it: a common procedure is to repeat the technique at various thresholds and finally select the one that would return the most statistically significant results from the application of NBS, as it is explained later in this subsection. Once the potential candidates are defined, the software performs the topological clustering of the supra-threshold edges, as it is assumed that the configuration of a non-chance structure of altered connectivity is more relevant and critical than a set of isolated connections. The final step of the method is to perform the FWER correction for each connected component found from the clustering, which is based on a permutation test including

10000 recombinations of patients and controls, and the size of the largest component is stored to build up a null distribution. Thus a corrected p-Value is assigned as the proportion of permutations for which the largest component was of the same size or greater. The threshold of significance for the p-Value was set at 0.05.

SC networks
The same NBS analysis could not be operated on the SC networks, again because in that case there is only one matrix per group instead of one per subject, which makes the application of a GLM impossible.
Therefore, to check the presence of altered connections between patients and controls, the correlation coefficients of the FC matrices of the two groups were transformed with a Fisher's z transformation and they were then compared element by element to calculate the z-score of the difference between each connection (i.e. the matrix element of patients with respect to the corresponding matrix element of controls):

$$z - score_{ij} = \frac{\left(\frac{1}{2}\ln\frac{1+\rho_{1,ij}}{1-\rho_{1,ij}}\right) - \left(\frac{1}{2}\ln\frac{1+\rho_{2},ij}{1-\rho_{2,ij}}\right)}{\sqrt{\frac{1}{n_1-3}+\frac{1}{n_2-3}}}$$

where $\rho_{1,ij}$ and $\rho_{2,ij}$ are the correlation coefficients between nodes i and j in patients and controls respectively and n_1 and n_2 are the numbers of subjects belonging to the BPD and healthy groups respectively.

4.7 Correlations with the clinical scores

An exploratory analysis, searching for a linear relationship between the topological measures and the clinical scales, was carried out. In particular, the AUCs of the global measures of the FC networks that resulted significantly varied (p-Value<0.05) between patients and controls were correlated with all the neuro-psychological scores described in section 4.1. The same was done also at nodal level, but in this case only the combinations of measures and nodes that passed the FDR were examined. The correlations were evaluated after having partialed out the nuisance variables of sex and age.
Since the scores of BIS, DERS, ARS, SHI and RRS were available for both patients and controls, the correlations were calculated for two different cases: by considering all the subjects together, and also separating the BPDs from the HCs. The correlations with BDI and WSAS, instead, were obviously estimated for patients only. This choice was taken to verify that the correlations observed across all subjects were actually supported also by intra-group correlations and were not artifacts emerging from the fact that the clinical scores significantly differ between BPDs and HCs.
Also in this case, the relationship between the network properties and the clinical scores could be investigated only for functional networks, since the SC ones do not present a measure for each subject by construction. Among the FC graphs three cases were examined: the full, the limbic, and the decomposed one at scale 4, which, as it will be shown in section 5, returned the most statistically significant results among the four wavelet decompositions. The occipital lobe was not investigated in this sense because it did not show significant variations between groups, as it is shown in chapter 5.

Chapter 5

Results

5.1 Comparison with the random networks

The results emerging from the comparison of the properties of the subjects' networks with respect to the random ones are reported in this section, for both patients and controls, and for each type of FC (full, limbic, occipital, wavelet-decomposed) and SC (full, limbic, occipital, females only) graphs.
For simplicity, in the following only the images retrieved from the full FC networks are reported, but the results can be perfectly extended also to the other types; in case of exceptions, it is explicitly said. Note that the following figures related to the FC networks were obtained after having averaged the results of the measures across the two groups of patients and controls separately, in order to have a single mean value at every density and for each measure. The same was done also for the corresponding random networks.

Degree and strength distributions
The degree distribution, which is equal for brain and random networks by construction, presents a skewed shape towards larger values at higher densities, whereas it assumes a decaying shape with a strong tail at lower densities, as expected since this indicates the likely presence of hubs in the network [10, 11].
Also the strength distributions of brain networks behave similarly over the entire range of densities; analogously, the ones retrieved from random networks present an almost equal shape, as a direct consequence of the fact that the strength distribution is preserved.
An example of strength distributions in patients and controls, compared to the distributions of the corresponding random networks, can be visualized in Fig. 5.1.

Characteristic path length
As one can see from Fig. 5.2, the characteristic path length decreases very quickly with the density, as expected since adding links on average will reduce the distance among nodes. The absolute values of the characteristic path length in subjects and randoms are almost equal over the range of densities, and differ visibly only at densities below 20%. Therefore, the ratio of the characteristic path length of brain networks with the one of random networks is actually $\sim$1, as needed by the small-worldness requirements.
In the SC network, the characteristic path lengths in subjects, and in particular in patients, tend to be slightly greater than in the corresponding random networks, as

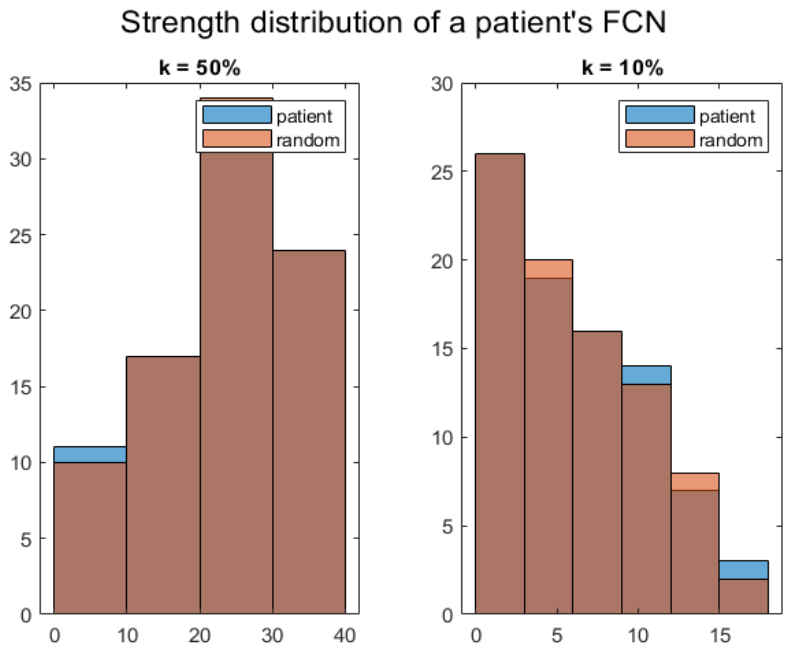

(a) Strength distribution in patients.

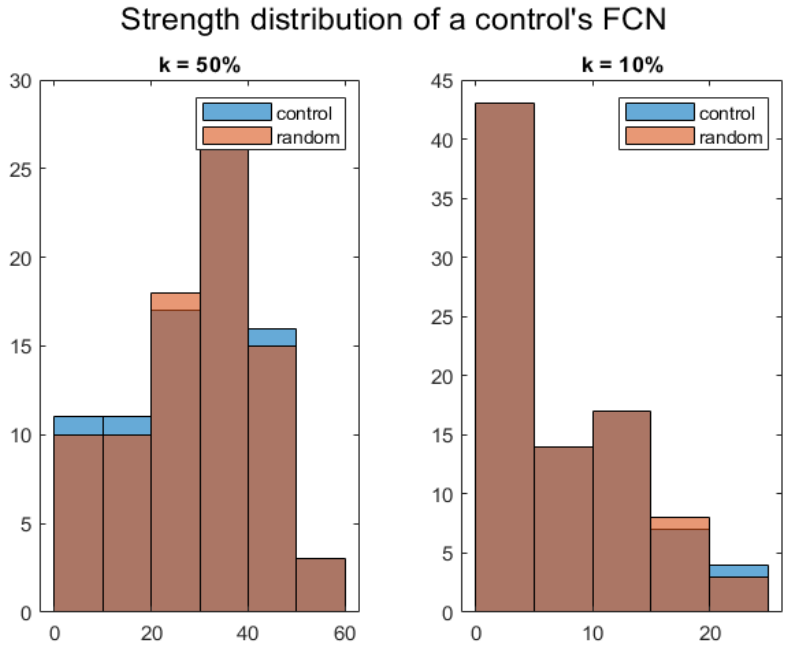

(b) Strength distribution in controls.

Figure 5.1: Histogram of the strength distribution for a single patient and a single control, compared with the results of the corresponding random network at two relevant densities: 50% and 10%. The distributions present shapes coherent with the presence of hubs.

it will be better described in the next section. Nevertheless the results confirm that the normalized values are close to 1 in both BPDs and HCs, making the definition of small-worldness viable.

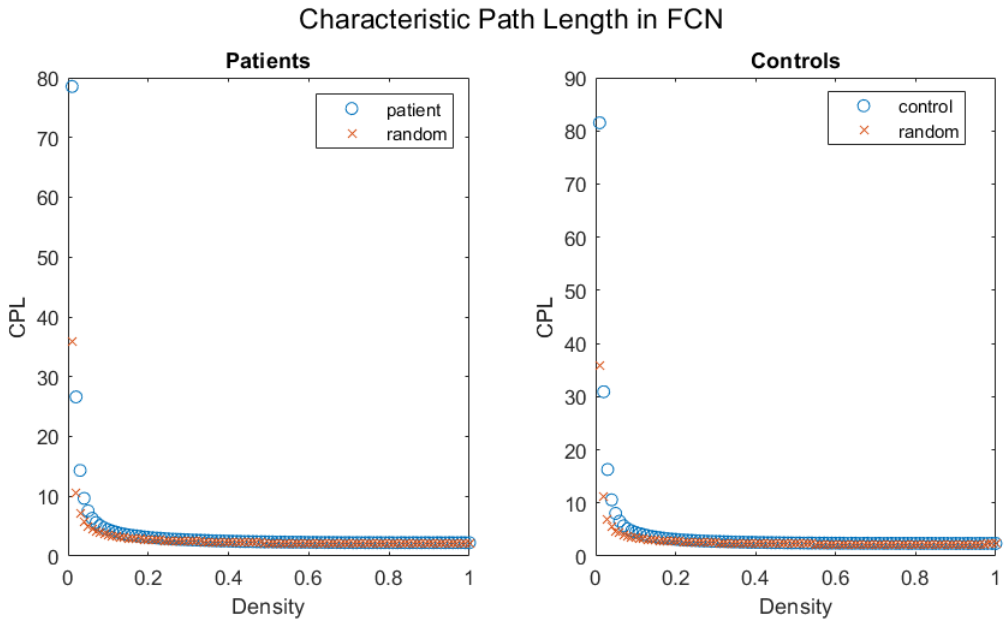

Figure 5.2: Characteristic path length as a function of density, averaged across patients and controls and compared to the results of the corresponding random networks. The quantity in subjects and randoms is almost equal over the entire range.

Global efficiency

The global efficiency, instead, is found higher in random networks, implying that the latter perform better in distant information transfer. The global efficiency continuously increases with the density, because adding links improves the connectivity among nodes in the network, but this occurs with different slopes along the density range: at low densities, adding links corresponds to a huge improvement, since the network is not fully connected yet, but as the edges between nodes start to increase, the advantage related to them decreases, up to a point where it is meaningless. This is characteristic of weighted networks, with respect to the binarized ones, shown later in this chapter, as the links that are progressively added with the increment of density have lower and lower weights, which implies that they contribute less to the network efficiency, as it can be deduced by Eq. 4.2. See Fig. 5.3 as an example.

Average local efficiency

Regarding the average local efficiency, one can clearly see that this quantity is significantly greater in brain networks, up to a density of about 50%, which can vary slightly basing on the type of network analysed. Note also that local efficiency has a maximum in the case of weighted networks: this is explained because the links that are progressively added with density have lower weights by construction, so that they tend not to benefit the nodal information transfer, since the latter is already mediated through more solid links. This can be deduced also by looking at Eq. 4.8. The results are shown in Fig. 5.4.

Average clustering coefficient

Qualitatively the results of the average clustering coefficient are close to those of the local efficiency, as one can see in Fig. 5.5, since they measure similar properties. Nevertheless quantitatively it is possible to observe that the difference between brain and random networks is even amplified. We can conclude that the efficiency of local information transfer

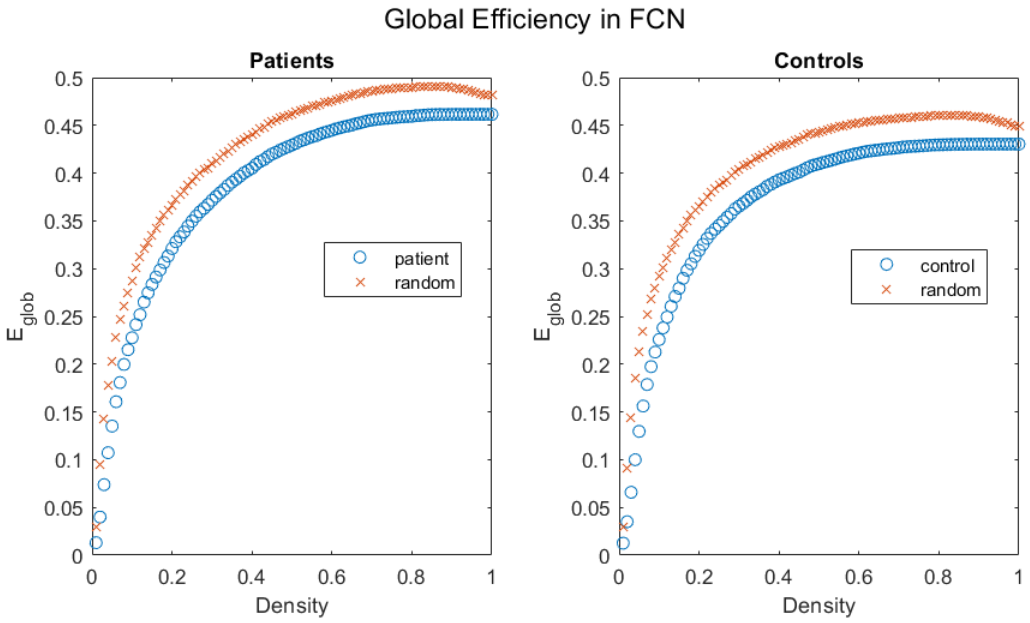

Figure 5.3: Global efficiency as a function of density, averaged across patients and controls and compared to the results of the corresponding random networks. The quantity is greater in randoms over the entire range.

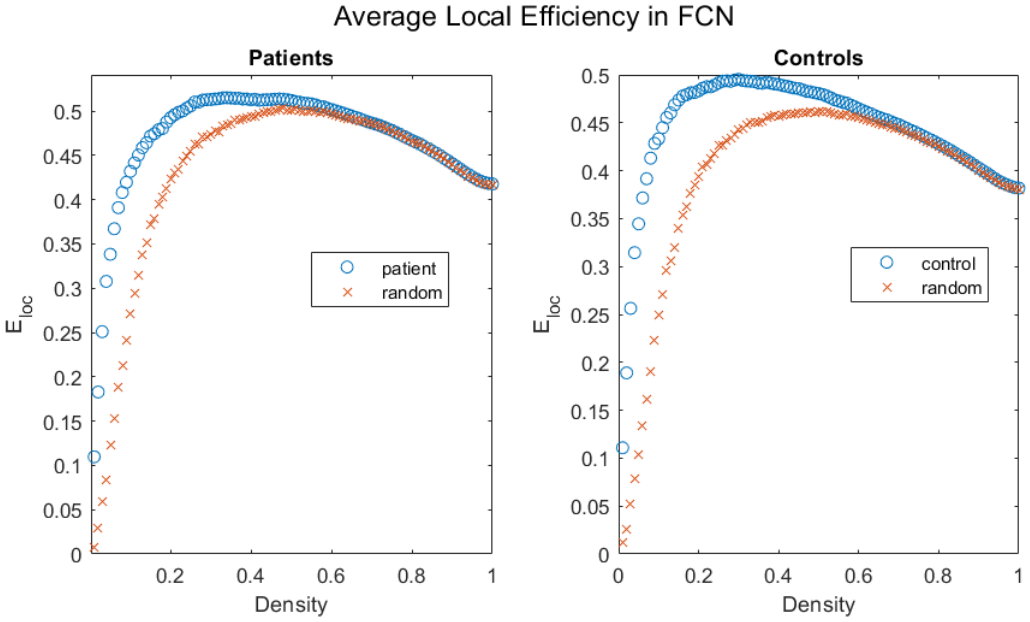

Figure 5.4: Local efficiency as a function of density, averaged across patients and controls and compared to the results of the corresponding random networks. The quantity is greater in subjects up to a density of about 50%.

in brain networks is considerably higher than that of random networks, as expected and required by the small-worldness hypothesis.

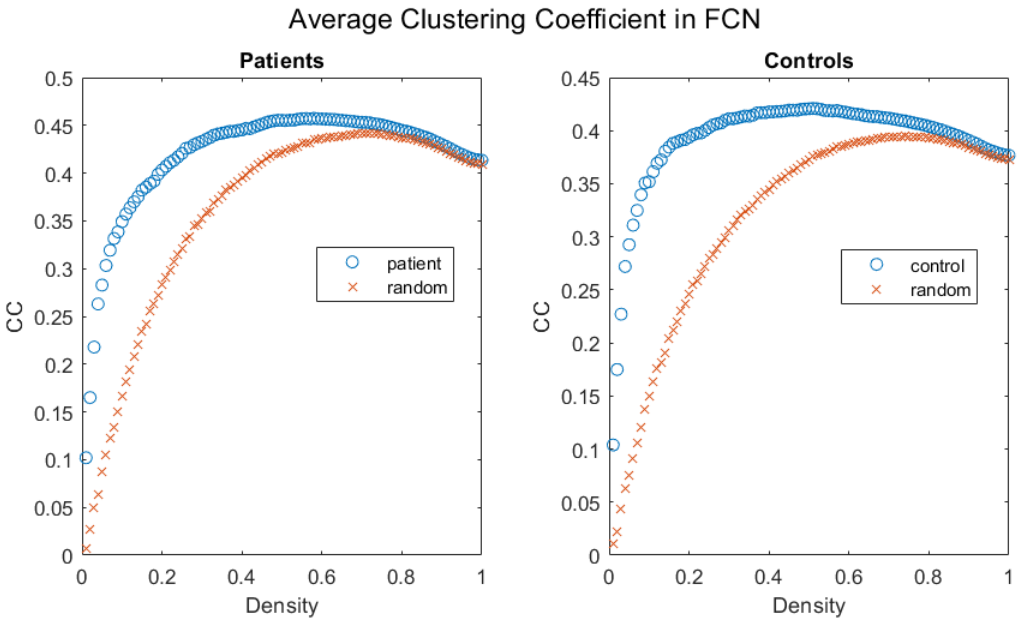

Figure 5.5: Clustering coefficient as a function of density, averaged across patients and controls and compared to the results of the corresponding random networks. The quantity is greater in subjects over the entire range, showing a greater difference with random networks, with respect to local efficiency.

5.2 Comparison between patients and controls

In this section, the differences found between patients and controls are reported, through the use of plots of the topological measures in subjects as a function of density, such as the ones in the previous section, with the inclusion of the graphs of the same quantities normalized by the ones obtained from random networks. In addition, summary tables are used, where the properties that were found to be significantly varied between the two groups are highlighted and collected with their corresponding p-Value. In case of local measures, besides the tables, also graphical representations of the brain, where the significant nodes or links are emphasized, are proposed in some cases to help the visualization.
For simplicity, all the plots are reported only for the full FC and SC networks, and they are shown in additional cases only when behaviors that meaningfully deviate from the represented situations need to be pointed out.

5.2.1 Functional Connectivity networks

Full network

Global properties

Mean Functional Connectivity As one could deduce by looking at the average connectivity matrices shown in Fig. 4.5, the mean connectivity in the full FC matrices of patients and controls differs. This was verified by building a boxplot of the mean connectivity of the matrices of patients and controls separately, which is reported in Fig. 5.6. The quantity results greater in patients.

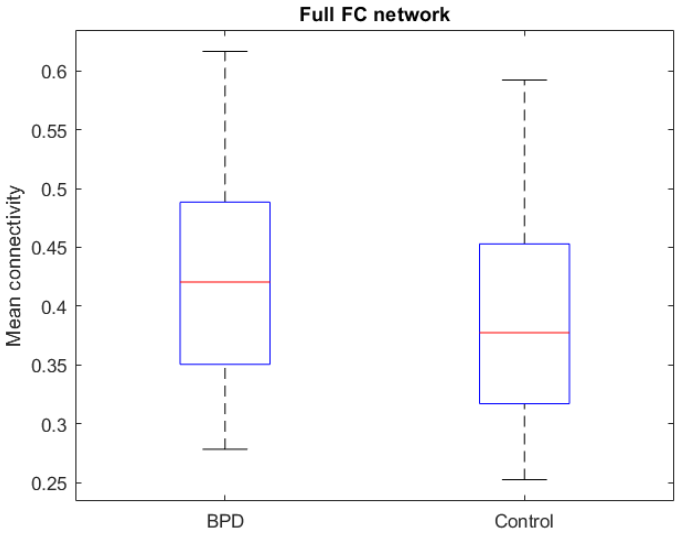

Figure 5.6: Boxplot of the mean connectivity of the full FC matrices in patients and controls. The quantity results higher in BPD subjects.

Characteristic path length The difference in characteristic path length between patients and controls, in absolute values and normalized by the corresponding random results, does not appear to be significant, as shown in Fig. 5.7. Nevertheless, the meaningful result is that the normalized value is close to 1 for both groups in a very wide range, excluding only really low densities. The small-worldness requirements are therefore satisfied beyond a density of ∼5%, where the normalized CPL is ∼1.5.

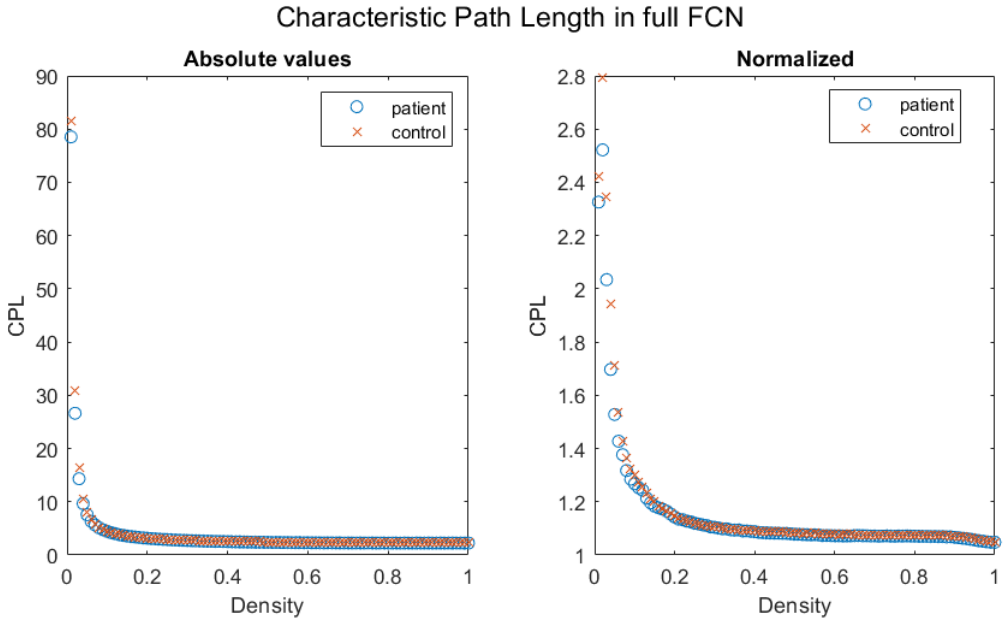

Figure 5.7: Characteristic path length as a function of density in patients and controls, in absolute values and normalized by the result of the corresponding random networks, in the full FC network. The quantity in BPDs and HCs is almost equal over the entire range and the normalized values are close to 1.

Global efficiency BPDs show higher global efficiency than HCs, in absolute values, beyond a density of ∼50%; nevertheless this distinction is canceled when passing to the normalized case. This is actually consistent with the results of the characteristic path length, since they measure the same property, i.e. the efficiency in distant information transfer, where patients and controls were found to be compatible.
Note that the normalized values are always inferior to 1, as it was shown in Fig. 5.3 that random networks dominate on this side.

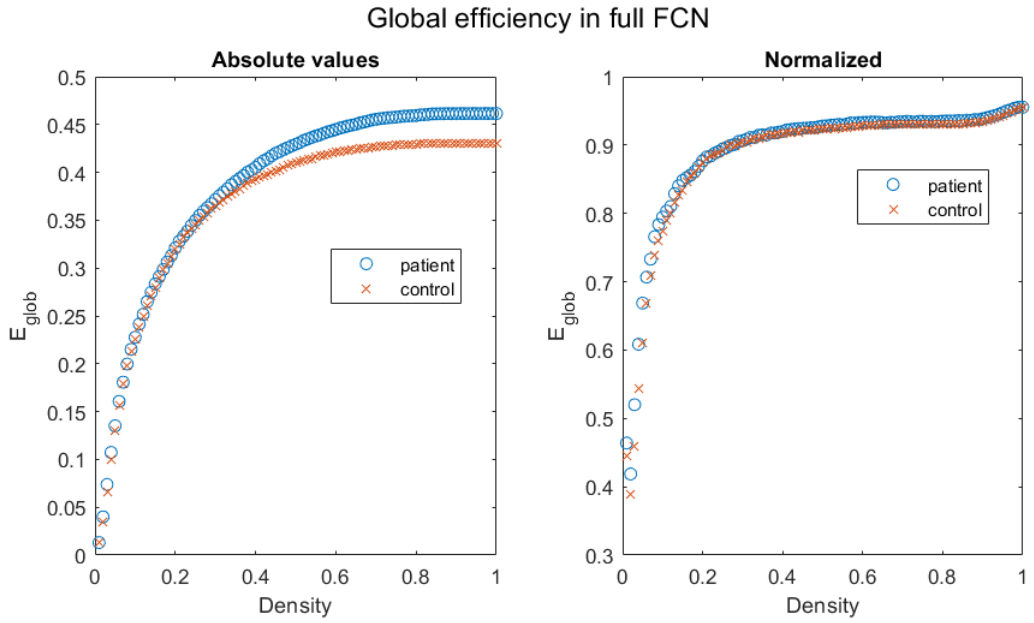

Figure 5.8: Global efficiency as a function of density in patients and controls, in absolute values and normalized by the result of the corresponding random networks, in the full FC network. The quantity is higher in BPDs, in absolute values, beyond a density of 50%, but it is comparable with HCs over the entire range when normalized.

Average local efficiency Also in local efficiency, BPDs appear to be dominating in absolute values, at least at densities higher than ∼20%. Nevertheless, this trend is inverted when the measures are normalized in a range of 5-40%, where controls show higher values, while above ∼50% the ratio is basically 1.
This inversion in trend between absolute and normalized values was actually seen in various averaged local measures across networks, as it will be shown further in the next paragraphs, and it is characteristic of the graphs in this study: this is interpreted as the fact that BPDs' networks have configurations more similar to a random graph than HCs' ones. This aspect is deepened in the discussion in chapter 6.

Average clustering coefficient The comments related to the average local efficiency are extendable to the average clustering coefficient, as the results are very similar, see Fig. 5.10. Nonetheless, it is meaningful to underline that the differences in average CC are amplified with respect to the ones found with average local efficiency.

Small-worldness As the difference of clustering coefficient between brain and random networks is much more significant than that of the characteristic path length, which is almost equal to 1, it is verified that the small-worldness is greater than 1 over the entire

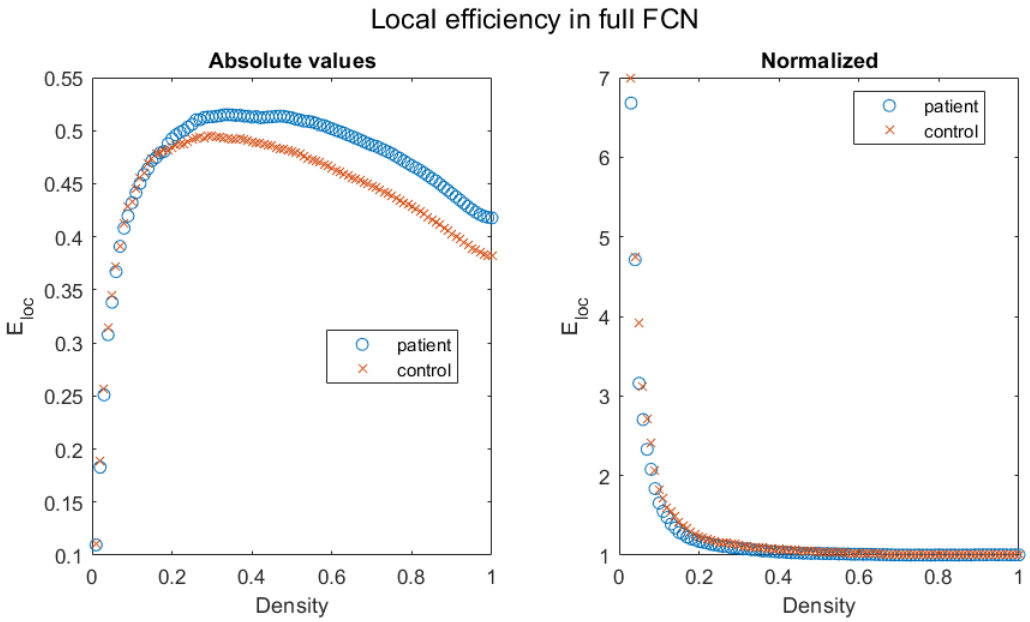

Figure 5.9: Average local efficiency as a function of density in patients and controls, in absolute values and normalized by the result of the corresponding random networks, in the full FC network. The quantity is higher in BPDs, in absolute values, beyond a density of 20%; when normalized, instead, controls dominate in a range of 5-40%.

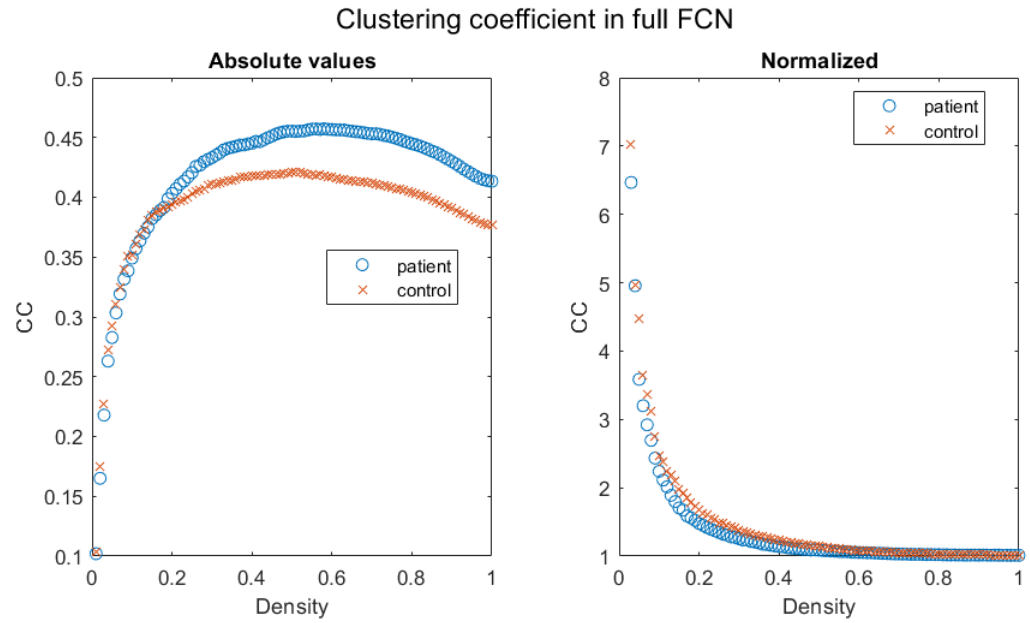

Figure 5.10: Average clustering coefficient as a function of density in patients and controls, in absolute values and normalized by the result of the corresponding random networks, in the full FC network. The quantity is higher in BPDs, in absolute values, beyond a density of 20%; when normalized, controls dominate in a range of 5-50%.

range of densities for both BPDs and HCs. This characteristic property, therefore, is verified in a range of about 5-50% in terms of density, where both the patients ad the controls have values greater than 1 and their characteristic path length is close to 1. Note, moreover, that a difference between the groups is visible up to a density of ∼60%,

as it can be seen from Fig. 5.11.

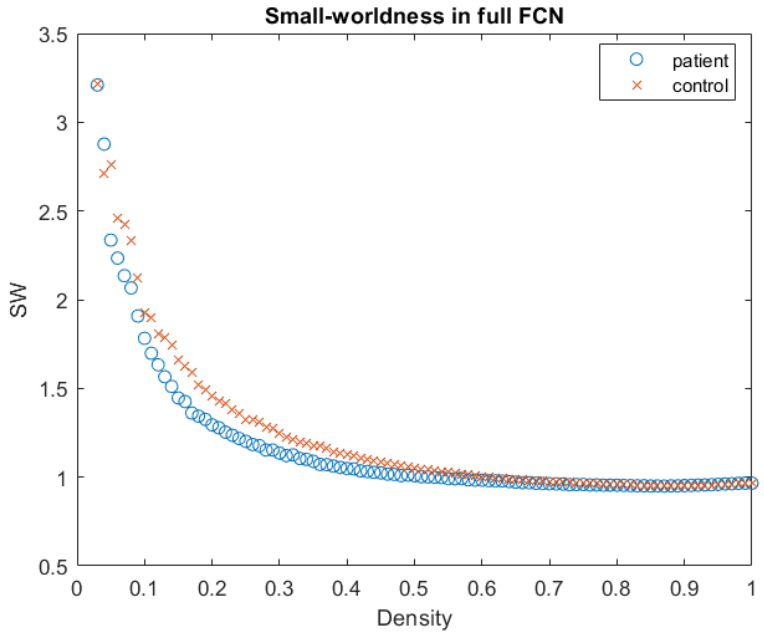

Figure 5.11: Small-worldness as a function of density in patients and controls, in the full FC network. The quantity is greater than 1 for both patients and controls up to a density of 50% and a difference between groups is visible up to 60%.

Largest Connected Component size The trend of the size of the largest connected component as a function of density shows that the 10% of the strongest weights constitute on average a connected component of about 70 elements out of 85, thus including a considerable part of the network. After this level, the increase is slower and the full connection is reached at about 70%, even if at 50% the nodes on average linked are ∼84 already. See Fig. 5.12.

Modularity coefficient The modularity coefficient appears to be significantly greater for controls with respect to patients over the entire range of densities, in particular at intermediate levels, between 20% and 70%. This suggests that a modular structure is present in the HCs in a more definite way. The plot is reported in Fig. 5.13.

Statistical significance The 10000 permutations test operated on the AUCs in the density range 5-50% of the topological measures listed above, after the regression-out of the nuisance variables of sex and age in each subject, returned the p-Values reported in Tab. 5.1.
The only global property that is increased in BPDs is the global efficiency, but not significantly from a statistical point of view, as well as the characteristic path length. On the other hand, the local efficiency, the clustering coefficient, the small-worldness, the LCC size and the modularity coefficient present p-Values inferior to 0.05. In particular, the modularity has an exceptionally low p-Value, as it could be expected because of the considerable difference shown in Fig. 5.13.

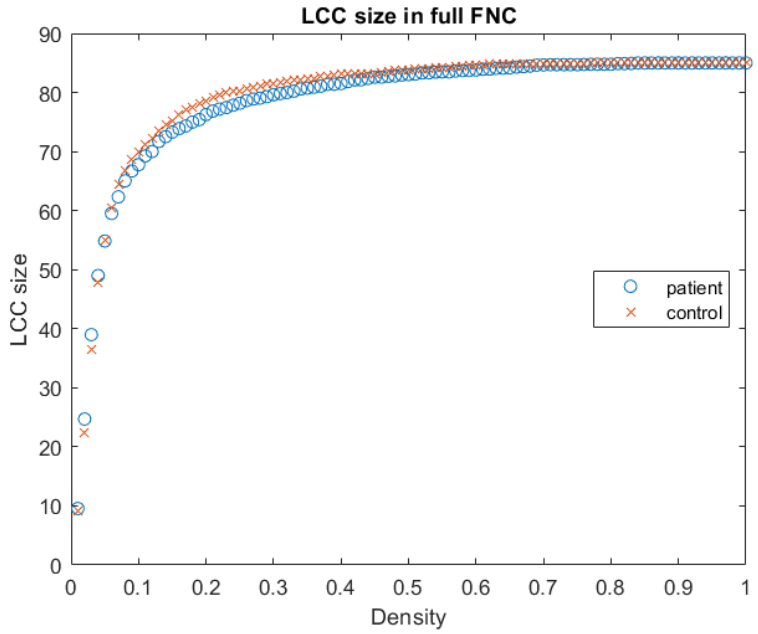

Figure 5.12: Largest connected component size as a function of density in patients and controls, in the full FC network. Full connectivity is reached at 70% of density, but, on average, at 50% 84 out of 85 nodes are already included.

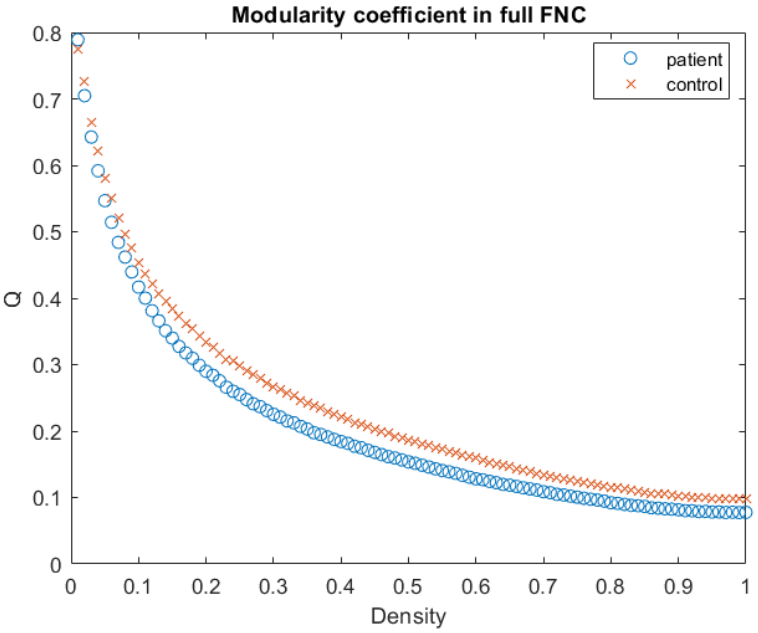

Figure 5.13: Modularity coefficient as a function of density in patients and controls, in the full FC network. The quantity is clearly greater in controls over the entire range of densities, especially in the central ones.

Local properties

In this paragraph, the nodes whose AUC of a measure was found significantly varied between patients and controls are reported. The p-Values and the corresponding nodes names that maintained the statistical significance (adjusted p-Value<0.05) also after the FDR correction are written in bold characters. The arrows indicate whether the quantity

	AUC in BPD	**AUC in HC**	**p-Value**
$CPL \downarrow$	0.5175	0.5230	0.1217
$E_{glob} \uparrow$	0.3944	0.3912	0.1467
$E_{loc} \downarrow$	0.5699	0.6089	**0.0263**
$CC \downarrow$	0.6842	0.7603	**0.0139**
$SW \downarrow$	0.5841	0.6430	**0.0225**
$LCCsize \downarrow$	34.5480	35.3339	**0.0313**
$Q \downarrow$	0.1209	0.1387	**0.0060**

Table 5.1: p-Values of the differences of the AUCs of the global measures between patients and controls. All except for the CPL and the E_{glob} are found lower in patients with p-Value inferior to 0.05.

is lower or higher in BPD patients and the number in brackets tells which system the node belongs to, referring to Tab. A.1: (1) frontal pole, (2) parietal lobe, (3) occipital lobe, (4) temporal lobe, (5) limbic lobe, (6) basal ganglia, (7) cerebellum cortex.

Degree The nodes of the full FC network whose degree is significantly varied are reported in Tab. 5.2. The number of increments is lower than the one of decrements. The system which counts the most variations is the limbic one, which also presents some of the lowest p-Values in the bilateral amygdala and entorhinal cortex, followed by the frontal and the temporal lobes. Nonetheless, none of the p-Values passed the FDR. Note also that there is a certain symmetry between the two hemispheres in terms of nodes significantly varied.

Strength Most of the nodes with statistically varied degree between patients and controls, were found to have different outcomes also in strength, as one may expect, and those that were detected in both measures also show the same characteristic of increment or decrement, as one can see from Tab 5.3 and Fig. 5.14. Nonetheless, there are some divergences between the two cases: firstly, a larger number of nodes are varied in strength; secondly, considerably more nodes have increased AUC rather than decreased. This is explained by the fact that the mean functional connectivity of the patients' networks is on average higher in patients, see Fig. 5.6.
Again, the system which presents the biggest number of varied nodes is the limbic one, which also includes some of the lowest p-Values, in bilateral amygdala and caudal anterior cingulate cortex (differently from the degree). Nevertheless, also in this case none passed the FDR.

Betweenness centrality The outcomes retrieved from betweenness centrality, reported in Tab. 5.4, show a quite different situation from the one depicted by the other centrality measures. First of all, there is not a symmetry between the left and the right hemisphere, as instead could be seen in degree and strength. Secondly, none of the nodes belong to the limbic system, which was instead important in relation to the other centrality measures. Moreover, all the p-Values are quite high, in particular if compared to the ones reported in Tab. 5.2 and 5.3, except for the left superior parietal lobule, which even passed the FDR.

	Degree		
	AUC in BPD	**AUC in HC**	**p-Value**
BS ↑ (0)	2.5302	1.3420	0.0206
L.FP ↓ (1)	3.9043	5.5555	0.0436
L.paraC ↑ (1)	15.6891	14.0691	0.0306
L.parsOR ↓ (1)	4.4741	6.0964	0.0128
R.paraC ↑ (1)	15.8396	13.4107	0.0034
R.parsOP ↑ (1)	9.7696	8.3504	0.0384
R.parsOR ↓ (1)	4.2711	5.6048	0.0283
L.LING ↑ (3)	14.9798	13.0623	0.0350
L.IT ↓ (4)	11.6928	14.1380	0.0226
L.MT ↓ (4)	11.4713	13.6730	0.0156
L.TP ↓ (4)	1.4993	3.3430	0.0086
R.IT ↓ (4)	12.3507	14.9495	0.0162
R.MT ↓ (4)	12.5606	14.4086	0.0321
L.AMY ↓ (5)	2.4009	5.1614	0.0023
L.cAC ↑ (5)	12.3915	10.4007	0.0157
L.ENTH ↓ (5)	1.3291	2.9616	0.0059
L.PC ↑ (5)	17.1104	15.8296	0.0427
R.AMY ↓ (5)	2.5396	5.8114	0.0012
R.HIP ↓ (5)	7.8694	9.8239	0.0233
R.cAC ↑ (5)	12.6691	10.4555	0.0184
R.ENTH ↓ (5)	0.8993	2.6339	0.0093
R.CAU ↑ (6)	12.1698	9.4720	0.0452

Table 5.2: Nodes whose degree presents significant variations (p-Value<0.05) between patients and controls in the full FC network. The numbers within brackets indicate which system the ROI belongs to.

	Strength		
	AUC in BPD	**AUC in HC**	**p-Value**
BS ↑ (0)	1.3928	0.6190	0.0066
L.cMF ↑ (1)	6.7645	5.8699	0.0245
L.FP ↓ (1)	2.2973	3.2173	0.0462
L.paraC ↑ (1)	10.4199	8.9752	0.0269
L.parsOR ↓ (1)	2.7472	3.4891	0.0382
R.paraC ↑ (1)	10.6310	8.6979	0.0058
R.parsOP ↑ (1)	6.4392	5.1486	0.0167
R.rMF ↑ (1)	7.6824	6.5744	0.0434
L.CUN ↑ (3)	9.6438	8.2731	0.0407
L.LING ↑ (3)	10.2928	8.5400	0.0175
L.PERIC ↑ (3)	8.0429	6.5012	0.0281
R.LING ↑ (3)	10.3938	8.7179	0.0294
R.PERIC ↑ (3)	8.1884	6.3101	0.0238
L.TP ↓ (4)	0.9021	1.6884	0.0387
R.TT ↑ (4)	12.2008	10.7483	0.0358
L.ACC ↓ (5)	1.8195	2.5161	0.0480
L.AMY ↓ (5)	1.4025	2.8421	0.0088
L.cAC ↑ (5)	7.9917	6.2734	0.0071
L.ENTH ↓ (5)	0.7011	1.4717	0.0135
L.PC ↑ (5)	11.5092	9.8298	0.0133
R.AMY ↓ (5)	1.5136	3.1690	0.0045
R.cAC ↑ (5)	8.3024	6.2697	0.0083
R.ENTH ↓ (5)	0.5142	1.2813	0.0227
L.THA ↑ (6)	10.0791	7.9934	0.0136
R.CAU ↑ (6)	7.6166	5.3116	0.0161
R.THA ↑ (6)	10.4618	8.1057	0.0165

Table 5.3: Nodes whose strength presents significant variations (p-Value<0.05) between patients and controls in the full FC network.

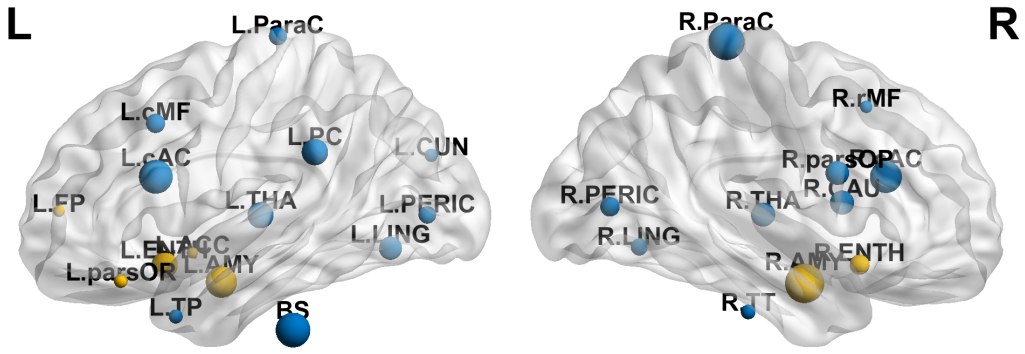

Figure 5.14: Nodes whose strength was found significantly varied between patients and controls in the full FC network. The dimension indicates the statistical significance of the difference and the color tells in which group the quantity was increased. Blue: increased in patients; yellow: increased in controls.

	Betweenness centrality		
	AUC in BPD	**AUC in HC**	**p-Value**
L.parsOP ↑ (1)	28.8889	17.9914	0.0445
R.FP ↓ (1)	9.9411	27.9807	0.0366
R.paraC ↑ (1)	46.5859	20.8254	0.0424
L.SP ↓ (2)	26.3178	63.0211	**0.0003**
L.FG ↓ (3)	51.2752	78.9754	0.0454
R.LOC ↑ (3)	13.4467	4.2889	0.0230
R.MT ↓ (4)	37.6741	61.1396	0.0195
R.THA ↑ (6)	74.4815	39.6550	0.0238
L.CER ↓ (7)	20.0004	38.9254	0.0396

Table 5.4: Nodes whose betweenness centrality presents significant variations (p-Value<0.05) between patients and controls in the full FC network. The left superior parietal lobule passed the FDR.

Participation coefficient The participation coefficient, in Tab. 5.5 and Fig. 5.15, shows asymmetric variations: in the right hemisphere there are more than twice the significant variations found in the left one. Among these variations, few more than the half of the AUC report a decrease in patients. Moreover in the right hemisphere, two regions, the amygdala and the rostral middle frontal gyrus are associated with particularly low p-Values which ensure their significance also after the FDR correction. This information, combined with the results for the right amygdala given by the degree and the strength, suggests that the role of this ROI is significantly reduced in patients in terms of centrality, and in particular in the integration of modules within the network. Other regions, especially in the frontal lobe, display very low p-Values. The same system also includes most of the nodes that were actually found varied, followed by the limbic one.

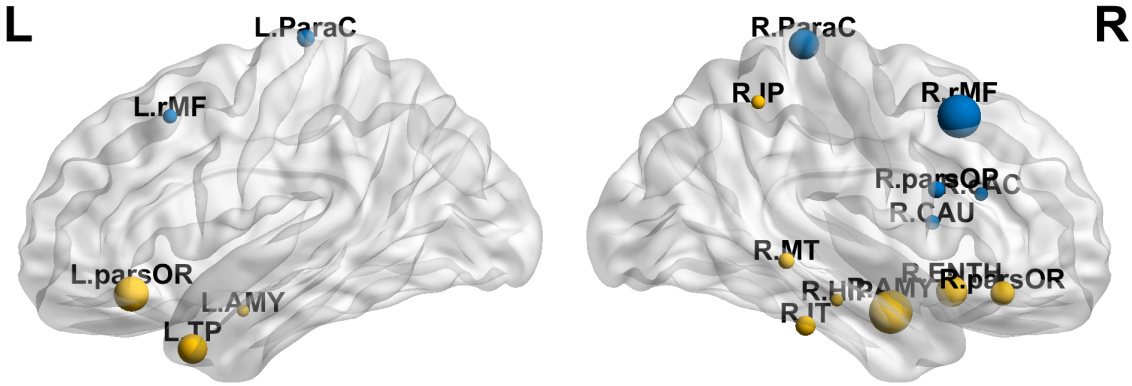

Figure 5.15: Nodes whose participation coefficient was found significantly varied between patients and controls in the full FC network. The dimension indicates the statistical significance of the difference and the color tells in which group the quantity was increased. Blue: increased in patients; yellow: increased in controls.

	Participation coefficient		
	AUC in BPD	**AUC in HC**	**p-Value**
L.paraC ↑ (1)	0.2285	0.1918	0.0230
L.parsOR ↓ (1)	0.0979	0.1525	0.0024
L.rMF ↑ (1)	0.2379	0.2077	0.0362
R.paraC ↑ (1)	0.2262	0.1803	0.0045
R.parsOP ↑ (1)	0.1697	0.1327	0.0254
R.parsOR ↓ (1)	0.0955	0.1400	0.0098
R.rMF ↑ (1)	0.2275	0.1807	**0.0008**
R.IP ↓ (2)	0.2179	0.2437	0.0379
L.TP ↓ (4)	0.0344	0.0781	0.0048
R.IT ↓ (4)	0.2287	0.2532	0.0172
R.MT ↓ (4)	0.2094	0.2388	0.0284
L.AMY ↓ (5)	0.0723	0.1100	0.0466
R.AMY ↓ (5)	0.0708	0.1314	**0.0008**
R.HIP ↓ (5)	0.1403	0.1648	0.0441
R.cAC ↑ (5)	0.1980	0.1606	0.0391
R.ENTH ↓ (5)	0.0201	0.0648	0.0038
R.CAU ↑ (6)	0.2105	0.1600	0.0346

Table 5.5: Nodes whose participation coefficient presents significant variations (p-Value<0.05) between patients and controls in the full FC network. Two regions, the right amygdala and the right rostral middle frontal gyrus passed the FDR.

Within-module strength On the other hand, for the within-module strength, in the left hemisphere twice the significant variations with respect to the right hemisphere were found, balancing the outcomes of the participation coefficient. In this case, a few more than the half of AUCs were demonstrated to be increased in patients, as it can be seen from Tab. 5.6. It is relevant to observe that more than half of the nodes significantly varied belong to the limbic system and some of them even have relatively low p-Values (even if none passed the FDR correction): this, combined with the other findings, is one of the main aspects that legitimates a deepened study of this system.

Local efficiency Also the local efficiency shows a quite asymmetric outcome, where most of the significant variations are in the left hemisphere, as it can be seen from Tab 5.7. This is actually explained by the fact that also the within-module strength displays this type of configuration: the modules are formed by nodes which are strictly interconnected to each other, and therefore it is likely that they are neighbors sharing many links, which translates in efficient local information transfer. The largest part of the variations is constituted by increments in patients, and the nodes are quite distributed among the limbic (the most numerous), the frontal, the parietal and the temporal lobes. The latter includes the nodes with the lowest p-Values, among which the left temporal pole passed the FDR.

Clustering coefficient As expected, the clustering coefficient returns results similar to those of the local efficiency, see Tab. 5.8 and Fig. 5.16. Nevertheless, in this case, there is not an asymmetry towards the left hemisphere, but the two parts are balanced. The

	Within-module strength		
	AUC in BPD	**AUC in HC**	**p-Value**
BS ↑ (0)	0.9268	0.3982	0.0062
L.FP ↓ (1)	1.7008	2.3879	0.0347
L.PCUN ↑ (2)	5.7071	5.0584	0.0220
R.PCUN ↑ (2)	5.4627	4.9073	0.0341
L.CUN ↑ (3)	5.7764	5.0023	0.0422
L.TP ↓ (4)	0.5598	1.1028	0.0216
R.TT ↑ (4)	3.5179	2.5117	0.0282
L.ACC ↓ (5)	1.2842	2.0196	0.0084
L.AMY ↓ (5)	0.9064	1.6712	0.0083
L.cAC ↑ (5)	4.8588	3.9628	0.0132
L.ENTH ↓ (5)	0.4718	1.0939	0.0053
L.INS ↑ (5)	6.1882	5.4625	0.0432
L.iC ↑ (5)	5.4013	4.7695	0.0385
L.MoF ↓ (5)	3.1791	3.7937	0.0364
R.AMY ↓ (5)	1.0474	1.8790	0.0154
R.INS ↑ (5)	6.1369	5.3397	0.0192
R.iC ↑ (5)	5.5464	4.7542	0.0097
R.LoF ↓ (5)	2.7497	3.3267	0.0423
R.MoF ↓ (5)	3.0478	3.7029	0.0332

Table 5.6: Nodes whose within-module strength presents significant variations (p-Value<0.05) between patients and controls in the full FC network.

largest number of significant variations occur, again, in the limbic system, even if with relatively high p-Values: the most significant variations in local efficiency of information transfer evidently arise from the temporal lobe, where three nodes even passed the FDR. This is also supported by the outcomes in terms of local efficiency shown in Tab. 5.7.

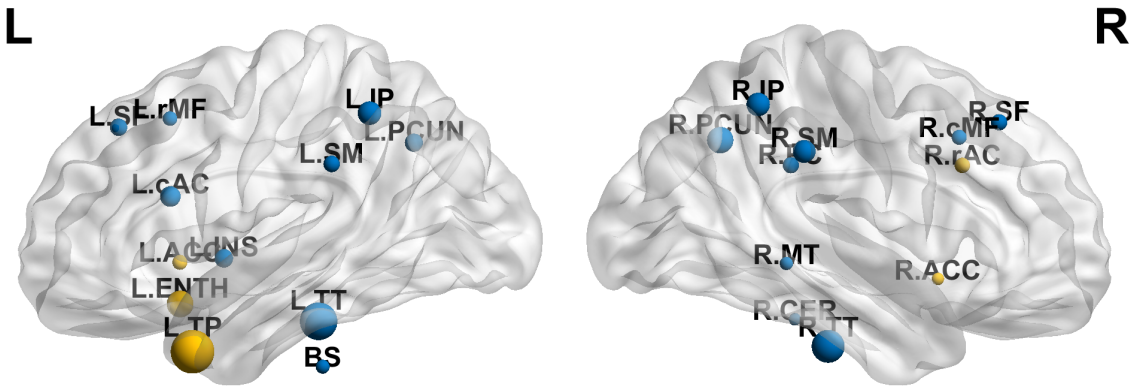

Figure 5.16: Nodes whose clustering coefficient was found significantly varied between patients and controls in the full FC network. The dimension indicates the statistical significance of the difference and the color tells in which group the quantity was increased. Blue: increased in patients; yellow: increased in controls.

	Local efficiency		
	AUC in BPD	**AUC in HC**	**p-Value**
BS ↑ (0)	0.1074	0.0709	0.0372
L.MF ↑ (1)	0.2316	0.2177	0.0377
L.SF ↑ (1)	0.2369	0.2192	0.0384
R.cMF ↑ (1)	0.2569	0.2368	0.0146
R.SF ↑ (1)	0.2360	0.2199	0.0259
L.IP ↑ (2)	0.2546	0.2328	0.0071
L.PCUN ↑ (2)	0.2705	0.2495	0.0189
L.SM ↑ (2)	0.2557	0.2352	0.0280
R.IP ↑ (2)	0.2558	0.2333	0.0102
R.PCUN ↑ (2)	0.2741	0.2483	0.0072
R.SM ↑ (2)	0.2710	0.2501	0.0194
L.TP ↓ (4)	0.0501	0.1189	**0.0003**
L.TT ↑ (4)	0.2469	0.1749	0.0022
R.TT ↑ (4)	0.2411	0.1748	0.0020
L.ACC ↓ (5)	0.1544	0.1952	0.0299
L.cAC ↑ (5)	0.2596	0.2289	0.0052
L.ENTH ↓ (5)	0.0553	0.1086	0.0038
L.INS ↑ (5)	0.2475	0.2277	0.0238
L.rAC ↓ (5)	0.2046	0.2431	0.0413
R.PC ↑ (5)	0.2527	0.2341	0.0274
R.rAC ↓ (5)	0.1926	0.2373	0.0415

Table 5.7: Nodes whose local efficiency presents significant variations (p-Value<0.05) between patients and controls in the full FC network. The left temporal pole passed the FDR.

	Clustering coefficient		
	AUC in BPD	**AUC in HC**	**p-Value**
BS ↑ (0)	0.1005	0.0660	0.0374
L.rMF ↑ (1)	0.1814	0.1679	0.0337
L.SF ↑ (1)	0.1786	0.1593	0.0214
R.cMF ↑ (1)	0.2181	0.1979	0.0315
R.SF ↑ (1)	0.1740	0.1588	0.0254
L.IP ↑ (2)	0.2023	0.1794	0.0078
L.PCUN ↑ (2)	0.2263	0.2018	0.0188
L.SM ↑ (2)	0.2086	0.1849	0.0248
R.IP ↑ (2)	0.2046	0.1799	0.0080
R.PCUN ↑ (2)	0.2329	0.2004	0.0049
R.SM ↑ (2)	0.2357	0.2094	0.0087
L.TP ↓ (4)	0.0444	0.1056	**0.0003**
L.TT ↑ (4)	0.2271	0.1558	**0.0008**
R.MT ↑ (4)	0.1966	0.1789	0.0418
R.TT ↑ (4)	0.2235	0.1597	**0.0017**
L.ACC ↓ (5)	0.1390	0.1755	0.0316
L.cAC ↑ (5)	0.2252	0.1965	0.0128
L.ENTH ↓ (5)	0.0505	0.0964	0.0046
L.INS ↑ (5)	0.1974	0.1744	0.0176
R.ACC ↓ (5)	0.1429	0.1742	0.0481
R.PC ↑ (5)	0.2024	0.1826	0.0261
R.rAC ↓ (5)	0.1776	0.2232	0.0294
R.CER ↑ (7)	0.1869	0.1706	0.0483

Table 5.8: Nodes whose clustering coefficient presents significant variations (p-Value<0.05) between patients and controls in the full FC network. The left temporal pole and the bilateral transverse temporal gyrus passed the FDR.

Hubs

The hubs, separated into integrating and segregating basing on the participation coefficient and the within-module strength, as explained in Section 4.5.2, are reported in Tab. 5.9 and Fig. 5.17. Recall that nodes which favour intermodular connectivity are called 'integrating', whereas 'segregating' are those that cover a central role within the module where they are assigned.

The hub nodes are quite symmetric between the left and the right hemisphere, even if their role may change in few cases. Regarding the difference between patients and controls, there is not a specific system where they mostly occur, but they are rather distributed among all the lobes. Note, moreover, that there is consistency between the differences in terms of hubs between BPDs and HCs and those in terms of participation coefficient and within-module strength: nodes with an integrating role in one group but not in the other also show a significantly increased participation coefficient, and the analogous happens for the segregating ones.

Composition of modules

The composition of modules is clearly important in interpreting the results of the mea-

	Left hemisphere		Right hemisphere	
	BPD	**HC**	**BPD**	**HC**
paraC (1)	Both	Segregating	Segregating	Segregating
PreCG (1)	Segregating	Segregating	Segregating	Segregating
rMF (1)	Integrating	-	Integrating	-
SF (1)	Integrating	Integrating	Integrating	Both
IP (2)	-	Integrating	-	Integrating
PostCG (2)	Segregating	Segregating	Segregating	Segregating
PCUN (2)	Segregating	-	-	-
SP (2)	Integrating	Both	Segregating	Segregating
CUN (3)	Segregating	-	Segregating	-
FG (3)	-	Both	-	Segregating
LING (3)	Segregating	Segregating	Segregating	Segregating
IT (4)	Integrating	Integrating	-	Integrating
MT (4)	-	-	-	Integrating
ST (4)	-	Integrating	-	-
INS (5)	Segregating	Segregating	Segregating	-
LoF (5)	-	Integrating	-	-
PC (5)	Integrating	Integrating	Integrating	Integrating
THA (6)	-	-	Integrating	-
CER (7)	-	-	-	Integrating

Table 5.9: Comparison of hub nodes in patients and controls in the full FC network: integrating are those nodes that have strong intermodular connections, segregating are those that have a central role within their module.

sures related to the modularity and the hubs. The configuration of communities obviously changes basing on the density of evaluation: at high values, in this case, about three subnetworks were found by the algorithm; this number increases at low densities, especially because of the removal of weak links and the rise of disconnected components, so that at k$\sim$10%, even eight modules can be found. Moreover, it must be considered that there can be (and actually are) differences also between BPDs and HCs at a fixed density, which can complicate the interpretation.
Clarified this, there were some regular aspects that repeated across the range of densities, except for very low values: the occipital and the limbic systems were often organized almost completely into two different modules, even if shared with few nodes from other lobes. This is another aspect that supports a separate comparison of the limbic and the occipital networks.
The composition of the modules at a density of 32% (chosen because it is in the middle of the density range studied and it is around the maximum of the local efficiency in absolute values for both patients and controls) in a BPD and a HC subjects is reported in the Appendix, in Tab. A.2 and A.3, as an example.

NBS analysis

Through the NBS analysis, significant and structured changes emerged only when looking for increased functional connectivity in patients with respect to controls, and not vice versa, which is consistent with the fact that the mean FC is greater for the firsts (Fig.

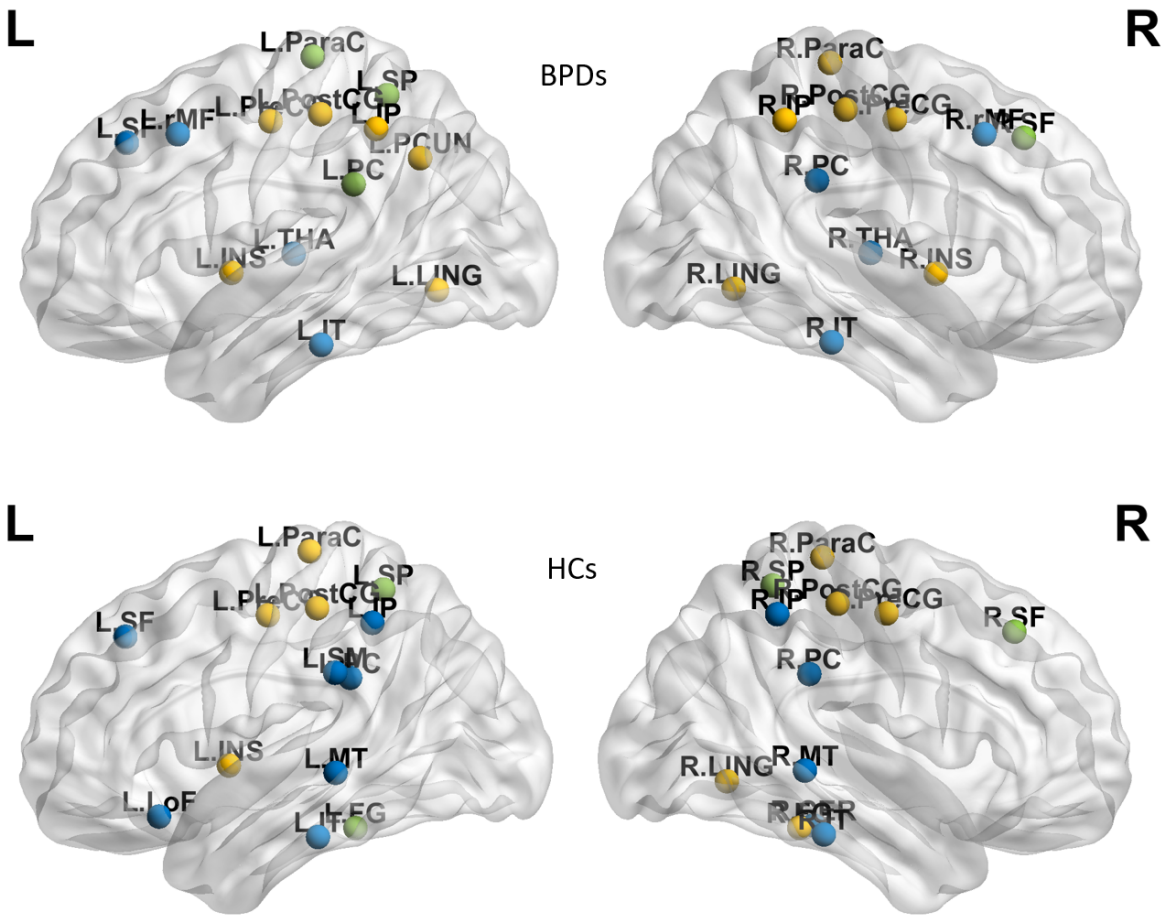

Figure 5.17: Hub nodes in patients and controls in the full FC network, where the color defines the role of the hub. Blue: integrating; yellow: segregating; green: both.

5.6).
The method was applied over a set of primary thresholds for the mass univariate test, from 2.05 to 4.5. Some of the outcomes of these tests are collected in Tab. 5.10, where the number of connected links and nodes is reported, along with the final p-Value of the analysis. It is possible to see that there is a local minimum in final p-Value using a threshold of 2.9 and a global minimum by thresholding at 4.0.

primary threshold	**# nodes**	**# links**	**p-Value**
2.05	no significant results		
2.5	63	115	0.0395
2.75	46	77	0.0307
2.9	36	52	0.0299
3.0	28	35	0.0304
3.25	6	10	0.0364
3.5	6	8	0.0209
4.0	5	6	0.0062
4.5	no significant results		

Table 5.10: Set of tests of the NBS analysis with different primary thresholds and the corresponding final p-Value, with the subnetwork characteristics.

The composition of the subnetwork at 2.9 consists of regions from all the different systems, not symmetric between the left and right hemisphere: Fig. 5.18, where the subnetwork and the corresponding boxplot of mean connectivity are reported, also show that the altered edges mainly connect regions belonging to different systems.
The one at 4.0, on the other hand, shows a quite symmetric structure, including the bilateral caudal anterior cingulate cortex, as it can be seen in Fig. 5.19, where it is particularly interesting to see the big difference in the mean connectivity given in the boxplot and the presence of two nodes of the limbic system. Nevertheless, note that this subnetwork is only composed by 5 nodes and 6 links, thus it is very selective with respect to the full FC network.

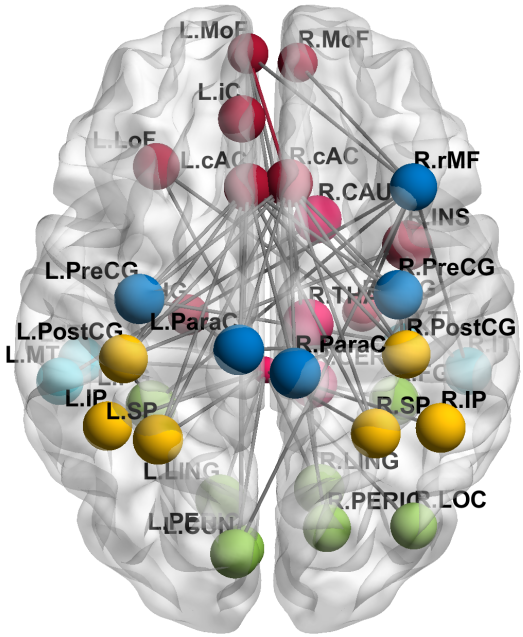

(a) Subnetwork of significantly altered connectivity, where colors represent the system the nodes belong to. Dark blue: frontal lobe; yellow: parietal lobe; green: occipital lobe; light blue: temporal lobe; dark red: limbic lobe; light red: basal ganglia, cerebellum and brain stem. Gray edges indicate connections between different modules.

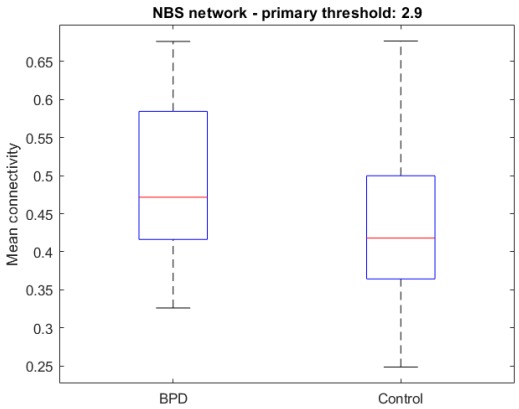

(b) Boxplot of the mean connectivity in the subnetwork, compared between BPDs and HCs

Figure 5.18: Subnetwork of significantly altered functional connectivity in the full FC network, as identified through NBS at primary threshold 2.9, with the corresponding boxplot of mean connectivity.

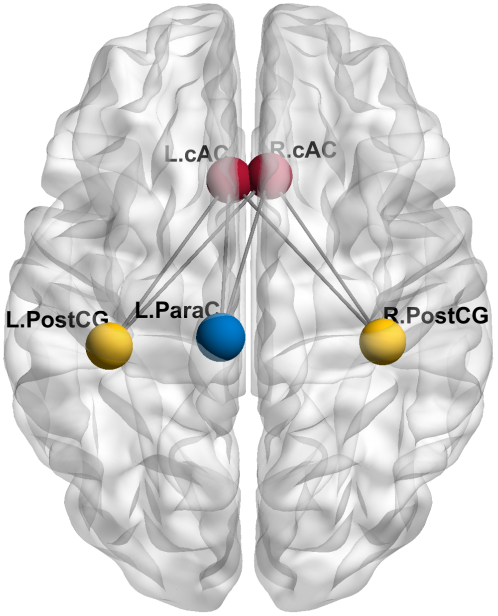

(a) Subnetwork of significantly altered connectivity, where colors represent the system assignment. Dark blue: frontal lobe; yellow: parietal lobe; dark red: limbic lobe. Gray edges indicate connections between different modules.

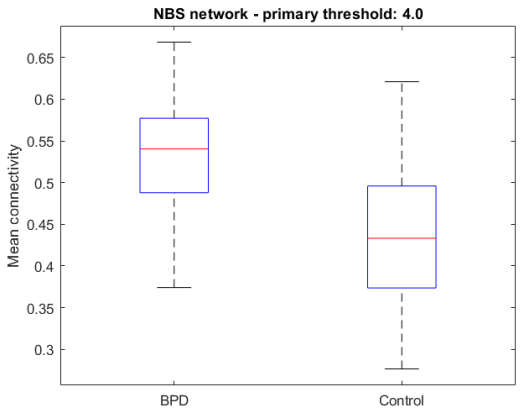

(b) Boxplot of the mean connectivity in the subnetwork, compared between BPDs and HCs

Figure 5.19: Subnetwork of significantly altered functional connectivity in the full FC network, as identified through NBS at primary threshold 4.0, with the corresponding boxplot of mean connectivity.

Binarized networks

As mentioned in section 4.4.1, the main purpose of the binarized networks was to verify the trends observed in the weighted ones and to check if relevant differences would emerge between the two; therefore they were evaluated only at a global level.
The normalized results indeed provided similar outcomes to those reported in the previous subsection: the same topological properties as the ones collected in Tab. 5.1 were significantly increased in controls also within the binarized graphs. On the other hand, the absolute values were not as distinct between patients and controls as it was observed in the weighted case and, in particular, the trend inversion was not that much clearly visible, if even existing. This means that such behavior must be related to weights of the links among the nodes, rather than their presence. This aspect will be deepened in the discussion in chapter 6.
Specifically, in Fig. 5.20, 5.21 and 5.22, the global efficiency, the clustering coefficient and the small-worldness of the binarized networks, taken as an example of the results, are plotted against the density. From the image of global efficiency, it is interesting to note that the quantity continuously increase with the density, oppositely to what happened in the weighted case: this is because the links that are added have all the same weights as the ones already present at lower densities, so that it is very likely that they provide a significant contribution in the increment of the efficiency in distant information transfer.
In terms of comparison between patients and controls, the global efficiency appears to be greater in the latter both in absolute and normalized values, in contrast to what emerged from the weighted case, but the difference is still not significant.

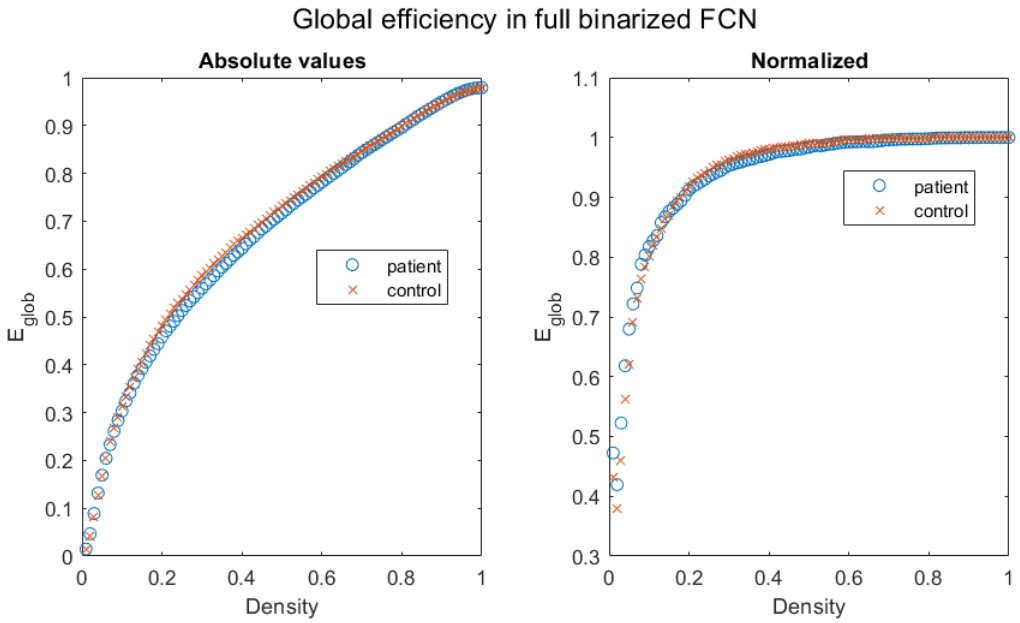

Figure 5.20: Global efficiency as a function of density in patients and controls, in absolute values and normalized by the result of the corresponding random networks, in the full binarized FC network. The quantity is slightly greater in controls in both cases, but the difference is not significant.

Regarding the clustering coefficient, a similar comment can be made on its behavior as a function of density: its constant increment is again due to the fact that all the newly added links have the same weight.

In this case, the absolute values in patients and controls intersect, so that it is not clear of the trend inversion observed in weighted networks is supported; nonetheless, the normalized values confirm that the difference is in favor of HCs.
Also the small-worldness supports the increment in controls that was identified within the weighted full FC network, ensuring that the properties that emerged under that condition are verified also in binarized networks, at least when they are normalized.

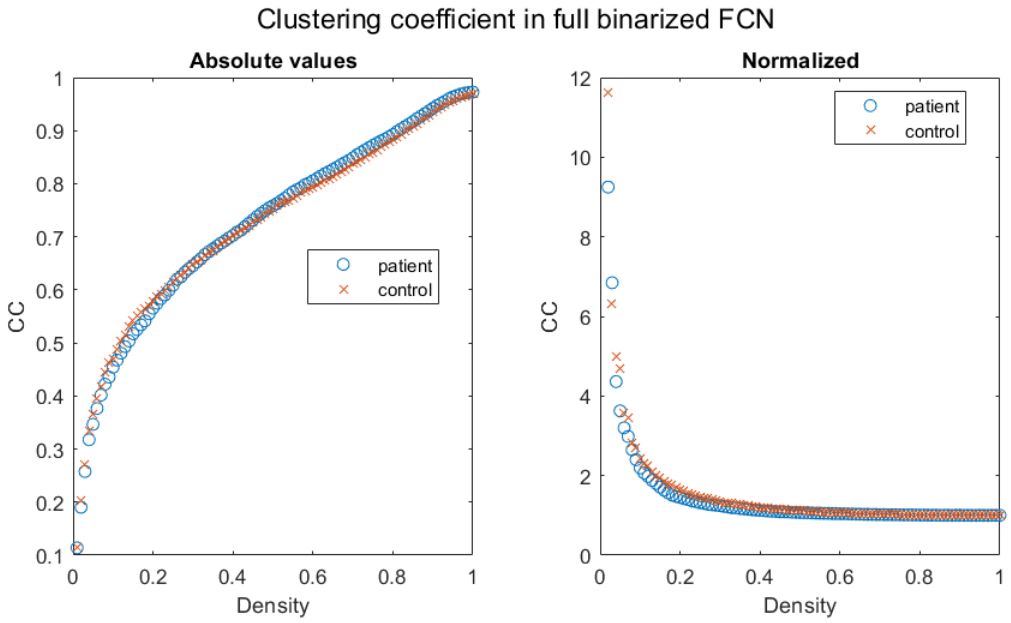

Figure 5.21: Average clustering coefficient as a function of density in patients and controls, in absolute values and normalized by the result of the corresponding random networks, in the full binarized FC network. The normalized quantity is greater in controls up to a density of ∼50%.

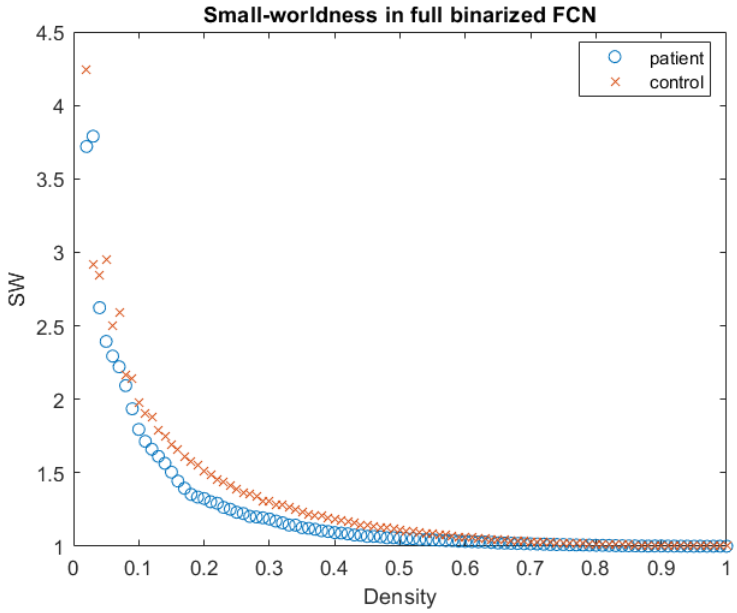

Figure 5.22: Small-worldness as a function of density in patients and controls, in the full binarized FC network. The quantity is greater in controls up to a density of ∼50%.

Limbic and occipital subnetworks

Global properties

At global level, in the limbic and the occipital subnetworks, the only (slightly) statistically significant variation found regarded the global efficiency in the occipital lobe, as it can be seen from Tab. 5.11 and 5.12, where the p-Values of the differences of each measure between patients and controls is reported. Besides the configuration of the network themselves, the absence of global variations might be related to the small dimensions of the subnetworks, which affect the emerging of such outcomes. Even if the results are not significant, it is interesting to observe that increments or decrements of the properties reported in the tables reflect what was obtained with full network (Tab. 5.1), except for the LCC size in the occipital system.

	AUC in BPD	**AUC in HC**	**p-Value**
$CPL \downarrow$	0.3313	0.3338	0.2502
$E_{glob} \uparrow$	0.2724	0.2707	0.2854
$E_{loc} \downarrow$	0.3850	0.3998	0.1725
$CC \downarrow$	0.4621	0.4889	0.1495
$SW \downarrow$	0.4171	0.4377	0.1922
$LCCsize \downarrow$	6.7311	6.8329	0.0877

Table 5.11: p-Values of the differences of the AUCs of the global measures between patients and controls within the limbic FC subnetworks. None of the differences is statistically significant.

	AUC in BPD	**AUC in HC**	**p-Value**
$CPL \downarrow$	0.2087	0.2138	0.0503
$E_{glob} \uparrow$	0.1928	0.1889	0.0425
$E_{loc} \downarrow$	0.2313	0.2467	0.2349
$CC \downarrow$	0.2479	0.2761	0.1781
$SW \downarrow$	0.2367	0.2572	0.2988
$LCCsize \downarrow$	1.9435	1.9350	0.2916

Table 5.12: p-Values of the differences of the AUCs of the global measures between patients and controls within the occipital FC subnetworks. The global efficiency, increased in BPDs is the only statistically significant result.

Moreover, it is relevant to note that the mean functional connectivity of the occipital lobe is higher than the one of the limbic system, as it is possible to see from Fig. 5.23 and looking back at the average FC matrices in Fig. 4.5. Nonetheless the difference in these terms between BPDs and HCs does not deviate much from what was observed in the full FC network.

Local properties

Regarding local measures, an evident difference between the occipital and the limbic subnetworks emerged. In particular, while the first showed only one significant difference between BPDs and HCs in clustering coefficient, see Tab. 5.13, the second presented many variations, especially within centrality measures, associated with very low p-Values.

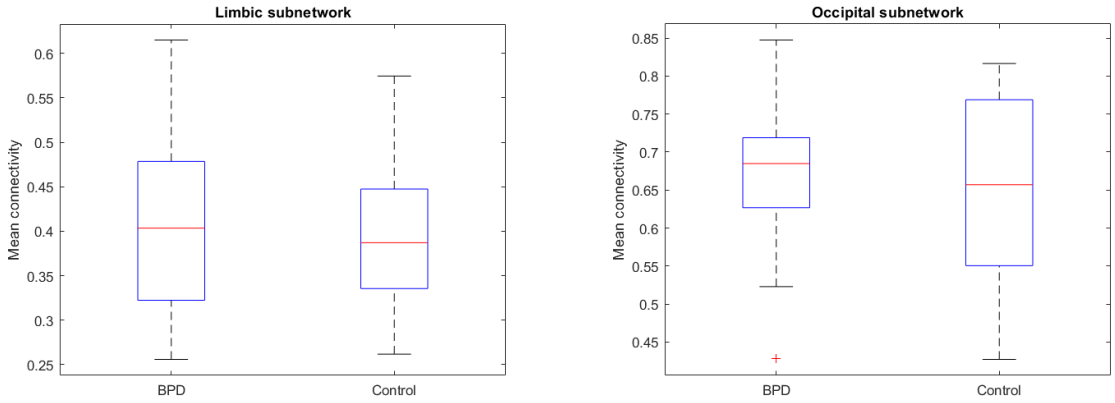

(a) Boxplot of the mean connectivity in the limbic FC subnetwork, compared between BPDs and HCs.

(b) Boxplot of the mean connectivity in the occipital FC subnetwork, compared between BPDs and HCs.

Figure 5.23: Boxplot of the mean connectivity in the limbic and in the occipital FC subnetworks, compared between patients and controls.

	Clustering coefficient - occipital FCN		
	AUC in BPD	**AUC in HC**	**p-Value**
R.LING ↓	0.0764	0.0926	0.0361

Table 5.13: Nodes within the occipital FC subnetwork whose clustering coefficient presents significant variations (p-Value<0.05) between patients and controls.

In particular, the results of degree and strength are reported in Tab. 5.14 and Tab. 5.15. The results are quite symmetric between the two measures (only the right isthmus of cingulate gyrus is added in the strength variations) and, within each quantity, also between the left and right hemispheres and the increment or decrement of the property. The most relevant result is that the p-Values associated to the same six regions for both the measures passed the FDR: the right amygdala (which often emerged also from the outcomes of the full FC network), the bilateral caudal anterior cingulate, the left entorhinal and the bilateral posterior cingulate cortices. Moreover, some nodes that did not exhibit significant variations in centrality measures within the full network were found to be modified in the limbic one: the bilateral medial orbitofrontal cortex, the right isthmus of cingulate gyrus and the right posterior cingulate cortex. This information suggests that such regions present differences only in connections within the subnetwork. The last centrality measure of betweenness centrality reported only the right amygdala as significantly varied, again showing quite different results with respect to degree and strength.

Regarding the measures of local efficiency and clustering coefficient, collected in Tab. 5.17 and Tab. 5.18, also in this case the significant variations found in the limbic subnetwork quantitatively overcame those of the occipital. Nevertheless, note that none of the regions passed the FDR. Moreover, the symmetry between measures and hemispheres that was found in centrality is not as respected in the two efficiency measures, where only the left insular and the rostral anterior cingulate cortices are repeated in both, the local efficiency and the clustering coefficient.
An interesting outcome is the presence of the bilateral hippocampus, which together

	Degree - limbic FCN		
	AUC in BPD	**AUC in HC**	**p-Value**
L.AMY ↓	1.3952	1.9863	0.0160
L.cAC ↑	2.4370	2.0441	**0.0073**
L.ENTH ↓	0.6102	1.1936	**0.0035**
L.MoF ↓	3.1152	3.4014	0.0441
L.PC ↑	3.4343	2.9559	**0.0039**
R.AMY ↓	1.3896	2.1334	**0.0030**
R.cAC ↑	2.5737	2.1368	**0.0078**
R.MoF ↓	2.9663	3.3370	0.0190
R.PC ↑	3.2370	2.7684	**0.0022**

Table 5.14: Nodes within the limbic FC subnetwork whose degree presents significant variations (p-Value<0.05) between patients and controls. A total of six nodes also passed the FDR.

	Strength - limbic FCN		
	AUC in BPD	**AUC in HC**	**p-Value**
L.AMY ↓	0.7978	1.1245	0.0356
L.cAC ↑	1.6247	1.3350	**0.0074**
L.ENTH ↓	0.3295	0.6098	**0.0086**
L.MoF ↓	2.0001	2.2080	0.0286
L.PC ↑	2.2830	1.9028	**0.0042**
R.AMY ↓	0.7973	1.1890	**0.0082**
R.cAC ↑	1.7117	1.3841	**0.0069**
R.iC ↑	1.9904	1.7890	0.0482
R.MoF ↓	1.9218	2.1706	0.0167
R.PC ↑	2.1415	1.7939	**0.0041**

Table 5.15: Nodes within the limbic FC subnetwork whose strength presents significant variations (p-Value<0.05) between patients and controls. A total of six nodes also passed the FDR.

	Betweenness centrality - limbic FCN		
	AUC in BPD	**AUC in HC**	**p-Value**
R.AMY ↓	2.2304	5.4204	0.0175

Table 5.16: Nodes within the limbic FC subnetwork whose betweenness centrality presents significant variations (p-Value<0.05) between patients and controls.

with the left rostral anterior cingulate and the right insular cortices did not appear in the full network.

Considering all the outcomes described in this paragraph, it is possible to state that, at least at local level, the limbic system is significantly more varied in BPD patients with respect to healthy controls than the occipital one.

	Local efficiency - limbic FCN		
	AUC in BPD	**AUC in HC**	**p-Value**
L.cAC ↑	0.1879	0.1739	0.0440
L.ENTH ↓	0.0635	0.0872	0.0448
L.INS ↑	0.1765	0.1575	0.0064
LrAC ↓	0.1481	0.1720	0.0286
R.INS ↑	0.1763	0.1619	0.0365
R.PC ↑	0.1693	0.1556	0.0414
R.rAC ↓	0.1421	0.1701	0.0409

Table 5.17: Nodes within the limbic FC subnetwork whose local efficiency presents significant variations (p-Value<0.05) between patients and controls.

	Clustering coefficient - limbic FCN		
	AUC in BPD	**AUC in HC**	**p-Value**
L.HIP ↑	0.1200	0.1047	0.0405
L.INS ↑	0.1582	0.1374	0.0065
L.rAC ↓	0.1303	0.1540	0.0380
R.HIP ↑	0.1209	0.1053	0.0301
R.rAC ↓	0.1321	0.1610	0.0334

Table 5.18: Nodes within the limbic FC subnetwork whose clustering coefficient presents significant variations (p-Value<0.05) between patients and controls.

Wavelet decomposition

Global properties

The networks obtained from the wavelet decomposition provided different outcomes basing on the frequency range of the subdivisions. The most evident deviation is between the network related to scale 1 (0.08-0.17 Hz) and the other three graphs: the first, in fact, returns opposite outcomes in the comparison between patients and controls with respect to scales 2 (0.04-0.08 Hz), 3 (0.02-0.04 Hz) and 4 (0.01-0.02 Hz). This can be deduced already from the boxplots of the mean connectivity in Fig. 5.24, where it is possible to observe that the highest frequency range is the only one where the MC of BPDs is inferior, on average, to that of HCs. From the boxplots, note also that the the mean connectivity increases as the frequency decreases and the difference between patients and controls is more evident in scales 3 (where it is maximum) and 4.

These characteristics were also revealed in all the other global measures carried out: as an example, the evolution of small-worldness with the density is shown in Fig. 5.25 for all the four scales. It can be observed that only in scale 1 the quantity is greater in patients with respect to controls, inverting the trend that was detected in the full FC network (Fig. 5.11) and also in the other three scales in which the signal was decomposed. Moreover, it is interesting to note that the difference between patients and controls increases as the frequency range decreases, so that the largest one is found always in scale 4. Thus, in general, scale 1 presents inverted trends with respect to the results of the full FCN, which are instead verified at lower frequency ranges in the decomposed networks, and scale 4 always tend to show the biggest difference between BPDs and HCs. The only

exceptions are the global efficiency and the characteristic path length, where largest difference is observed at scale 3. Nevertheless, the comparisons for these two measures were found to be statistically significant only at scale 1, as an additional demonstration of the inversion that occurs in this frequency range. These outcomes and the ones related to the other scales and measures can be seen in Tab. 5.19, which includes the p-Values of the differences of the global measures for all the decomposed networks. It is evident that the scale 4 shows the most significant variations, among the ones with p-Value<0.05 (i.e. local efficiency, clustering coefficient, small-worldness, largest connected component size and modularity): therefore it was selected for the further analysis of local properties.

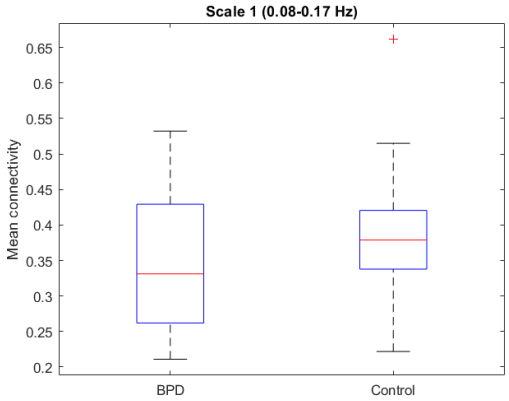

(a) Boxplot of the mean connectivity in the wavelet-decomposed network at scale 1, compared between BPDs and HCs.

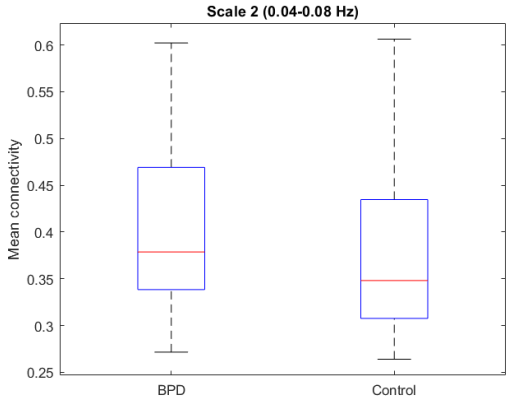

(b) Boxplot of the mean connectivity in the wavelet-decomposed network at scale 2, compared between BPDs and HCs.

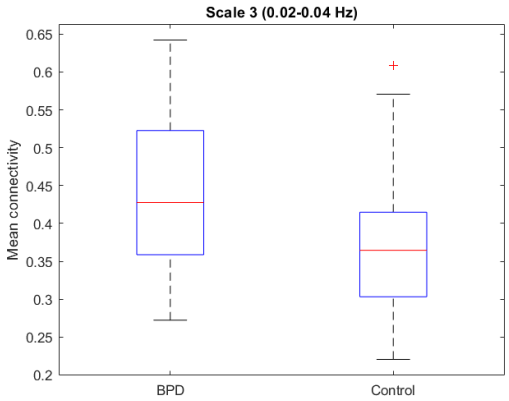

(c) Boxplot of the mean connectivity in the wavelet-decomposed network at scale 3, compared between BPDs and HCs.

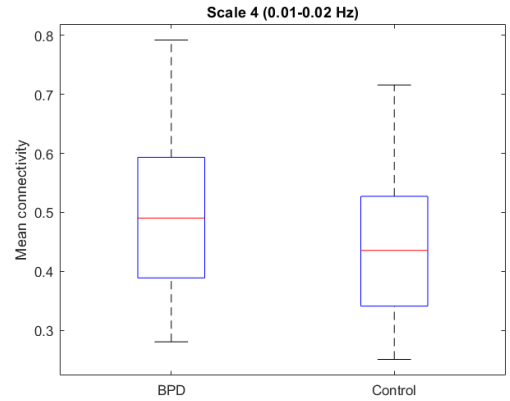

(d) Boxplot of the mean connectivity in the wavelet-decomposed network at scale 4, compared between BPDs and HCs.

Figure 5.24: Boxplots of the mean connectivity in all ranges of the wavelet-decomposed networks, compared between patients and controls.

	Scale 1		
	AUC in BPD	**AUC in HC**	**p-Value**
$CPL \uparrow$	0.5187	0.5092	**0.0204**
$E_{glob} \downarrow$	0.3931	0.3999	**0.0215**
$E_{loc} \uparrow$	0.5327	0.5245	0.3593
$CC \uparrow$	0.6246	0.6059	0.3048
$SW \downarrow$	0.5341	0.5397	0.4693
$LCCsize \uparrow$	34.0152	33.2761	0.1839
$Q \uparrow$	0.1115	0.1036	0.1932
	Scale 2		
	AUC in BPD	**AUC in HC**	**p-Value**
$CPL \downarrow$	0.5154	0.5173	0.3592
$E_{glob} \uparrow$	0.3958	0.3945	0.3559
$E_{loc} \downarrow$	0.5579	0.5963	**0.0155**
$CC \downarrow$	0.6664	0.7383	**0.0091**
$SW \downarrow$	0.5732	0.6342	**0.0093**
$LCCszie \downarrow$	34.7783	35.3084	0.0962
$Q \downarrow$	0.1201	0.1349	**0.0099**
	Scale 3		
	AUC in BPD	**AUC in HC**	**p-Value**
$CPL \downarrow$	0.5142	0.5247	0.0623
$E_{glob} \uparrow$	0.3962	0.3898	0.0748
$E_{loc} \downarrow$	0.5853	0.6236	**0.0236**
$CC \downarrow$	0.7129	0.7868	**0.0122**
$SW \downarrow$	0.6147	0.6677	**0.0344**
$LCCsize \downarrow$	35.4585	36.2054	**0.0195**
$Q \downarrow$	0.1279	0.1452	**0.0077**
	Scale 4		
	AUC in BPD	**AUC in HC**	**p-Value**
$CPL \downarrow$	0.5230	0.5297	0.1695
$E_{glob} \uparrow$	0.3912	0.3869	0.1753
$E_{loc} \downarrow$	0.5850	0.6588	**0.0019**
$CC \downarrow$	0.7119	0.8537	**0.0006**
$SW \downarrow$	0.6042	0.7111	**0.0010**
$LCCsize \downarrow$	35.4376	36.6105	**0.0022**
$Q \downarrow$	0.1272	0.1555	**0.0002**

Table 5.19: p-Values of the differences of the global measures between patients and controls in the wavelet-decomposed networks. Scale 4 is the most significantly varied and scale 1 presents inverted outcomes with respect to the other scales and the full FC network.

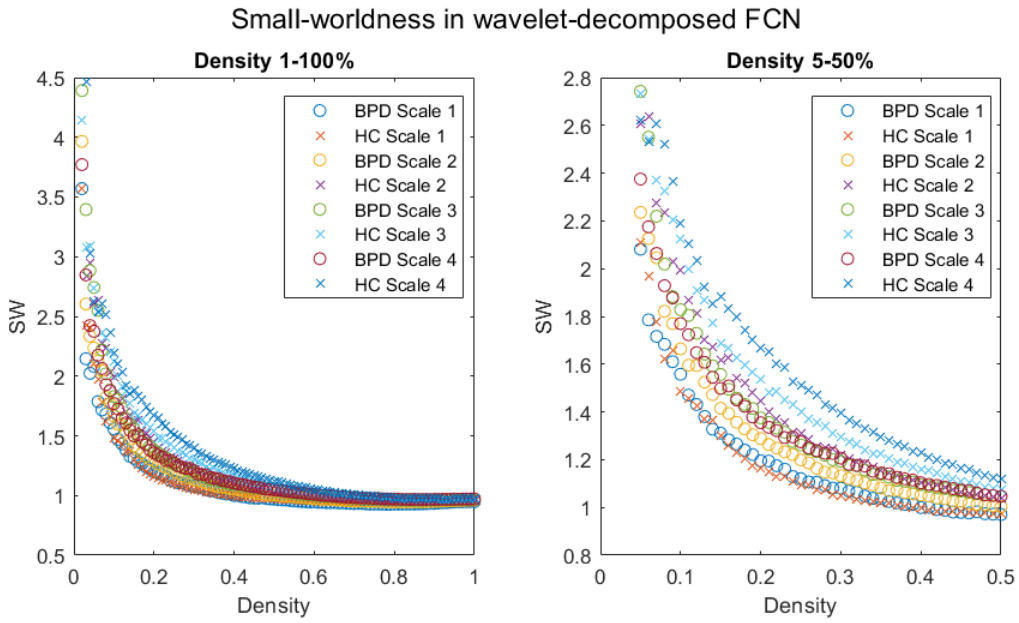

Figure 5.25: Small-worldness as a function of density in patients and controls of the wavelet-decomposed FCN. Scale 1 is the only where the quantity is lower in controls with respect to patients; the difference between BPDs and HCs is highest in scale 4.

Local properties - scale 4 network

Degree and strength Tab. 5.20 and 5.21 collect the information on nodes whose degree and strength, respectively, were found to be significantly varied between patients and controls in the scale 4 network among the wavelet decomposition.
Interestingly, in comparison with the outcomes of the full FCN, many nodes were found to be significantly varied with respect to these two properties, and especially many of those also passed the FDR: 17 in degree and 11 in strength. Despite this difference in the outcomes of the FDR correction between the two properties, the total number of regions involved is slightly higher in strength.
Nonetheless, the two measures are quite similar in terms of the nodes exhibited, and both show symmetric results between the hemispheres, except for the basal ganglia, which predominantly diverge in the right one. The variations particularly affect the limbic system, where also the majority of the nodes that passed the FDR are found. Note again the presence of the amygdala, also on the left in the scale 4 network, and the insular cortex, which did not emerge under the previous conditions. Note also that, while in the limbic and in the frontal lobes the variations are balanced between those higher patients and those higher in controls, among the basal ganglia there is a prevalence of the first case and in the temporal lobe of the second.

	Degree		
	AUC in BPD	**AUC in HC**	**p-Value**
BS ↑ (0)	6.9917	4.6246	0.0137
L.FP ↓ (1)	3.7420	6.2813	**0.0078**
L.parsOR ↓ (1)	5.4265	7.7586	0.0181
R.FP ↓ (1)	4.7357	7.8980	**0.0086**
R.parsOP ↑ (1)	9.8672	8.2030	0.0352
R.parsOR ↓ (1)	4.2619	7.9429	**0.0003**
L.LING ↑ (3)	14.1941	11.1793	**0.0046**
R.LING ↑ (3)	14.6607	11.7407	**0.0053**
L.IT ↓ (4)	10.1881	13.6791	**0.0050**
L.MT ↓ (4)	9.4193	12.1762	**0.0051**
L.TP ↓ (4)	3.4815	8.0830	**0.0001**
R.MT ↓ (4)	10.9063	13.0818	0.0157
L.AMY ↓ (5)	5.7519	9.4246	**0.0024**
L.HIP ↓ (5)	8.7513	11.1577	0.0191
L.cAC ↑ (5)	12.3946	10.2677	0.0236
L.ENTH ↓ (5)	4.1250	7.0391	**0.0049**
L.MoF ↓ (5)	6.4980	8.8964	**0.0070**
L.PC ↑ (5)	16.4993	13.9618	**0.0074**
R.AMY ↓ (5)	5.1341	9.8141	**0.0004**
R.cAC ↑ (5)	13.6274	10.0648	**0.0012**
R.ENTH ↓ (5)	3.4294	6.5198	**0.0084**
R.INS ↑ (5)	14.7352	12.7675	**0.0099**
R.MoF ↓ (5)	6.6200	8.8836	0.0180
L.THA ↑ (6)	15.4054	12.8218	0.0345
R.CAU ↑ (6)	12.6913	10.0238	0.0310
R.THA ↑ (6)	15.4530	12.2214	**0.0092**
R.VEN ↓ (6)	9.9644	12.3632	0.0156

Table 5.20: Nodes whose degree presents significant variations (p-Value<0.05) between patients and controls in scale 4 wavelet-decomposed network. 17 of these, especially in the limbic system, passed the FDR.

	Strength		
	AUC in BPD	**AUC in HC**	**p-Value**
BS ↑ (0)	4.9626	3.0595	0.0098
L.cMF ↑ (1)	7.5122	6.2496	0.0270
L.FP ↓ (1)	2.6494	4.2805	0.0125
L.parsOR ↓ (1)	3.8736	5.1978	0.0432
R.FP ↓ (1)	3.4980	5.5700	0.0176
R.paraC ↑ (1)	10.7819	9.2058	0.0478
R.parsOP ↑ (1)	7.5907	5.9231	0.0164
R.parsOR ↓ (1)	3.0530	5.3029	**0.0013**
L.CUN ↑ (3)	9.7830	7.9314	0.0264
L.LING ↑ (3)	11.2097	8.2656	0.0023
R.LING ↑ (3)	11.5828	8.6815	**0.0024**
R.PERIC ↑ (3)	8.3485	6.2876	0.0292
L.IT ↓ (4)	7.5307	9.8631	0.0181
L.MT ↓ (4)	7.0511	8.7242	0.0248
L.TP ↓ (4)	2.5196	5.4927	**0.0003**
L.AMY ↓ (5)	4.0583	6.4622	**0.0060**
L.cAC ↑ (5)	9.4805	7.4112	0.0151
L.ENTH ↓ (5)	2.9163	4.6406	0.0184
L.INS ↑ (5)	12.0639	10.4099	0.0427
L.MoF ↓ (5)	4.7253	6.5175	**0.0045**
L.PC ↑ (5)	12.9971	10.1779	**0.004**
R.AMY ↓ (5)	3.7515	6.8426	**0.0026**
R.cAC ↑ (5)	10.5379	7.1646	**0.0005**
R.ENTH ↓ (5)	2.3029	4.2168	0.0130
R.INS ↑ (5)	11.5897	9.4484	**0.0043**
R.MoF ↓ (5)	4.8549	6.4919	0.0159
R.PC ↑ (5)	11.4648	9.2886	0.0195
L.THA ↑ (6)	11.8697	9.0640	0.0126
R.CAU ↑ (6)	9.6479	7.0215	0.0139
R.PUT ↑ (6)	9.6859	7.5276	0.0450
R.THA ↑ (6)	11.9051	8.7656	**0.0054**
R.VEN ↓ (6)	7.1884	8.6678	0.0466

Table 5.21: Nodes whose strength presents significant variations (p-Value<0.05) between patients and controls in scale 4 wavelet-decomposed network. 11 of these, especially in the limbic system, passed the FDR.

Betweenness centrality As observed also in the previous cases, betweenness centrality provides divergent results with respect to the other centrality measures. In particular, there is not a symmetry between the two hemispheres, both in terms of the quality and the quantity of the nodes involved, whose BC is mostly decreased in patients with respect to controls.
Note also that the limbic system is not found to be particularly varied, as instead it was seen for degree and strength, but it is rather replaced by the frontal and the temporal lobes; within the latter it was also found the only node whose p-Value passed the FDR correction, the left inferior temporal gyrus.
Tab. 5.22 summarizes these results.

	Betweenness centrality		
	AUC in BPD	**AUC in HC**	**p-Value**
L.cMF ↑ (1)	34.4615	23.1093	0.0432
L.parsTR ↑ (1)	16.8030	9.8479	0.0396
R.FP ↓ (1)	10.2052	40.4261	0.0089
R.paraC ↑ (1)	43.8230	19.8800	0.0108
R.parsOR ↓ (1)	5.6219	13.8564	0.0051
L.SP ↓ (2)	27.3648	46.6636	0.0338
R.LOC ↑ (3)	30.0059	8.5882	0.0228
L.IT ↓ (4)	27.1970	72.5721	**0.0002**
L.TP ↓ (4)	12.0052	41.0589	0.0211
R.IT ↓ (4)	32.7793	76.8393	0.0191
R.MT ↓ (4)	33.5533	58.7218	0.0063
R.ENTH ↓ (5)	8.3737	25.6264	0.0166
R.rAC ↑ (5)	20.6385	7.1821	0.0141

Table 5.22: Nodes whose betweenness centrality presents significant variations (p-Value<0.05) between patients and controls in scale 4 wavelet-decomposed network. The left inferior temporal gyrus is the only node whose p-Value passed the FDR.

Participation coefficient The outcomes for the participation coefficient, reported in Tab. 5.23, show a considerable presence of the frontal lobe, with respect to the other systems. Even if the variations of some nodes, particularly within this lobe, are associated to very low p-Values, none of them passed the FDR.
Nonetheless it is meaningful to note the presence of the insular cortex and the basal ganglia, as well as other regions found also in degree and strength, which suggest that their variation in connectivity are related to their integration with the modules of the network.

	Participation coefficient		
	AUC in BPD	**AUC in HC**	**p-Value**
BS ↑ (0)	0.1531	0.1032	0.0064
L.FP ↓ (1)	0.0691	0.1068	0.0488
L.paraC ↑ (1)	0.2203	0.1853	0.0464
L.PreCG ↑ (1)	0.1984	0.1637	0.0448
L.rMF ↑ (1)	0.2113	0.1650	0.0236
R.FP ↓ (1)	0.0733	0.1283	0.0062
R.paraC ↑ (1)	0.2178	0.1726	0.0181
R.parsOP ↑ (1)	0.1604	0.0973	0.0026
R.parsOR ↓ (1)	0.0025	0.1541	0.0007
R.PreCG ↑ (1)	0.1884	0.1341	0.0028
R.rMF ↑ (1)	0.2033	0.1472	0.0056
L.LING ↑ (3)	0.2061	0.1654	0.0189
R.LOC ↑ (3)	0.1698	0.1217	0.0368
L.IT ↓ (4)	0.1950	0.2354	0.0086
L.MT ↓ (4)	0.1719	0.2031	0.0367
L.TP ↓ (4)	0.0817	0.1373	0.0084
L.cAC ↑ (5)	0.2030	0.1557	0.0200
L.ENTH ↓ (5)	0.0894	0.1457	0.0086
L.INS ↑ (5)	0.2229	0.1905	0.0473
R.cAC ↑ (5)	0.2208	0.1545	0.0044
R.ENTH ↓ (5)	0.0875	0.1362	0.0418
R.INS ↑ (5)	0.2217	0.1729	0.0088
R.CAU ↑ (6)	0.2274	0.1608	0.0031
R.PUT ↑ (6)	0.2229	0.1732	0.0138
R.THA ↑ (6)	0.2421	0.1838	0.0079
L.CER ↑ (7)	0.2164	0.1813	0.0494

Table 5.23: Nodes whose participation coefficient presents significant variations (p-Value<0.05) between patients and controls in scale 4 wavelet-decomposed network.

Within-module strength On the other hand, concerning the within-module strength, whose outcomes are collected in Tab. 5.24, two aspects clearly emerge: firstly, the quantities are mostly decreased in patients within all lobes, except for the occipital, where the trend is opposite; secondly, the limbic system includes the greatest number of variation (as in the full network), among which the right amygdala also passed the FDR. Note that, within the full network, this ROI was significantly varied in both the participation coefficient (where it also passed the FDR) and the within-module strength, whereas is the scale 4 network it is present only in the latter. Also the left temporal pole, detected also in other centrality measures within the scale 4 network, passed the FDR.

	Within-module strength		
	AUC in BPD	**AUC in HC**	**p-Value**
L.FP ↓ (1)	2.3521	3.4872	0.0230
R.parsOR ↓ (1)	2.7942	3.8086	0.0215
L.CUN ↑ (3)	6.7696	5.6809	0.0339
L.LING ↑ (3)	7.3145	6.2108	0.0252
R.LING ↑ (3)	7.4221	6.2450	0.0112
L.IT ↓ (4)	4.6136	6.0039	0.0220
L.MT ↓ (4)	4.7693	5.9380	0.0211
L.TP ↓ (4)	1.8266	3.9904	**0.0001**
R.TP ↓ (4)	1.5766	2.6896	0.0285
R.TT ↑ (4)	5.1830	4.0072	0.0489
L.ACC ↓ (5)	3.1544	4.3753	0.0364
L.AMY ↓ (5)	2.7554	4.4094	0.0018
L.ENTH ↓ (5)	2.1610	3.3425	0.0149
L.MoF ↓ (5)	4.0165	5.4831	0.0044
L.PC ↑ (5)	6.9994	6.0996	0.0418
R.AMY ↓ (5)	2.5742	4.9203	**0.0003**
R.ENTH ↓ (5)	1.6207	2.9328	0.0036
R.MoF ↓ (5)	4.0483	5.4228	0.0108
L.PAL ↓ (6)	3.4727	4.6420	0.0437
R.VEN ↓ (6)	4.5189	5.8800	0.0103

Table 5.24: Nodes whose within-module strength presents significant variations (p-Value<0.05) between patients and controls in scale 4 wavelet-decomposed network. The left temporal pole and the right amygdala passed the FDR

Local efficiency and clustering coefficient The results for the local efficiency and the clustering coefficient, very similar to each other, are reported in Tab. 5.25 and 5.26. The properties of the regions involved are mostly increased in patients, confirming what was observed in the full network, even though in this case, no p-Values passed the FDR correction. Nonetheless note that there is a correspondence between the sign of the variations in local efficiency and clustering coefficient with those of the within-module strength.
The most varied system is the limbic one, where also the lowest p-Values are found, followed by the temporal one: similar results were observed also in the full network, where the left temporal pole and the transverse temporal gyrus even passed the FDR.

	Local efficiency		
	AUC in BPD	**AUC in HC**	**p-Value**
BS ↑ (0)	0.2144	0.1710	0.0382
R.cMF ↑ (1)	0.2818	0.2605	0.0184
R.SF ↑ (1)	0.2731	0.2547	0.0381
L.SP ↑ (2)	0.2938	0.2703	0.0172
L.SM ↑ (2)	0.2904	0.2688	0.0325
R.PCUN ↑ (2)	0.3071	0.2898	0.0338
R.SP ↑ (2)	0.2932	0.2764	0.0480
R.SM ↑ (2)	0.3060	0.2871	0.0373
L.CUN ↑ (3)	0.3053	0.2848	0.0333
L.FG ↑ (3)	0.2959	0.2739	0.0275
L.ST ↑ (4)	0.2837	0.2564	0.0278
L.TP ↓ (4)	0.1446	0.2179	0.0022
L.TT ↑ (4)	0.2905	0.2287	0.0026
R.TP ↓ (4)	0.1270	0.1799	0.0374
R.TT ↑ (4)	0.2819	0.2228	0.0030
L.AMY ↓ (5)	0.1876	0.2437	0.0045
L.cAC ↑ (5)	0.2962	0.2571	0.0021
L.ENTH ↓ (5)	0.1528	0.2095	0.0071
L.INS ↑ (5)	0.2866	0.2650	0.0300
L.PC ↑ (5)	0.2881	0.2589	0.0081
R.AMY ↓ (5)	0.1802	0.2359	0.0056
R.cAC ↑ (5)	0.2938	0.2642	0.0123
R.iC ↑ (5)	0.3027	0.2844	0.0211
R.PC ↑ (5)	0.2936	0.2612	0.0039
R.CER ↑ (7)	0.2745	0.2441	0.0101

Table 5.25: Nodes whose local efficiency presents significant variations (p-Value<0.05) between patients and controls in scale 4 wavelet-decomposed network.

	Clustering coefficient		
	AUC in BPD	**AUC in HC**	**p-Value**
R.cMF ↑ (1)	0.2310	0.2148	0.0455
R.SF ↑ (1)	0.2098	0.1902	0.0203
L.SP ↑ (2)	0.2415	0.2170	0.0187
L.SM ↑ (2)	0.2397	0.2125	0.0200
R.PCUN ↑ (2)	0.2608	0.2418	0.0428
R.SM ↑ (2)	0.2634	0.2413	0.0360
L.FG ↑ (3)	0.2407	0.2147	0.0286
L.ST ↑ (4)	0.2281	0.2042	0.0434
L.TP ↓ (4)	0.1288	0.1824	0.0098
L.TT ↑ (4)	0.2569	0.1959	0.0023
R.IT ↑ (4)	0.2266	0.2044	0.0492
R.TP ↓ (4)	0.1106	0.1584	0.0339
R.TT ↑ (4)	0.2447	0.1932	0.0053
L.AMY ↓ (5)	0.1596	0.2007	0.0213
L.cAC ↑ (5)	0.2532	0.2134	0.0039
L.ENTH ↓ (5)	0.1346	0.1753	0.0184
L.INS ↑ (5)	0.2257	0.2056	0.0448
L.PC ↑ (5)	0.2247	0.1978	0.0154
R.AMY ↓ (5)	0.1535	0.1929	0.0155
R.cAC ↑ (5)	0.2426	0.2191	0.0405
R.iC ↑ (5)	0.2527	0.2322	0.0179
R.PC ↑ (5)	0.2367	0.2046	0.0068
R.CER ↑ (7)	0.2322	0.1966	0.0026

Table 5.26: Nodes whose clustering coefficient presents significant variations (p-Value<0.05) between patients and controls in scale 4 wavelet-decomposed network.

5.2.2 Structural covariance networks

In the following, the plots as a function of density are reported up to 85% of the latter. The reason is that, after having set the negative weights to 0, the maximum density in patients was 79% and in controls 85%.

Full network

Global properties

Characteristic path length As mentioned in section 5.1, the characteristic path length of the SC networks of subjects slightly differ from that of random networks: this deviation is especially marked in patients, so that a discrepancy between the normalized values of BPDs and HCs is clearly visible over the full range of densities, as it can be seen from Fig. 5.26. Nevertheless, the normalized quantity is close enough to 1 to ensure the verification of the small-worldness requirements. Note also that the characteristic path length is greater in patients also in absolute values.
Another aspect to underline is that the continuous decrease as a function of the density seen in the full FC networks is not so smoothly repeated in this case, especially when

the measures are normalized. This is due in particular to the fact that the plots are not retrieved from an average value over the quantities of a set of networks, as it was in the FC case, but are described only by one value per group. Therefore, on a global level, this is particularly evident at low densities, where the graph starts to be considerably disconnected and the links, over which the properties are calculated, decrease in number. Additionally, it must be considered that the SC matrices are less accurate than the FC ones in finding true correlations, since the series over which the Pearson's coefficients were calculated, are quite short (27 for patients' matrix, 28 for controls', against the 180 of the FC graphs). As a consequence, this kind of behavior is present also in other global measures, as it is shown in the next paragraphs.

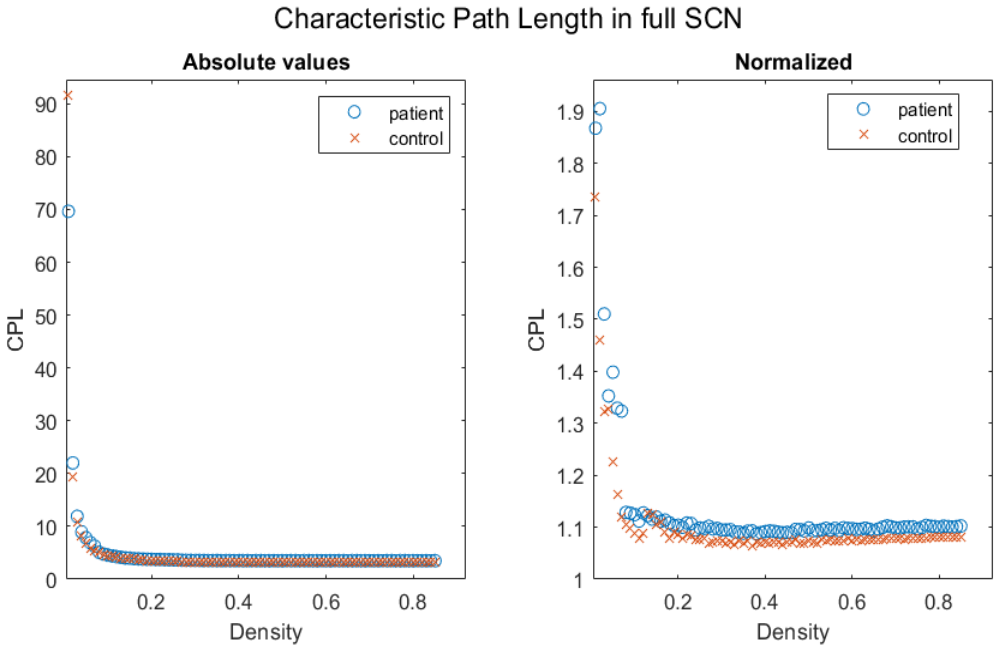

Figure 5.26: Characteristic path length as a function of density in patients and controls, in absolute values and normalized by the result of the corresponding random networks, in the full SC network. The normalized quantity appears to differ between BPDs and HCs, but it is close to 1 over almost the entire range.

Global efficiency As shown in Fig. 5.27, the global efficiency returns outcomes that are perfectly consistent with the results found through the characteristic path length: the first is increased in controls, both in absolute and normalized values, starting from a density of 10-15%, as well as the second is shorter in HCs.
Nevertheless, it is important to underline this trend is inverted with respect to what was found in the FC networks, where the global efficiency was incremented in patients. This is another characteristic aspect of the SC networks: the absolute values of the measures, which were often found to be increased in patients in the FC graphs, tend instead to be decreased in this case, as it is shown further in the following paragraphs of this section.

Note also that in the SC networks the decrease of the slope of the increment in global efficiency as a function of the density is even more evident than in the FC network: the quantity remains unchanged after a density of ∼30%, where, as it is shown later in this subsection, the network is fully connected. The fact that the constant behavior is not seen in the FC networks is because, in that case, the values of global efficiency in the plots

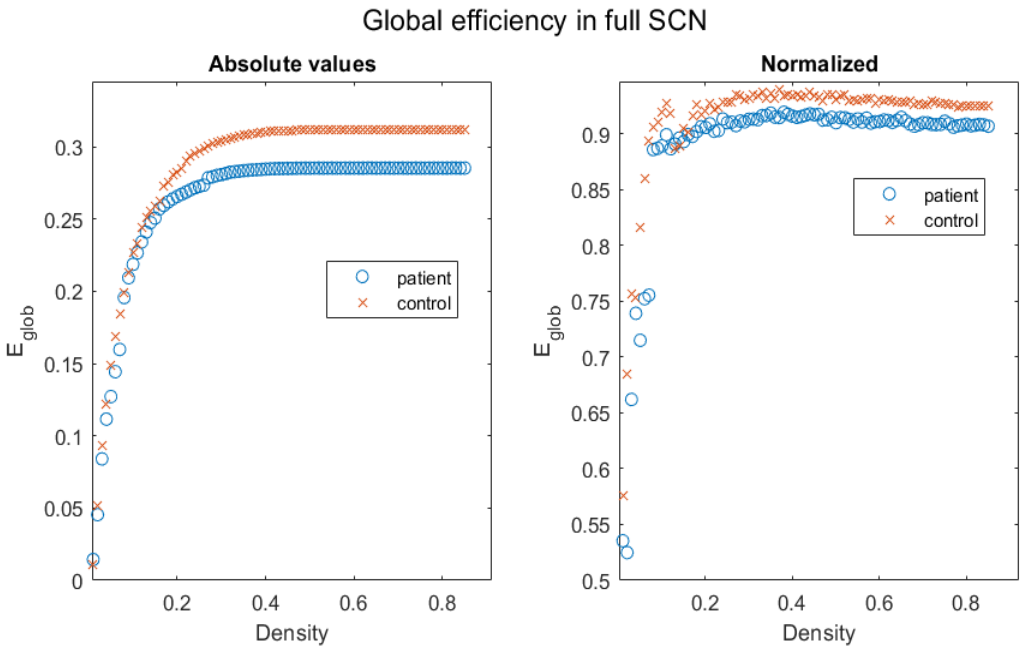

Figure 5.27: Global efficiency as a function of density in patients and controls, in absolute values and normalized by the result of the corresponding random networks, in the full SC network. The absolute values are increased in controls, as well as the normalized ones.

are calculated as the average of the quantity for each subject: since they become fully connected at different densities, the global efficiency continuously increase in a group until the networks of all the subjects within that group are indeed fully connected. It is clear, though, that once a weighted network is fully connected through the strongest links, the global efficiency is unlikely to increase, even if the density does, because the new links added have lower weights and therefore they tend not to contribute significantly to the connectivity among nodes.

Average local efficiency and clustering coefficient Also the absolute values of the average local efficiency are increased in controls, starting from a density of about 15-20%, see Fig. 5.28. Nonetheless, this deviation is canceled when passing to the normalized values, so that they are perfectly compatible with each other.
For this measure, it is particularly evident also in the absolute values that the smooth behavior seen in the FC case ceases to be verified, for the reasons described in the paragraph on characteristic path length.
Very similar is the trend of the average clustering coefficient, reported in Fig. 5.29, which is increased in patients in absolute terms, but is perfectly comparable between patients and controls when normalized.

Small-worldness As expected by recalling the considerations described above on the characteristic path length and the average clustering coefficient of the full SC network, it can be seen from Fig. 5.30 that the small-worldness in patients and controls is comparable over the entire range of densities. The requirements of $SW > 1$ are verified up to a density of about 50%, which allows to state that this property is present in that range, but small discrepancies between BPDs and HCs are visible only up to 30%. Moreover these variations appear to be quite random and do not show a clear tendency in favour

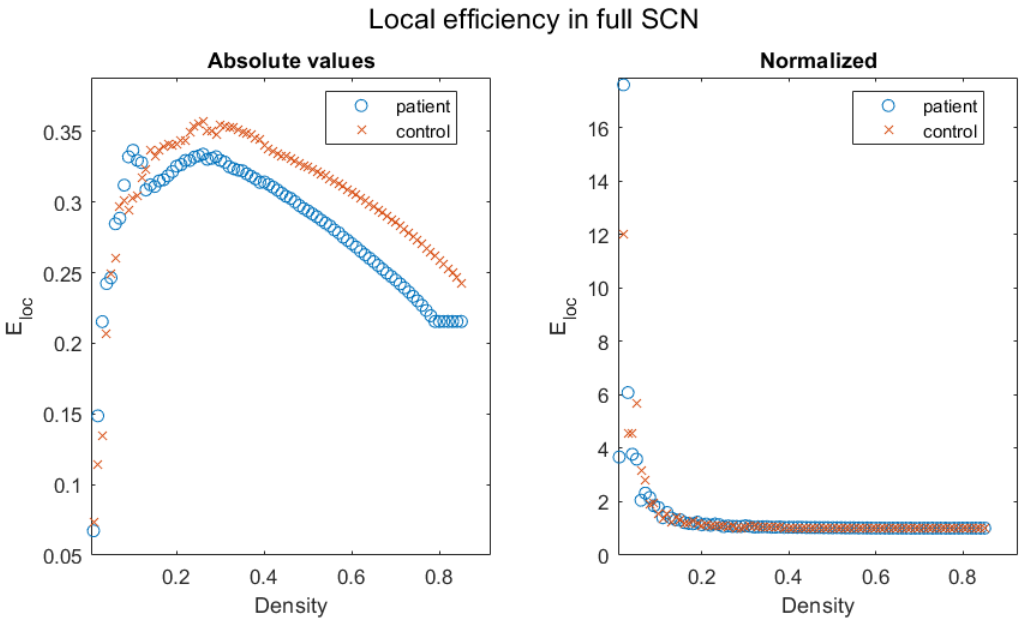

Figure 5.28: Local efficiency as a function of density in patients and controls, in absolute values and normalized by the result of the corresponding random networks, in the full SC network. The absolute values are increased in controls, whereas the normalized ones are basically equal to those of patients over the entire range.

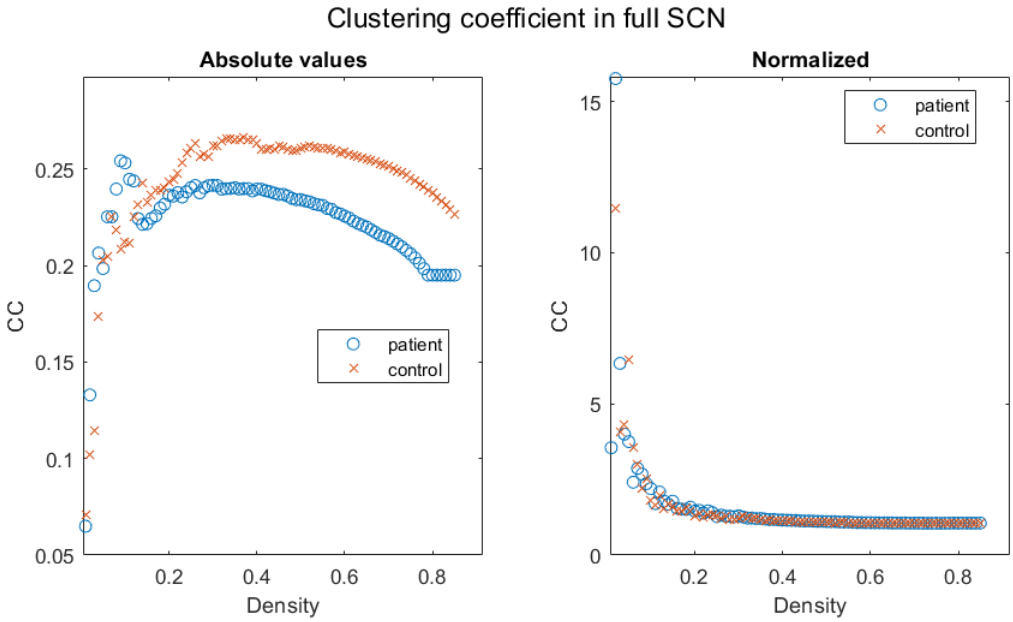

Figure 5.29: Clustering coefficient as a function of density in patients and controls, in absolute values and normalized by the result of the corresponding random networks, in the full SC network. The absolute values are increased in controls, whereas the normalized ones are basically equal to those of patients over the entire range.

of one of the two groups.

Largest connected component size As it is possible to see from Fig. 5.31, the largest connected component reaches the full connectivity at a density of ∼30% in both

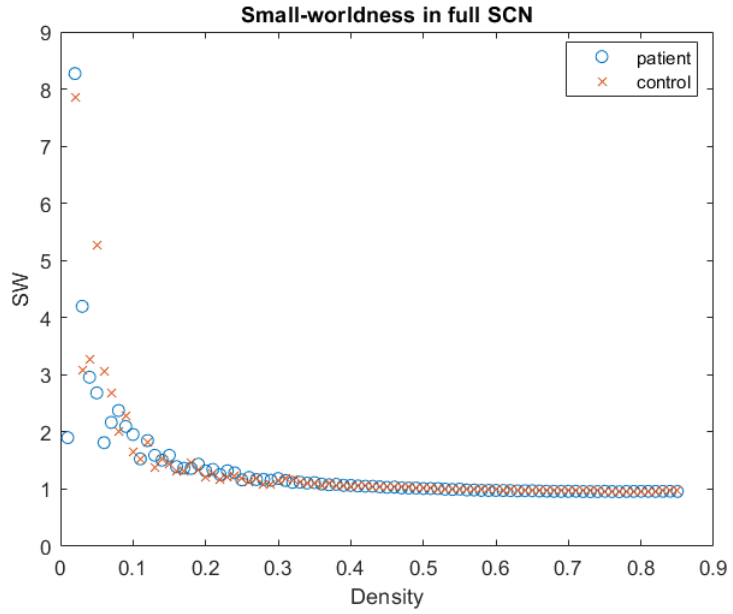

Figure 5.30: Small-worldness as a function of density in patients and controls, in the full SC network. The quantity is greater than 1 for both patients and controls up to a density of 50%, but an inconsistent difference between groups is visible only up to 30%.

patients and controls, as anticipated by the comments on the global efficiency of the SC networks. This, combined with the outcomes of small-worldness, was the criterion to set 30% as the maximum density value for the investigation of the local properties.
It is also interesting to note that the LCC size in HCs is greater up to a density of 7%, after which the one of patients abruptly increases, overcoming the one of controls up to ∼20%, after which they are basically equal. This means that between 7% and 8% the set of links added connect a sub-module to the largest connected component of the network.

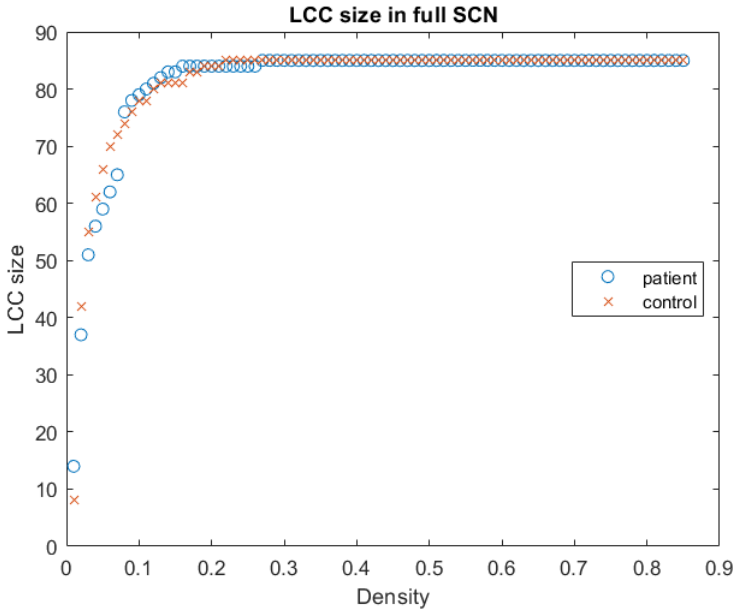

Figure 5.31: Largest connected component size as a function of density in patients and controls, in the full SC network. Full connectivity is reached at ∼30% of density.

Modularity coefficient Even the modularity coefficient, which was the most significantly varied property in FC networks, is basically the same between patients and controls in the SC networks. The central part of the curve, reported in Fig. 5.32, is again the one where there is the biggest deviation between BPDs and HCs, but it is evident that it is not significant enough to distinguish the two groups.

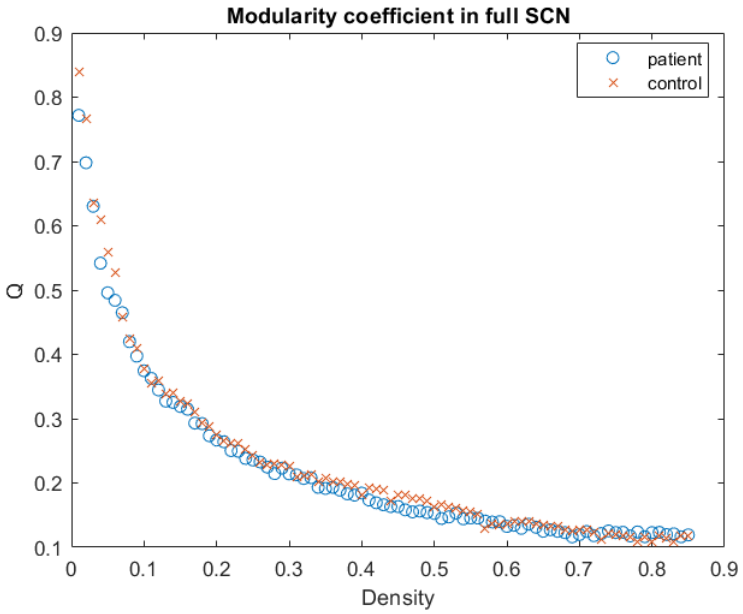

Figure 5.32: Modularity as a function of density in patients and controls, in the full SC network. The quantity is basically equal between patients and controls over the entire range of densities.

Statistical significance The 10000 permutations of the assignments of subjects to patients or control groups and the calculation of the properties described above at each repetition, returned the p-Value reported in Tab. 5.27. The properties are found to be mostly decreased in patients, but this is not a meaningful result, since, as it was expected by looking at all the plots related to the SC networks, none of the variations are statistically significant.

	AUC in BPD	**AUC in HC**	**p-Value**
$CPL \uparrow$	0.2833	0.2734	0.1910
$E_{glob} \downarrow$	0.2213	0.2288	0.2056
$E_{loc} \downarrow$	0.3499	0.3578	0.8853
$CC \uparrow$	0.4256	0.4205	0.9415
$SW \downarrow$	0.3721	0.3821	0.8805
$LCCsize \downarrow$	20.2000	20.2550	0.9395
$Q \downarrow$	0.0776	0.0796	0.8390

Table 5.27: p-Values of the differences of the AUCs of the global measures between patients and controls in the full SC network. None of the variations are statistically significant.

Local properties

Consistently with the findings obtained from the global properties, also at a local level the full SC networks did not show many significant variations, so that none of them even passed the FDR correction.

Centrality measures Tab. 5.28 and 5.3 collect the significant variations between patients and controls at a local level in the full SC networks in terms of degree and strength respectively.
It is immediately evident that the number of nodes involved is way inferior to that found in all the types of the FC networks. Nonetheless it is interesting to observe some results. Firstly, the most influenced system seems to be still the limbic one, among which the right amygdala is found varied again, together with the right hippocampus and the left entorhinal cortex. Secondly, it must be specified that the degree/strength of the nodes just mentioned were found significantly lower in patients in the full FC networks, whereas in this case they are all increased. The same inversion in the trend is detected for the right rostral middle frontal gyrus, whereas the right lateral occipital was not found within the full FC networks.

	Degree		
	AUC in BPD	**AUC in HC**	**p-Value**
R.rMF ↓ (1)	1.2650	7.2300	0.0121
L.ENTH ↑ (5)	3.8750	0.4250	0.0350
R.AMY ↑ (5)	7.2500	1.6400	0.0486
R.HIP ↑ (5)	8.1200	1.9450	0.0046

Table 5.28: Nodes whose degree presents significant variations (p-Value<0.05) between patients and controls in the full SC network.

	Strength		
	AUC in BPD	**AUC in HC**	**p-Value**
R.rMF ↓ (1)	0.5074	3.7220	0.0085
R.LOC ↓ (3)	0.8004	3.5135	0.0440
L.ENTH ↑ (5)	1.8311	0.2273	0.0351
R.HIP ↑ (5)	4.4024	0.9851	0.0065

Table 5.29: Nodes whose strength presents significant variations (p-Value<0.05) between patients and controls in the full SC network.

Regarding the betweenness centrality, it provides quite different outcomes with respect to the other centrality measures, as it was already seen for the other networks, even if there are also some confirmations. In particular, the right rostral middle frontal gyrus and hippocampus are significantly varied also in this case and in the same verse as for the other centrality measures. Nonetheless the betweenness centrality of these regions was not significantly varied in the full FC network. The results are reported in Tab. 5.30.

Module-related measures As for the other local measures, also the participation coefficient and the within-module strength did not provide many significant outcomes,

	Betweenness centrality		
	AUC in BPD	**AUC in HC**	**p-Value**
R.rMF ↓ (1)	0.7900	67.8300	0.0321
R.PostCG ↑ (2)	105.0200	11.2500	0.0114
R.ST ↑ (4)	219.3200	63.2600	0.0384
L.PC ↓ (5)	0	39.8100	0.0255
R.HIP ↑ (5)	123.38	4.8500	0.0064
L.VEN ↓ (6)	7.8900	91.3000	0.0345

Table 5.30: Nodes whose betweenness centrality presents significant variations (p-Value<0.05) between patients and controls in the full SC network.

which are collected in Tab. 5.31 and 5.32. Still, from the results we can retrieve information on the previous findings about the centrality measures: in particular, the variation in degree and strength of the left entorhinal cortex are related to variations in its integration with the other modules in the network, whereas those of the left lateral occipital sulcus and right hippocampus to variations in their centrality role within the community where they are located (through the community optimization of the Louvain algorithm, whose characterization is described in the next paragraphs).

	Participation coefficient		
	AUC in BPD	**AUC in HC**	**p-Value**
R.paraC ↑ (1)	0.1694	0	0.0066
L.CUN ↓ (3)	0.0062	0.1225	0.0380
L.ENTH ↑ (5)	0.1530	0.0247	0.0319

Table 5.31: Nodes whose participation coefficient presents significant variations (p-Value<0.05) between patients and controls in the full SC network.

	Within-module strength		
	AUC in BPD	**AUC in HC**	**p-Value**
L.LOC ↓ (3)	0.4062	1.5861	0.0342
R.HIP ↑ (5)	2.2868	0.5622	0.0165

Table 5.32: Nodes whose within-module strength presents significant variations (p-Value<0.05) between patients and controls in the full SC network.

Local efficiency measures The outcomes of local efficiency and clustering coefficient, quite consistent with each other as it can be seen from Tab. 5.33 and 5.34, mostly present variations in the limbic system, among which it is possible to see once more the left entorhinal cortex, even if only in the first of the two properties.
Among the other nodes significantly varied, the only one that was present also in FC networks is the right rostral anterior cingulate cortex, for which there is an inversion in the verse of the difference, too.

	Local efficiency		
	AUC in BPD	**AUC in HC**	**p-Value**
L.PostCG ↓ (2)	0.0511	0.0984	0.0473
L.FG ↓ (3)	0.0295	0.1114	0.0070
L.ENTH ↑ (5)	0.0818	0.0023	0.0348
L.iC ↓ (5)	0.0297	0.1186	0.0095
R.PC ↑ (5)	0.0852	0.0088	0.0329
R.rAC ↑ (5)	0.1136	0.0083	0.0099

Table 5.33: Nodes whose local efficiency presents significant variations (p-Value<0.05) between patients and controls in the full SC network.

	Clustering coefficient		
	AUC in BPD	**AUC in HC**	**p-Value**
L.FG ↓ (3)	0.0167	0.0921	0.0029
L.iC ↓ (5)	0.0236	0.1059	0.0074
R.rAC ↑ (5)	0.0979	0.0083	0.0132

Table 5.34: Nodes whose clustering coefficient presents significant variations (p-Value<0.05) between patients and controls in the full SC network.

Hubs

The integrating and segregating hub nodes are collected in Tab. 5.35 and Fig. 5.33: they are more than the ones of the FC networks, even if many nodes are repeated also in this case. Nevertheless, most of those nodes have changed their role in the SC network, which is actually consistent with the fact that the participation coefficient and the within-module strength of some nodes differ between patients and controls with opposite signs in the full FC and in the SC networks. Beside this, it should also be noted that there is not much symmetry neither between the left and right hemisphere within the same group of subjects, nor within patients and controls. Also in this case, the hubs are quite distributed among all the systems of the brain, making it difficult to infer on specific and meaningful variations.

Composition of modules

In the full SC network, the composition of modules did not reflect the subdivision in anatomical systems, which instead was considerably more supported in the full FC graph. Also in this case, obviously, the assignment of nodes changed with the density and also between patients and controls. The most evident aspect was that the subdivisions were often asymmetric between the left and the right hemisphere, so that it occurred that some small modules were formed only by nodes belonging to a single hemisphere. Nevertheless, it was verified that, across densities, the occipital lobe was generally mostly unified into a single community; the limbic system, instead, was always divided into different modules, moreover shared with many other regions. The separate study of the limbic system, therefore, would not be supported by the underlying structure of the networks, but it was still carried out, as it is shown in the next paragraphs, both for comprehensiveness and because it was found that it was the most affected by significant variations also in full FC networks.

In general, it is evident that in the case of the full SC network the subdivision in modules

	Left hemisphere		Right hemisphere	
	BPD	**HC**	**BPD**	**HC**
paraC (1)	Segregating	-	Integrating	-
PreCG (1)	Both	Segregating	-	Segregating
rMF (1)	Integrating	-	-	Integrating
SF (1)	-	Segregating	-	-
IP (2)	Integrating	Integrating	-	-
PostCG (2)	-	-	Integrating	-
PCUN (2)	-	Segregating	-	Segregating
SP (2)	-	-	-	Integrating
FG (3)	-	-	-	Integrating
LOC (3)	-	-	-	Integrating
IT (4)	Integrating	-	Integrating	-
MT (4)	Segregating	Integrating	-	Integrating
ST (4)	-	Segregating	Both	Segregating
TP (4)	-	-	Integrating	Integrating
AMY (5)	Both	-	Segregating	-
HIP (5)	Segregating	-	Segregating	-
INS (5)	Integrating	-	-	-
iC (5)	-	-	-	Integrating
LoF (5)	Segregating	Segregating	Segregating	-
PHG (5)	Integrating	-	-	-
CAU (6)	Integrating	-	-	-
PUT (6)	-	-	-	Integrating
THA (6)	Segregating	Segregating	Segregating	Both
VEN (6)	Segregating	Segregating	Segregating	-
CER (7)	-	Integrating	-	Integrating

Table 5.35: Comparison of hub nodes in patients and controls in the full SC network: integrating are those nodes that have strong intermodular connections, segregating are those that have a central role within their module.

does not provide supporting results, but rather delegitimizes the properties found under this frame. As an example, the modules found at a density of 32%, chosen for comparison with the results derived from the FC networks, are reported in Tab A.4 and A.5. Even though the density is outside of the range selected for the integration, it was verified that the results are extendable also to lower densities.

Analysis of altered connectivity

As described in Section 4.6.2, the analysis of the altered connectivity could not be carried with the NBS method, as for the FC networks, but it was achieved through the calculation of the z-score of the element-wise difference between the Pearson's correlation matrices of patients and controls (shown in Fig. 4.9), which is reported in Fig. 5.34.
After the conversion of the z-scores to the corresponding p-Values, 73 differences higher in patients and 134 higher in controls were found to be statistically significant. Nevertheless, the FDR correction returned one variation only among these, higher in patients, between the left and the right caudate nucleus.

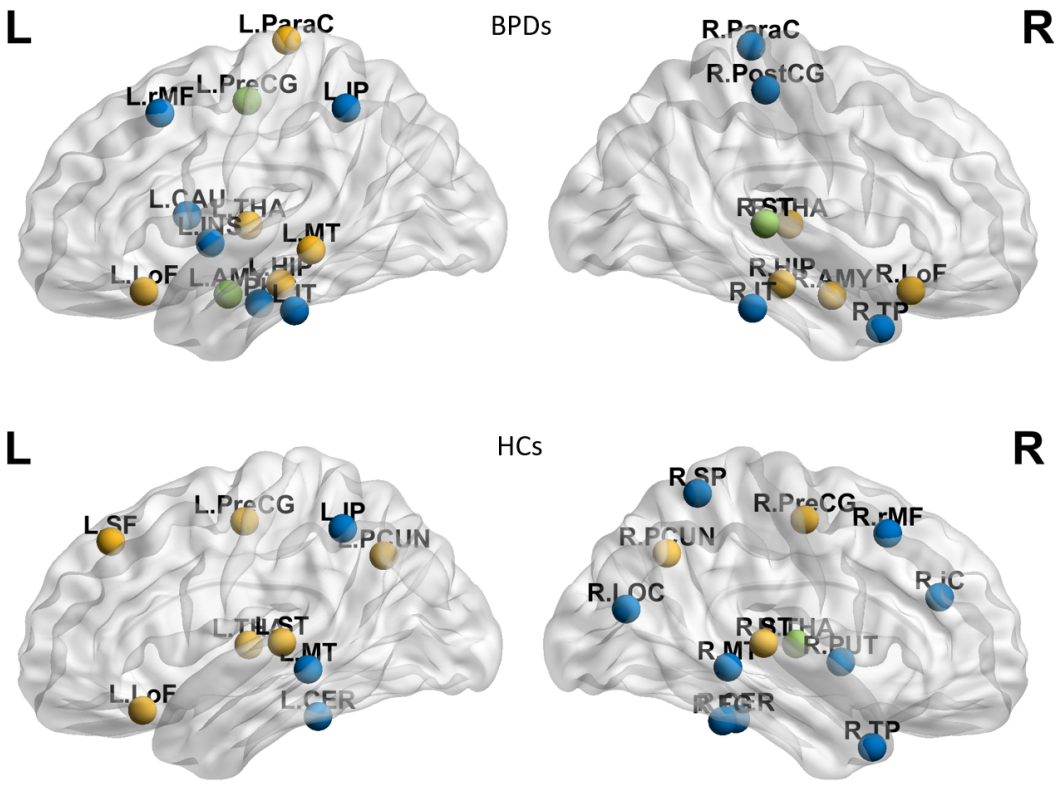

Figure 5.33: Hub nodes in patients and controls in the full SC network, where the color defines the role of the hub. Blue: integrating; yellow: segregating; green: both.

Therefore, also from this point of view, it appears that there are no consistent variations between patients and controls in the SC networks.

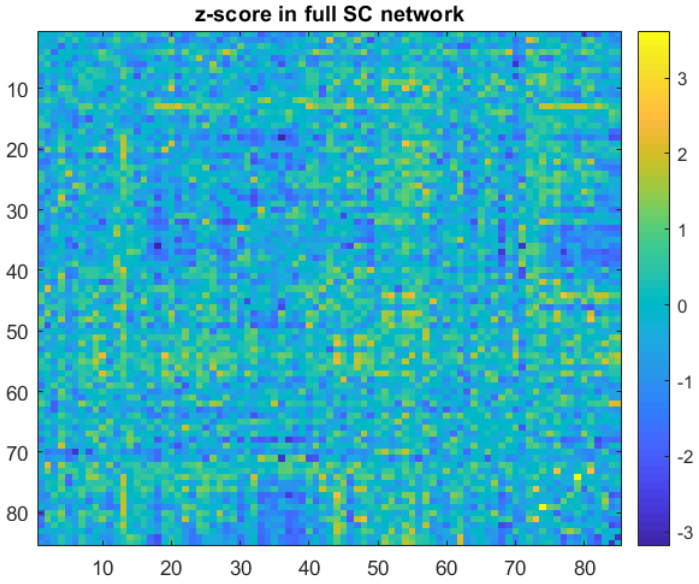

Figure 5.34: Matrix of the z-scores of the difference of the correlation values between patients and controls in the full SC network. Positive values indicate that the correlation coefficient is higher in patients, negative that it is higher in controls.

Limbic and occipital subnetworks

Global properties

As it could be expected by the outcomes obtained from the full SC network, also the limbic and occipital SC subnetworks did not provide any significant result at global level for any measure. For simplicity, the table of p-Values is not reported here.

Local properties

Even at local level, the occipital subnetwork alone did not present any significant variation for any measure, which is actually consistent with the expectations.

On the other hand, the limbic system showed some significant variations in the centrality measures, which are reported in Tab. 5.36, 5.37 and 5.38. The nodes involved, i.e. the right parahippocampal gyrus in degree and strength and the right insular cortex in betweenness centrality, were not previously detected, neither in the limbic and occipital FC subnetworks, nor in the full SC network. Moreover, the p-Value of the differences are quite high, so that none of the results passed the FDR correction, making these outcomes not very relevant for further interpretation.

	Degree - limbic SCN		
	AUC in BPD	**AUC in HC**	**p-Value**
R.PHG ↓	0.3500	2.9550	0.0381

Table 5.36: Nodes within the limbic SC subnetwork whose degree presents significant variations (p-Value<0.05) between patients and controls.

	Strength - limbic SCN		
	AUC in BPD	**AUC in HC**	**p-Value**
R.PHG ↓	0.1705	1.2534	0.0380

Table 5.37: Nodes within the limbic SC subnetwork whose strength presents significant variations (p-Value<0.05) between patients and controls.

	Betweenness centrality - limbic SCN		
	AUC in BPD	**AUC in HC**	**p-Value**
R.INS ↑	19.6600	0.3600	0.0322

Table 5.38: Nodes within the limbic SC subnetwork whose betweenness centrality presents significant variations (p-Value<0.05) between patients and controls.

Finally, from the point of view of efficiency in local information transfer, no significant deviations were detected neither in the limbic system.
Combining these findings, we can state that the separate study of the two lobes did not provide new observations within the SC frame. Moreover, between the two systems, a clear difference in terms of statistically significant results did not emerge.

Females-only network

Global properties

The global results obtained by the comparison of female patients and controls are very

similar to those retrieved from the full set of subjects. The main difference regards the efficiency in distant information transfer, represented by the measures of characteristic path length and global efficiency: if the full networks showed a difference between BPDs and HCs, even though it was not statistically significant, within the subset of females only such difference is even reduced, as it can be seen from Fig. 5.35. This could suggest that healthy male subjects may show higher global efficiency in SC networks with respect to BPD ones; nevertheless the numbers involved in this study are too low to make inferential statistic in this sense.

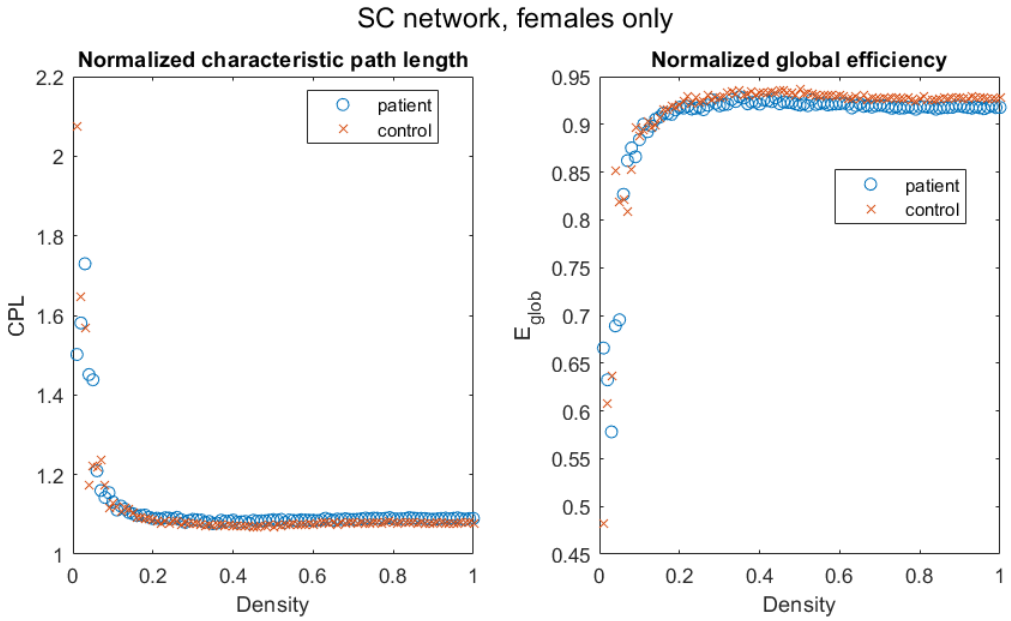

Figure 5.35: Normalized characteristic path length and global efficiency as a function of density in patients and controls, in the SC networks of females only.

As one can deduce from the considerations described above, it is evident that also for the subset of females only there is not a statistically significant difference between the global properties of the SC networks of patients and controls.

Local properties

Since the differences between patients and controls were found reduced at a global level, it should be expected that also from the local perspective the outcomes would not provide many statistically significant variations. This was actually verified, as it is shown in this paragraph, and none of the deviations between BPDs and HCs could pass the FDR correction.

Centrality measures The degree and strength were significantly varied only in the left caudate nucleus, as it is reported in Tab. 5.39 and 5.40, which previously appeared only in the analysis of altered connections, as the weight of its link with the right caudate nucleus was found to be significantly increased in patients. The sign of the variation is in accord with this observation.

The betweenness centrality returned again deviating results with respect to degree and strength, which are collected in Tab. 5.41. It is possible to note the presence of the right

	Degree - females SCN		
	AUC in BPD	**AUC in HC**	**p-Value**
L.CAU ↑	6.4700	1.8400	0.0259

Table 5.39: Nodes within the SC subnetwork of females subjects, whose degree presents significant variations (p-Value<0.05) between patients and controls.

	Degree - females SCN		
	AUC in BPD	**AUC in HC**	**p-Value**
L.CAU ↑	3.4357	0.9760	0.0382

Table 5.40: Nodes within the SC subnetwork of females subjects, whose strength presents significant variations (p-Value<0.05) between patients and controls.

amygdala, which was often found to be varied in this study, and the right hippocampus, which emerged also from the analysis of all subjects.

	Betweenness centrality - females SCN		
	AUC in BPD	**AUC in HC**	**p-Value**
R.AMY ↑ (5)	57.4700	0.2300	0.0257
R.HIP ↑ (5)	126.1400	7.0800	0.0434

Table 5.41: Nodes within the SC subnetwork of females subjects, whose betweenness centrality presents significant variations (p-Value<0.05) between patients and controls.

Module-related measures The participation coefficient, in Fig. 5.42, is the measure which presents the highest number of variations and also the most significant ones, even if none passing the FDR. The quantity is mostly increased in patients and the limbic system is mainly involved. Within the latter, the left entorhinal cortex is the only region which was found modified also in the participation coefficient of the all-subjects network, but it is meaningful also to underline the presence of the amygdala and the right isthmus of cingulate gyrus, whose p-Values are particularly low.

	Participation coefficient - females SCN		
	AUC in BPD	**AUC in HC**	**p-Value**
R.PostCG ↑ (2)	0.1652	0.0744	0.0185
L.AMY ↑ (5)	0.1658	0.0069	0.0044
L.ENTH ↑ (5)	0.1372	0.0179	0.0350
R.AMY ↑ (5)	0.1719	0.0168	0.0085
R.iC ↓ (5)	0.0259	0.1655	0.0033
L.PUT ↑ (6)	0.1398	0.0241	0.0342

Table 5.42: Nodes within the SC subnetwork of females subjects, whose participation coefficient presents significant variations (p-Value<0.05) between patients and controls.

The within-module strength, in Tab. 5.43 does not provide as numerous results, yet note that left lateral occipital sulcus was present also among the significant variations of the same measures in the full SC network.

	Within-module strength - females SCN		
	AUC in BPD	**AUC in HC**	**p-Value**
L.LOC ↓ (3)	0.3449	1.9388	0.0284
R.MoF ↓ (5)	0.2106	1.4982	0.0406

Table 5.43: Nodes within the SC subnetwork of females subjects, whose within-module strength presents significant variations (p-Value<0.05) between patients and controls.

Local efficiency measures From the local efficiency and the clustering coefficient, reported respectively in Tab. 5.44 and 5.45, only one ROI per measure emerged: the left lateral occipital sulcus for the first and the right amygdala for the second. Also in this case, these regions were not found to be varied in the full SC network.

	Local efficiency - females SCN		
	AUC in BPD	**AUC in HC**	**p-Value**
L.LOC ↓ (3)	0.0476	0.1155	0.0431

Table 5.44: Nodes within the SC subnetwork of females subjects, local efficiency presents significant variations (p-Value<0.05) between patients and controls.

	Clustering coefficient - females SCN		
	AUC in BPD	**AUC in HC**	**p-Value**
R.AMY ↓ (5)	0.0543	0.1149	0.0408

Table 5.45: Nodes within the SC subnetwork of females subjects, clustering coefficient presents significant variations (p-Value<0.05) between patients and controls.

To summarize the results for the SC networks retrieved from female subjects only, we can observe that, also in this case, there is not a strong significance in the difference between patients and controls. Moreover, there is not a strong accord with the results found in the full FC network, even if some results are repeated. Nevertheless, there is a certain degree of consistency among the outcomes of the females-only network alone, in particular regarding some nodes, such as the right amygdala.

5.3 Correlation with the clinical scores

As described in section 4.7, an exploratory analysis of the correlation of the clinical scores with the AUCs of the topological measures was performed global. In particular, the properties selected for this investigation were the global measures that resulted significantly varied and the local ones which also passed the FDR correction.
In this section, the reported results consist of the partial correlation coefficients (ρ) and their p-Values, under two different conditions. The first was to look for a single correlation through the data of all subjects, recalling that only the scores of BIS, DERS, ARS, SHI and RRS could be investigated in this sense, since those are available for both BPDs and HCs. The second condition was to explore correlations separately for patients and controls: in this case, also the BDI and WSAS scores of patients were included. This was repeated for all the types of the FC networks, except for the occipital one, which was previously proven not to be significant.

In the tables of correlations and p-Values, to help the visualization, the combinations that were found to be statistically significant are written in bold characters, and those that passed the FDR are also written in italic. For simplicity, the plots of the linear regressions between the clinical scores and the AUC of the measures are shown only for those combinations that were found to be statistically significant in both the cases of all subjects merged into a single group and of patients or controls separately. The reason behind this choice is that the correlations across all subjects were, in several cases, clearly biased, even if they passed the FDR correction, because of the net separation of patients and controls due especially to the deviation in their clinical scores: the verification of the existence of a correlation in the two types of evaluations, therefore, is considered as a consolidation of the results, so that such outcomes are considered the most reliable. To show this issue, only the plots related to the global properties across all subjects are reported for the full FC network, as an exception to the rule described above.
Additionally, note that the correlations with the SHI scale were considered reliable only when present in patients, because among controls there was an evident bias, due to the fact that most of them scored 0, the minimum value, in this clinical evaluation. As it will be more clear by looking at the images related to this scale, reported in this section, this made the correlations involving SHI in HCs evidently artificial.
This extended analysis has allowed to characterize the relationship between the networks measures and the clinical scores in both the groups of subjects. Results suggest possible future directions in the correlation analysis.

5.3.1 All subjects

Full FC network

Global measures

The partial correlation coefficients of the global measures in the full FC network with the clinical scores across all subjects are reported in Tab. 5.46, along with the corresponding p-Values.
The DERS correlates significantly and negatively with the normalized average correlation coefficient and the modularity coefficient, and also RRS does with the latter. From the corresponding plots in Fig. 5.36 and Fig. 5.37, it is quite evident that the correlation is actually due to the considerable difference of the clinical score between patients and controls, as it can be deduced from the fact that the line separates almost perfectly BPDs from HCs. This issue, which invalidates the reliability of the correlations, was observed frequently throughout the analysis across all subjects, as mentioned above.

Local measures

Concerning the local measures, the ones that presented p-Values that passed the FDR correction in the full FC networks were the betweenness centrality, the participation coefficient, the local efficiency and the clustering coefficient.

Betweenness centrality The results in terms of correlation of the betweenness centrality are reported in Tab. 5.47. As it can be seen, the betweenness centrality of the only node that passed the FDR for that property, not only significantly correlates with all the clinical scores across all subjects with negative slope, but also all the correlations passed the FDR correction.

	Partial correlation				
	BIS	**DERS**	**ARS**	**SHI**	**RRS**
E_{loc}	-0.0383	-0.2478	-0.1027	-0.1134	-0.2217
CC	-0.0875	**-0.2864**	-0.1318	-0.1586	-0.2678
SW	-0.0608	-0.2156	-0.1085	-0.1150	-0.2069
$LCCsize$	0.0023	-0.2032	-0.0849	-0.0727	-0.1672
Q	-0.1876	**-0.3208**	-0.1581	-0.2067	**-0.3143**
	p-Value				
	BIS	**DERS**	**ARS**	**SHI**	**RRS**
E_{loc}	0.7856	0.0737	0.4642	0.4186	0.1105
CC	0.5334	**0.0376**	0.3470	0.2567	0.0525
SW	0.6656	0.1210	0.4391	0.4121	0.1371
$LCCsize$	0.9869	0.1446	0.5456	0.6051	0.2315
Q	0.1786	**0.0192**	0.2580	0.1375	**0.0219**

Table 5.46: Partial correlation coefficients and corresponding p-Values of the AUCs of the global measures in the full FC network with the clinical scores, across all subjects. The combinations that were found to be statistically significant are written in bold characters.

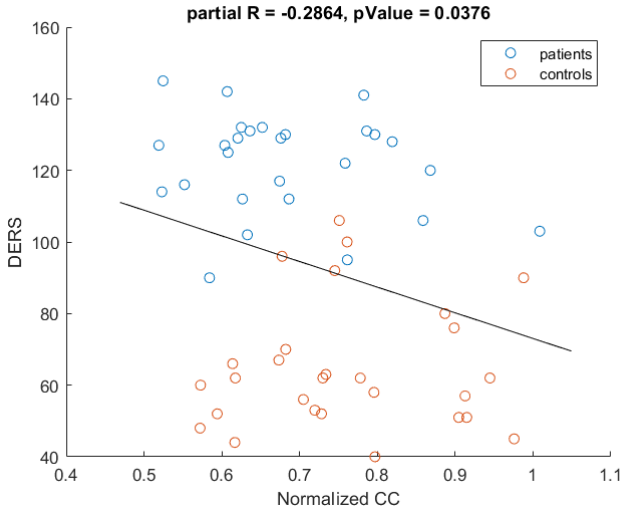

Figure 5.36: Correlation of the DERS with the average normalized clustering coefficient in the full FC network, across all subjects.

Referring to Fig. 5.38, the correlation appear to be quite consistent; nevertheless, it is clear that the coefficient would have very different values when considering patients and controls separately.

Participation coefficient For the participation coefficient, two ROIs passed the FDR: the right amygdala and the right rostral middle frontal gyrus.
The correlation coefficients and the p-Values, reported in Tab. 5.48, show that all the clinical scores negatively correlates with the participation coefficient of the amygdala with a significant p-Value; on the other hand, only the BIS and the DERS do with the rostral middle frontal gyrus, but those positive correlations are also statistically verified after the FDR correction. In this case, no correspondence was found in patients or

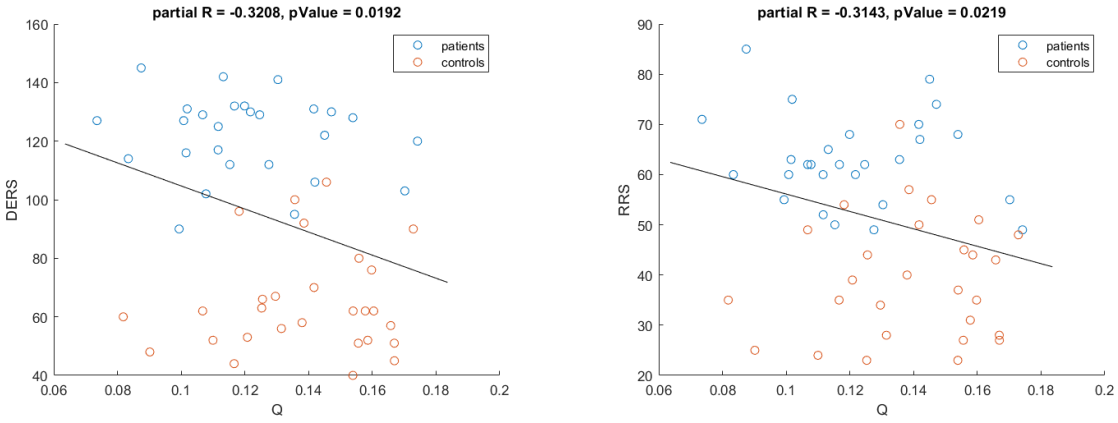

(a) *(b)*

Figure 5.37: Correlation of BIS and DERS with the modularity coefficient in the full FC network, across all subjects.

BC - Full FCN					
	Partial correlation				
	BIS	**DERS**	**ARS**	**SHI**	**RRS**
L.SP (2)	***-0.4337***	***-0.4757***	***-0.3443***	***-0.3602***	***-0.3906***
	p-Value				
	BIS	**DERS**	**ARS**	**SHI**	**RRS**
L.SP (2)	***0.0012***	***0.0003***	***0.0116***	***0.0081***	***0.0038***

Table 5.47: Partial correlation coefficients and corresponding p-Values of the nodal AUCs of the betweenness centrality in the full FC network with the clinical scores, across all subjects. The combinations that were found to be statistically significant are written in bold characters, and those that passed the FDR are also written in italic.

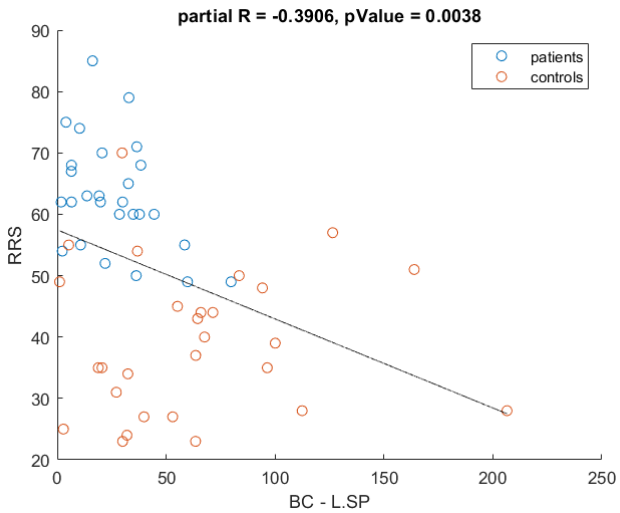

Figure 5.38: Correlation of RRS with the betweenness centrality of the left superior parietal lobule in the full FC network, across all subjects.

controls separately

PC - Full FCN					
	Partial correlation				
	BIS	**DERS**	**ARS**	**SHI**	**RRS**
R.rMF (1)	***0.4299***	***0.4032***	0.2645	0.2629	0.2641
R.AMY (5)	**-0.3044**	**-0.3422**	**-0.3196**	**-0.3264**	**-0.2873**
	p-Value				
	BIS	**DERS**	**ARS**	**SHI**	**RRS**
R.rMF (1)	***0.0013***	***0.0028***	0.0556	0.0572	0.0560
R.AMY (5)	**0.0267**	**0.0121**	**0.0197**	**0.0171**	**0.0370**

Table 5.48: Partial correlation coefficients and corresponding p-Values of the nodal AUCs of the participation coefficient in the full FC network with the clinical scores, across all subjects.

Local efficiency The left temporal pole is the only region that passed the FDR correction in local efficiency. The correlations in Tab. 5.49 show that DERS, SHI and RRS negatively correlate with the AUCs of the local efficiency of the region, and the first two also passed the FDR.
Also in this case there was no correspondence with the separate evaluations.

E_{loc} *- Full FCN*					
	Partial correlation				
	BIS	**DERS**	**ARS**	**SHI**	**RRS**
L.TP (4)	-0.1869	***-0.4147***	-0.2247	***-0.3395***	**-0.3078**
	p-Value				
	BIS	**DERS**	**ARS**	**SHI**	**RRS**
L.TP (4)	0.1803	***0.0020***	0.1057	***0.0129***	**0.0250**

Table 5.49: Partial correlation coefficients and corresponding p-Values of the nodal AUCs of the local efficiency in the full FC network with the clinical scores, across all subjects.

Clustering coefficient Finally, the clustering coefficient had three nodes that satisfied the criterion of FDR: the left temporal pole and the bilateral transverse temporal gyrus. Consistently with the results obtained for the local efficiency, the correlations are found only with DERS, SHI and RRS, as it is reported in Tab. 5.50. In particular, they are negative for the temporal pole, and positive for the transverse temporal gyrus.
Among these, the only combination that passed the FDR is the clustering coefficient of the left temporal pole with the DERS, similarly to the outcomes obtained for local efficiency: the same comments can be extended to this case.

Finally, it is meaningful to underline that the sign of the correlations is consistent with the sign of the variations between patients and controls: since the clinical scales are built so that the scores increase with the severity of the conditions, positive correlations correspond to the increment of the topological measure in BPDs, whereas the opposite occurs for the negative ones.

CC - Full FCN					
	Partial correlation				
	BIS	**DERS**	**ARS**	**SHI**	**RRS**
L.TP (4)	-0.2003	***-0.4154***	-0.2268	**-0.3389**	**-0.3153**
L.TT (4)	0.2323	**0.3713**	0.2312	**0.3513**	**0.2838**
R.TT (4)	0.2410	**0.3564**	0.2570	**0.3013**	**0.2921**
	p-Value				
	BIS	**DERS**	**ARS**	**SHI**	**RRS**
L.TP (4)	0.1504	***0.0020***	0.1024	**0.0131**	**0.0215**
L.TT (4)	0.0942	**0.0062**	0.0957	**0.0099**	**0.0394**
R.TT (4)	0.0822	**0.0088**	0.0632	**0.0283**	**0.0338**

Table 5.50: Partial correlation coefficients and corresponding p-Values of the nodal AUCs of the clustering coefficient in the full FC network with the clinical scores, across all subjects.

Limbic subnetwork

In the limbic subnetwork, the only significant variations that passed the FDR were within the local measures of degree and strength. In particular, the regions of interest in this sense were the same for both the properties: the bilateral caudal anterior cingulate cortex, the bilateral amygdala and the left entorhinal cortex.
All the correlations with the clinical scores and their p-Values are collected in Tab. 5.51 and 5.52 for degree and strength respectively. All the nodes show significant correlations with various clinical scores, in particular the left caudal anterior cingulate cortex and the right amygdala and posterior cingulate cortex. The latter is the only one which presents a correlation that passed the FDR correction, i.e. the one with DERS, which is plotted in Fig. 5.39, as it is verified also for patients and controls separately. In this case, even if the line separates quite well patients and controls, it appears that the positive trend persists in patients and controls separately.

Finally, from the point of view of the clinical scores the DERS is definitely the one that correlates the most with these centrality measures.

Deg - Limbic FCN					
	Partial correlation				
	BIS	**DERS**	**ARS**	**SHI**	**RRS**
L.cAC (5)	**0.2906**	**0.3285**	**0.3617**	**0.3093**	0.2080
L.ENTH (5)	-0.2639	**-0.3033**	-0.1939	-0.2236	-0.1269
L.PC (5)	0.2302	**0.3434**	0.1826	0.2302	0.2347
R.AMY (5)	**-0.3816**	**-0.3542**	**-0.3292**	-0.2119	**-0.3033**
R.cAC (5)	**0.3264**	**0.2935**	**0.3253**	0.2013	0.2464
R.PC (5)	0.1656	***0.4453***	**0.2954**	**0.3107**	**0.3743**
	p-Value				
	BIS	**DERS**	**ARS**	**SHI**	**RRS**
L.cAC (5)	**0.0348**	**0.0163**	**0.0078**	**0.0242**	0.1351
L.ENTH (5)	0.0562	**0.0273**	0.1643	0.1074	0.3652
L.PC (5)	0.0973	**0.0118**	0.1907	0.0972	0.0907
R.AMY (5)	**0.0048**	**0.0093**	**0.0161**	0.1277	**0.0273**
R.cAC (5)	**0.0171**	**0.0329**	**0.0175**	0.1484	0.0753
R.PC (5)	0.2360	***0.0008***	**0.0318**	**0.0236**	**0.0058**

Table 5.51: Partial correlation coefficients and corresponding p-Values of the nodal AUCs of the degree within the limbic FC network with the clinical scores, across all subjects.

Str - Limbic FCN					
	Partial correlation				
	BIS	**DERS**	**ARS**	**SHI**	**RRS**
L.cAC (5)	0.2226	**0.3126**	**0.2903**	**0.3391**	0.1948
L.ENTH (5)	**-0.2794**	**-0.2968**	-0.1903	-0.2063	-0.1137
L.PC (5)	0.1628	**0.3306**	0.1693	**0.2753**	0.2422
R.AMY (5)	**-0.3920**	**-0.3344**	**-0.3191**	-0.1535	**-0.2820**
R.cAC (5)	0.2327	**0.2883**	0.2433	0.2678	0.2317
R.PC (5)	0.0971	**0.3746**	0.2292	**0.3209**	**0.3038**
	p-Value				
	BIS	**DERS**	**ARS**	**SHI**	**RRS**
L.cAC (5)	0.1091	**0.0227**	**0.0350**	**0.0130**	0.1621
L.ENTH (5)	**0.0427**	**0.0309**	0.1724	0.1383	0.4187
L.PC (5)	0.2443	**0.0156**	0.2257	**0.0460**	0.0806
R.AMY (5)	**0.0037**	**0.0144**	**0.0198**	0.2724	**0.0408**
R.cAC (5)	0.0935	**0.0363**	0.0792	0.0525	0.0951
R.PC (5)	0.4892	**0.0057**	0.0988	**0.0191**	**0.0270**

Table 5.52: Partial correlation coefficients and corresponding p-Values of the nodal AUCs of the strength within the limbic FC network with the clinical score, across all subjectss.

Scale 4 network

Global measures

At a global level, in the scale 4 of the wavelet-decomposed networks, significant differences were detected for all measures, except for the characteristic path length and the global efficiency. The properties of the correlations of the global quantities with

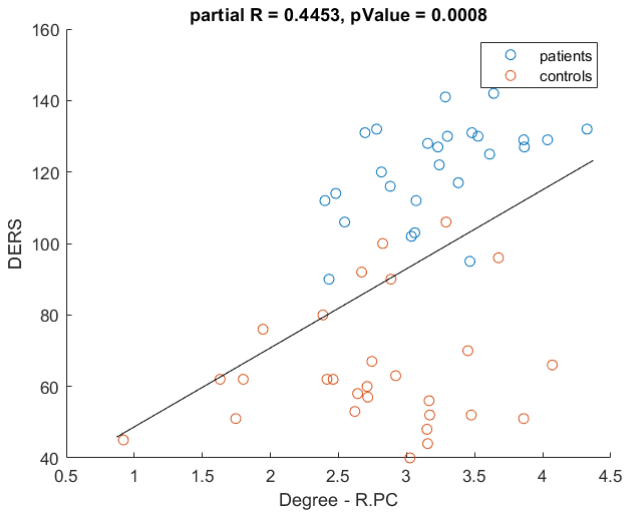

Figure 5.39: Correlation of DERS with the degree of the right posterior cingulate cortex in the limbic FC network, across all subjects.

the clinical scores are reported in Tab. 5.53. All the correlations are negative, since the normalized global quantities were increased in controls in each case, and the largest connected component size is the topological measure that correlates the most with the clinical scores.

	Partial correlation				
	BIS	**DERS**	**ARS**	**SHI**	**RRS**
E_{loc}	-0.1641	-0.2671	-0.2051	-0.2665	-0.1845
CC	-0.2466	**-0.3220**	-0.2300	**-0.3176**	-0.2366
SW	-0.2041	-0.2522	-0.2024	**-0.2809**	-0.1816
$LCCsize$	-0.1352	**-0.3144**	-0.1741	**-0.2940**	**-0.3035**
Q	**-0.3623**	**-0.3799**	-0.2210	**-0.3706**	**-0.3046**
	p-Value				
	BIS	**DERS**	**ARS**	**SHI**	**RRS**
E_{loc}	0.2402	0.0532	0.1406	0.0537	0.1861
CC	0.0751	**0.0187**	0.0976	**0.0205**	0.0880
SW	0.1428	0.0685	0.1462	**0.0416**	0.1931
$LCCsize$	0.3345	**0.0219**	0.2126	**0.0326**	**0.0271**
Q	**0.0077**	**0.0050**	0.1118	**0.0063**	**0.0266**

Table 5.53: Partial correlation coefficients and corresponding p-Values of the AUCs of the global measures in the scale 4 network with the clinical scores, across all subjects.

For several of the relationships investigated here, the same considerations illustrated in the previous paragraphs could be repeated here: it is unclear whether the correlations that emerged are reliable, because of a certain degree of separation between patients and controls.

Local measures

At local level, the scale 4 networks presented the most numerous and significant variations in degree and strength, but also in betweenness centrality and within-module strength some regions passing the FDR were detected.

Degree Tab. 5.54 collects the correlation coefficients between the degree and the clinical scores, with their p-Values. Note that in this case the statistically significant outcomes are more than half of the total combinations, and a considerable number of the latter also passed the FDR correction.
The left and right frontal poles are the only regions that do not show correlations with the clinical scores. On the other hand, the bilateral amygdala and the right pars orbitalis present correlations with all the neuro-psychological scales, and among the most significant ones, even if the lowest p-Value is associated to the correlation of the degree of the left inferior temporal gyrus with the SHI.
Also in this case, the DERS is the score that appears to correlate the most with the degree and provides also some of the lowest p-Values in this sense. On the opposite side, the ARS is the scale that correlates less with the topological measures, and none of the statistically significant results passed the FDR.

Among all the statistically significant correlations, only two found their correspondence in patients or controls separately: the one with the left inferior temporal gyrus, in Fig. 5.40, and the one with the right thalamus in Fig. 5.41.

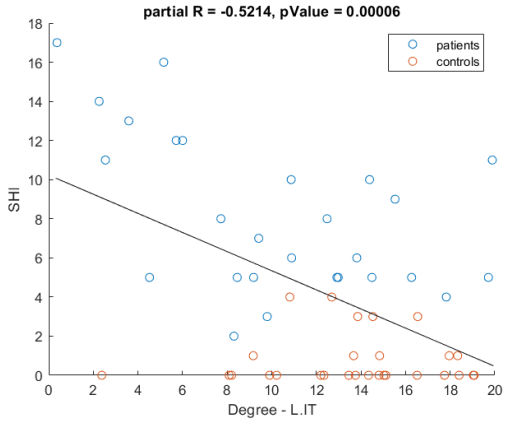

Figure 5.40: Correlation of SHI with the degree of the left inferior temporal gyrus in the scale 4 network, across all subjects.

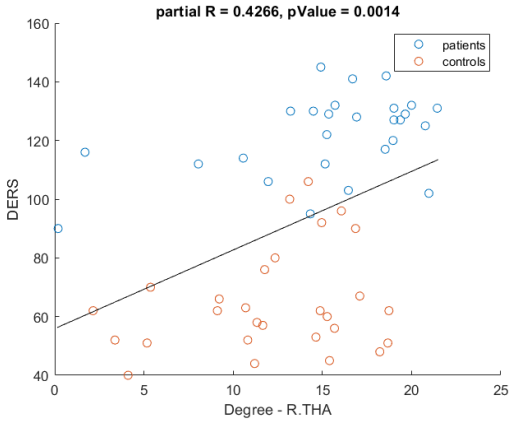

Figure 5.41: Correlation of DERS with the degree of the right thalamus in the scale 4 network, across all subjects.

Deg - Scale 4 FCN					
	Partial correlation				
	BIS	**DERS**	**ARS**	**SHI**	**RRS**
L.FP (1)	-0.2489	-0.2167	-0.1300	-0.1439	-0.2309
R.FP (1)	-0.2172	-0.1988	-0.1892	-0.1630	-0.2087
R.parsOR (1)	***-0.4532***	***-0.4417***	**-0.3331**	***-0.4567***	***-0.3948***
L.LING (3)	**0.3166**	0.2452	0.1232	***0.3563***	**0.3323**
R.LING (3)	**0.3382**	**0.2961**	0.2151	0.2485	***0.3805***
L.IT (4)	***-0.3840***	**-0.3408**	-0.2047	***-0.5214***	-0.1110
L.MT (4)	***-0.4396***	***-0.3866***	-0.1954	-0.2686	**-0.3389**
L.TP (4)	**-0.2908**	***-0.4029***	-0.2433	**-0.2999**	**-0.3223**
L.AMY (5)	**-0.2846**	***-0.3579***	**-0.3317**	**-0.2772**	***-0.4107***
L.cAC (5)	0.2182	0.2465	**0.3024**	0.1861	0.1970
L.MoF (5)	-0.2446	**-0.3103**	**-0.2773**	**-0.2800**	**-0.2814**
L.PC (5)	0.2400	***0.3606***	0.1288	**0.3093**	***0.3601***
R.AMY (5)	***-0.4224***	***-0.4196***	**-0.3454**	**-0.3192**	***-0.3787***
R.cAC (5)	***0.4468***	***0.3567***	**0.3156**	0.2647	**0.3222**
R.ENTH (5)	-0.2233	**-0.2901**	-0.1732	-0.2209	-0.2668
R.INS (5)	0.2669	***0.3707***	**0.3338**	**0.3194**	**0.3266**
R.THA (6)	**0.3382**	***0.4266***	0.2508	**0.3227**	**0.3084**
	p-Value				
	BIS	**DERS**	**ARS**	**SHI**	**RRS**
L.FP (1)	0.0723	0.1192	0.3535	0.3040	0.0963
R.FP (1)	0.1183	0.1537	0.1749	0.2435	0.1336
R.parsOR (1)	***0.0007***	***0.0009***	**0.0148**	***0.0006***	***0.0034***
L.LING (3)	**0.0209**	0.0768	0.3794	***0.0088***	**0.0150**
R.LING (3)	**0.0133**	**0.0314**	0.1219	0.0728	***0.0049***
L.IT (4)	***0.0045***	**0.0125**	0.1414	***0.0001***	0.4286
L.MT (4)	***0.0010***	***0.0042***	0.1608	0.0518	**0.0130**
L.TP (4)	**0.0347**	***0.0028***	0.0791	**0.0291**	**0.0186**
L.AMY (5)	**0.0389**	***0.0085***	**0.0152**	**0.0445**	***0.0023***
L.cAC (5)	0.1166	0.0751	**0.0278**	0.1821	0.1575
L.MoF (5)	0.0775	**0.0237**	**0.0444**	**0.0423**	**0.0412**
L.PC (5)	0.0834	***0.0080***	0.3578	**0.0242**	***0.0081***
R.AMY (5)	***0.0016***	***0.0018***	**0.0113**	**0.0198**	***0.0052***
R.cAC (5)	***0.0008***	***0.0088***	**0.0213**	0.0554	**0.0186**
R.ENTH (5)	0.1080	**0.0351**	0.2149	0.1119	0.0534
R.INS (5)	0.0534	***0.0063***	**0.0146**	**0.0198**	**0.0170**
R.THA (6)	**0.0133**	***0.0014***	0.0701	**0.0184**	**0.0247**

Table 5.54: Partial correlation coefficients and corresponding p-Values of the nodal AUCs of the degree in the scale 4 network with the clinical scores, across all subjects.

Strength The correlations of the clinical scores with the strengths reflect what was found for the degree, as it can be seen from Tab. 5.55: the right amygdala and, in particular, the right pars orbitalis are the two regions which correlate most significantly with the neuro-psychological scales, even though in this case even more combinations have a p-Value inferior to 0.05, also after the FDR correction. It is meaningful to observe that, beside the DERS, which was already found to be strongly related to the degree, also the RRS shows significant correlations with the strengths of every node involved.

Str - Scale 4 FCN					
	Partial correlation				
	BIS	**DERS**	**ARS**	**SHI**	**RRS**
R.parsOR (1)	***-0.4410***	***-0.4099***	**-0.3197**	***-0.4346***	***-0.3704***
L.LING (3)	**0.3093**	**0.2737**	0.1195	***0.3879***	***0.3514***
R.LING (3)	**0.3213**	**0.3241**	0.1918	**0.2874**	***0.4020***
L.TP (4)	-0.2672	***-0.3738***	-0.2253	-0.2506	**-0.2886**
L.AMY (5)	**-0.2754**	***-0.3324***	**-0.3214**	-0.2142	***-0.3792***
L.MoF (5)	**-0.2933**	***-0.3315***	**-0.3099**	**-0.2823**	**-0.2830**
L.PC (5)	0.2345	***0.3718***	0.1249	***0.3497***	***0.3525***
R.AMY (5)	***-0.3959***	***-0.3849***	**-0.3255**	-0.2617	***-0.3435***
R.cAC (5)	***0.3941***	***0.3725***	0.2603	**0.3106**	**0.3178**
R.INS (5)	0.2562	***0.4014***	**0.2999**	***0.3664***	***0.3365***
R.THA (6)	**0.3271**	**0.4245**	0.2154	***0.3425***	**0.3009**
	p-Value				
	BIS	**DERS**	**ARS**	**SHI**	**RRS**
R.parsOR (1)	***0.0009***	***0.0023***	**0.0196**	***0.0011***	***0.0063***
L.LING (3)	**0.0242**	**0.0473**	0.3940	***0.0041***	***0.0099***
R.LING (3)	**0.0190**	**0.0179**	0.1688	**0.0369**	***0.0029***
L.TP (4)	0.0531	***0.0058***	0.1049	0.0704	**0.0361**
L.AMY (5)	**0.0459**	***0.0150***	**0.0189**	0.1235	***0.0051***
L.MoF (5)	**0.0331**	***0.0153***	**0.0239**	**0.0406**	**0.0401**
L.PC (5)	0.0910	***0.0061***	0.3729	***0.0103***	***0.0096***
R.AMY (5)	***0.0033***	***0.0044***	**0.0174**	0.0583	***0.0118***
R.cAC (5)	***0.0035***	***0.0060***	0.0597	**0.0236**	**0.0204**
R.INS (5)	0.0640	***0.0029***	**0.0291**	***0.0070***	***0.0137***
R.THA (6)	**0.0168**	***0.0015***	0.1213	***0.0121***	**0.0286**

Table 5.55: Partial correlation coefficients and corresponding p-Values of the nodal AUCs of the strength in the scale 4 network with the clinical scores, across all subjects.

In this case, only one interpolation was significant also for patients or controls separately, i.e. the one of the strength of the right lingual gyrus with RRS, reported in Fig. 5.42.

Betweenness centrality The only node to present significant variations in betweenness centrality is the right inferior temporal gyrus, whose correlations with the clinical scores can be found in Tab. 5.56. The quantity negatively correlates with BIS, DERS and RRS; among these, the first and the third also passed the FDR correction. Also in this case no correspondence with the results of patients and controls were identified.

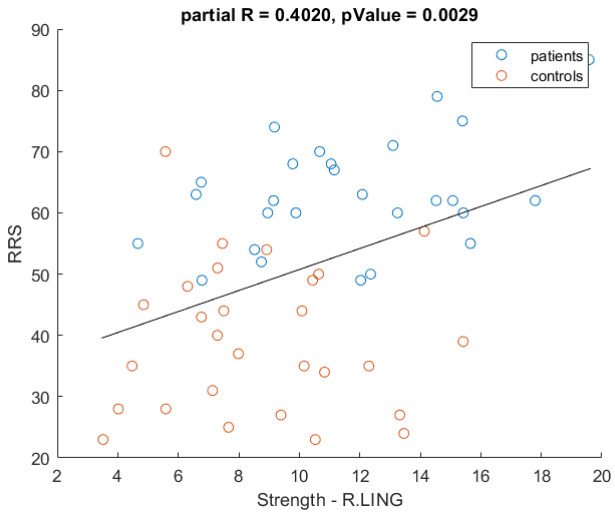

Figure 5.42: Correlation of RRS with the strength of the right lingual gyrus in the scale 4 network, across all subjects.

BC - Scale 4 FCN					
	Partial correlation				
	BIS	**DERS**	**ARS**	**SHI**	**RRS**
R.IT (4)	***-0.3993***	**-0.3028**	-0.2565	-0.1999	***-0.3723***
	p-Value				
	BIS	**DERS**	**ARS**	**SHI**	**RRS**
R.IT (4)	***0.0031***	**0.0275**	0.0638	0.1512	***0.0060***

Table 5.56: Partial correlation coefficients and corresponding p-Values of the AUC of the betweenness centrality of the right inferior temporal gyrus in the scale 4 network with the clinical scores, across all subjects.

Within-module strength Regarding the within-module strength, the nodes involved were the left temporal pole and the right amygdala. For the first region, the quantity correlates with all the clinical scores, whereas for the second it does not correlate with SHI. Nonetheless, in the latter case, the p-Values tend to be considerably lower, as it is reported in Tab. 5.57. Note that the lowest p-Values correspond again to the correlations with DERS and RRS.
Even for this measure, no correspondence were detected with the case of the separate evaluation of patients and controls.

As a final comment on these results, the partial correlations between the topological measures and the clinical scores, even if statistically significant, are not particularly strong: their absolute values overcome 0.5 only in one case (the degree of the left inferior temporal gyrus in the scale 4 network with the SHI) and rarely pass 0.4.

modStr - Scale 4 FCN					
	Partial correlation				
	BIS	**DERS**	**ARS**	**SHI**	**RRS**
L.TP (4)	**-0.3333**	***-0.4359***	**-0.2982**	**-0.3296**	***-0.4039***
R.AMY (5)	***-0.4464***	***-0.4823***	***-0.4032***	-0.2580	***-0.4119***
	p-Value				
	BIS	**DERS**	**ARS**	**SHI**	**RRS**
L.TP (4)	**0.0148**	***0.0011***	**0.0301**	**0.0159**	***0.0027***
R.AMY (5)	***0.0008***	***0.0003***	***0.0028***	0.0622	***0.0022***

Table 5.57: Partial correlation coefficients and corresponding p-Values of the nodal AUCs of the within-module strength in the scale 4 network with the clinical scores, across all subjects.

5.3.2 Patients and controls separately

Full FC network

Global measures

The correlation tables related to the global measures are presented separately for patients and controls in Tab. 5.58.
The first aspect that emerge is that the correlations behave differently with respect to the evaluation for all the subjects as one group: in this case, in fact, the results exhibit considerably more relationships between the global measures and the clinical scores. In particular, the statistically significant relationships found involve mainly BIS, ARS and SHI, whereas the DERS, which was clearly the most meaningful scale in the previous case, here appears to be not as important.
Moreover, there is also an evident difference between patients and controls: their global measures, in fact, correlate with different clinical scores. The ones of BPDs tend to correlate with BIS and ARS, whereas those of control with SHI. Nevertheless, the latter are clearly artificial and emerge only because of the fact that many healthy controls scored 0 in the SHI scale.
It is worth to underline that such correlations in patients are all positive, while in controls, even if not statistically significant, they are $\sim$0 for BIS and negative for ARS, thus the same trend is not reproduced within the two groups. The only exception is given by the modularity coefficient, for which also BIS correlates negatively in controls.

Local measures

Betweenness centrality Recalling that the betweenness centrality showed only one significant variation after FDR among nodes, i.e. the left superior parietal lobule, the correlation tables for patients and controls are reported in Tab. 5.59 for patients and controls separately.
The only significant correlation is negative, with RRS, and the plot is reported in Fig. 5.43, since it was present also across all subjects, Nevertheless, note that there is a crucial difference with that case: here, the negative correlation in ensured only in BPDs, whereas HCs actually present a slightly positive, non-significant one.

BPDs							
	Partial correlation						
	BIS	**DERS**	**ARS**	**SHI**	**RRS**	**BDI**	**WSAS**
E_{loc}	**0.4594**	-0.2336	**0.4596**	0.0720	-0.1621	-0.1680	-0.0312
CC	**0.4504**	-0.2308	**0.4464**	0.0496	-0.1780	-0.1275	0.0084
SW	**0.5046**	-0.1019	**0.4641**	0.0934	-0.1282	-0.1145	-0.0485
$LCCSize$	**0.5626**	-0.0076	0.3937	0.1996	0.0484	-0.1826	-0.2013
Q	**0.4155**	-0.1786	0.3477	0.0597	-0.2412	-0.0801	-0.0110
	p-Value						
	BIS	**DERS**	**ARS**	**SHI**	**RRS**	**BDI**	**WSAS**
E_{loc}	**0.0209**	0.2610	**0.0208**	0.7323	0.4387	0.4326	0.8825
CC	**0.0239**	0.2670	**0.0253**	0.8139	0.3947	0.5526	0.9680
SW	**0.0101**	0.6280	**0.0194**	0.6571	0.5415	0.5942	0.8178
$LCCsize$	**0.0034**	0.9711	0.0515	0.3387	0.8184	0.3932	0.3346
Q	**0.0389**	0.3930	0.0886	0.7768	0.2454	0.7100	0.9583

HCs					
	Partial correlation				
	BIS	**DERS**	**ARS**	**SHI**	**RRS**
E_{loc}	0.0412	0.0964	-0.2541	**0.4573**	0.0439
CC	-0.0359	0.0738	-0.2860	**0.4081**	0.0124
SW	-0.0287	0.1473	-0.2517	**0.4490**	0.0805
$LCCSize$	0.0513	0.1392	-0.1234	**0.4075**	0.0694
Q	-0.2514	0.0616	-0.2129	0.3034	0.0369
	p-Value				
	BIS	**DERS**	**ARS**	**SHI**	**RRS**
E_{loc}	0.8416	0.6394	0.2104	**0.0188**	0.8314
CC	0.8618	0.7200	0.1567	**0.0385**	0.9522
SW	0.8893	0.4728	0.2148	**0.0214**	0.6958
$LCCSize$	0.8033	0.4977	0.5482	**0.0388**	0.7361
Q	0.2155	0.7649	0.2963	0.1319	0.8579

Table 5.58: Partial correlation coefficients and corresponding p-Values of the AUCs of the global measures in the full FC network with the clinical scores, across patients and controls separately.

This is a clear example of what was mentioned in the previous section: the correlations across all subjects are biased by the difference in clinical scores of patients and controls, but the two groups tend to show different behaviors in this sense.

Participation coefficient Among the correlations within patients and controls separately, it was quite rare to observe significant ones with respect to the rate at which they were seen across all subjects. This could already be verified when looking for correlations of the AUCs of the participation coefficient, as it reported in Tab. 5.60: no significant correlations emerged in any combination in both BPDs and HCs.

Local efficiency Also in local efficiency there is only one region involved, the left temporal pole, see Tab. 5.61.

BPDs - BC - Full FCN							
	Partial correlation						
	BIS	**DERS**	**ARS**	**SHI**	**RRS**	**BDI**	**WSAS**
L.SP (2)	0.1882	-0.2124	-0.0237	-0.2311	**-0.4175**	-0.1424	-0.2072
	p-Value						
	BIS	**DERS**	**ARS**	**SHI**	**RRS**	**BDI**	**WSAS**
L.SP (2)	0.3677	0.3080	0.9106	0.2663	**0.0378**	0.5069	0.3202

HCs - BC - Full FCN					
	Partial correlation				
	BIS	**DERS**	**ARS**	**SHI**	**RRS**
L.SP (2)	-0.3340	-0.1773	-0.1028	0.2580	0.0244
	p-Value				
	BIS	**DERS**	**ARS**	**SHI**	**RRS**
L.SP (2)	0.0954	0.3862	0.6174	0.2032	0.9059

Table 5.59: Partial correlation coefficients and corresponding p-Values of the nodal AUCs of the betweenness centrality in the full FC network with the clinical scores, across patients and controls separately.

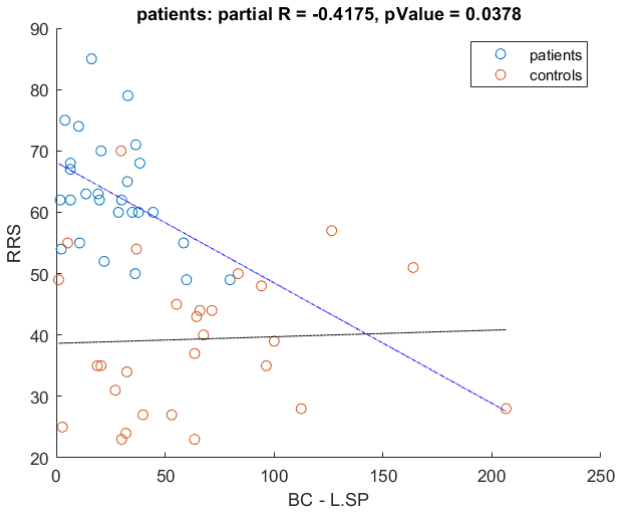

Figure 5.43: Correlation of RRS with the betweenness centrality of the left superior parietal lobule in the full FC network, across patients and controls separately.

In this case, no significant correlations were found in patients, while in controls there was only one with BIS, which also passed the FDR. In this latter case, the correlation in patients, even if not statistically significant, reflects the same trend that is observed in HCs. Nevertheless, the same correlation was not detected across all subjects.

Clustering coefficient Very similarly to local efficiency, as it can be seen from Tab. 5.62, also for the clustering coefficient the only significant correlation found was between the *CC* of the left temporal pole and the BIS of controls. None of the other combinations, in fact, revealed the presence of relationships between the clinical scores and the AUC of the topological measure, neither in patients nor in controls. Moreover, the only correlation detected did not pass the FDR correction.

BPDs - PC - Full FCN							
	Partial correlation						
	BIS	**DERS**	**ARS**	**SHI**	**RRS**	**BDI**	**WSAS**
R.AMY (5)	0.1228	-0.0808	-0.1693	-0.0196	0.1084	-0.3939	-0.2302
R.PC (5)	0.1984	0.1852	0.2031	-0.1408	0.0019	0.0184	0.0610
	p-Value						
	BIS	**DERS**	**ARS**	**SHI**	**RRS**	**BDI**	**WSAS**
R.AMY (5)	0.5587	0.7011	0.4185	0.9260	0.6060	0.0568	0.2682
R.PC (5)	0.3417	0.3753	0.3302	0.5019	0.9930	0.9320	0.7722

HCs - PC - Full FCN					
	Partial correlation				
	BIS	**DERS**	**ARS**	**SHI**	**RRS**
R.AMY (5)	-0.0584	0.1784	0.0195	0.1156	0.0789
R.PC (5)	0.2335	0.0680	-0.2188	0.0098	-0.1341
	p-Value				
	BIS	**DERS**	**ARS**	**SHI**	**RRS**
R.AMY (5)	0.7768	0.3832	0.9246	0.5739	0.7015
R.PC (5)	0.2509	0.7413	0.2828	0.9623	0.5138

Table 5.60: Partial correlation coefficients and corresponding p-Values of the nodal AUCs of the participation coefficient in the full FC network with the clinical scores, across patients and controls separately.

BPDs - E_{loc} - Full FCN							
	Partial correlation						
	BIS	**DERS**	**ARS**	**SHI**	**RRS**	**BDI**	**WSAS**
L.TP (4)	0.0507	-0.2491	0.1575	-0.0073	0.0640	-0.0634	0.0540
	p-Value						
	BIS	**DERS**	**ARS**	**SHI**	**RRS**	**BDI**	**WSAS**
L.TP (4)	0.8098	0.2298	0.4520	0.9725	0.7612	0.7684	0.7975

HCs - E_{loc} - Full FCN					
	Partial correlation				
	BIS	**DERS**	**ARS**	**SHI**	**RRS**
L.TP (4)	***0.5645***	0.2359	0.1218	0.2625	0.1430
	p-Value				
	BIS	**DERS**	**ARS**	**SHI**	**RRS**
L.TP (4)	***0.0027***	0.2460	0.5535	0.1951	0.4859

Table 5.61: Partial correlation coefficients and corresponding p-Values of the nodal AUCs of the local efficiency in the full FC network with the clinical scores, across patients and controls separately.

BPDs - CC - Full FCN							
	Partial correlation						
	BIS	**DERS**	**ARS**	**SHI**	**RRS**	**BDI**	**WSAS**
L.TP (4)	0.0452	-0.2169	0.1768	0.0196	0.0574	-0.0449	0.0367
L.TT (4)	-0.2210	0.1776	-0.2549	0.1659	-0.0760	-0.1731	-0.1585
R.TT (4)	-0.1689	0.1984	-0.2226	0.0904	-0.0967	0.1516	0.1094
	p-Value						
	BIS	**DERS**	**ARS**	**SHI**	**RRS**	**BDI**	**WSAS**
L.TP (4)	0.8301	0.2976	0.3978	0.9258	0.7852	0.8348	0.8617
L.TT (4)	0.2884	0.3957	0.2188	0.4280	0.7182	0.4187	0.4491
R.TT (4)	0.4197	0.3417	0.2849	0.6675	0.6455	0.4795	0.6026

HCs - CC - Full FCN					
	Partial correlation				
	BIS	**DERS**	**ARS**	**SHI**	**RRS**
L.TP (4)	**0.5396**	0.2192	0.0976	0.2185	0.1359
L.TT (4)	-0.0824	-0.1095	0.0752	-0.2530	-0.0487
R.TT (4)	-0.0358	-0.1107	0.0790	-0.2181	-0.0089
	p-Value				
	BIS	**DERS**	**ARS**	**SHI**	**RRS**
L.TP (4)	**0.0044**	0.2821	0.6354	0.2835	0.5081
L.TT (4)	0.6891	0.5944	0.7150	0.2124	0.8132
R.TT (4)	0.8621	0.5903	0.7014	0.2844	0.9655

Table 5.62: Partial correlation coefficients and corresponding p-Values of the nodal AUCs of the clustering coefficient in the full FC network with the clinical scores, across patients and controls separately.

Limbic subnetwork

Degree and strength The degree revealed only one significant correlation in patients, in the right posterior cingulate cortex with DERS, as it was already hypothesized by looking at Fig. 5.39. In Fig. 5.44, it is in fact shown the existence of a positive correlation, which is statistically significant only in patients (ρ=0.5152, p-Value=0.0084), but is also present in controls.
Among HCs three significant relationships were revealed, two of which with SHI within left entorhinal and left posterior cingulate cortices (which again were clearly biased by the fact that most of the controls score 0, the minimum value for that scale) and the last, positive, with RRS within the left entorhinal cortex; the latter, nonetheless, is associated to a p-Value of 0.0433, which is not low enough to pass the FDR correction. The results summarizing the degree are collected in Tab.5.63.
Also the strength shows similar outcomes, as it can be seen from Tab. 5.64, where the only significant correlation in patients is again within the right anterior cingulate cortex with DERS, but in this case it is not as significant (p-Value=0.0395), and in controls it is within the left entorhinal cortex, again with the SHI.

BPDs - Deg - Limbic FCN							
	Partial correlation						
	BIS	**DERS**	**ARS**	**SHI**	**RRS**	**BDI**	**WSAS**
L.cAC	0.1947	0.0488	0.2956	0.2051	-0.2871	-0.1146	0.0488
L.ENTH	-0.1517	-0.3601	-0.0324	-0.0025	-0.0088	-0.2465	-0.1920
L.PC	0.0694	0.3680	-0.1371	0.0640	0.2679	0.1791	-0.1626
R.AMY	-0.1968	0.0072	-0.1701	0.2016	-0.1964	-0.1323	-0.2180
R.cAC	0.1978	-0.1235	0.1764	-0.0959	-0.1299	-0.2068	0.2076
R.PC	-0.1306	**0.5152**	-0.1313	0.1835	0.3136	0.2229	-0.0333
	p-Value						
	BIS	**DERS**	**ARS**	**SHI**	**RRS**	**BDI**	**WSAS**
L.cAC	0.3511	0.8169	0.1514	0.3254	0.1641	0.5938	0.8168
L.ENTH	0.4690	0.0770	0.8777	0.9905	0.9666	0.2455	0.3578
L.PC	0.7416	0.0703	0.5135	0.7611	0.1954	0.4024	0.4375
R.AMY	0.3456	0.9729	0.4163	0.3338	0.3467	0.5378	0.2951
R.cAC	0.3433	0.5565	0.3990	0.6485	0.5361	0.3322	0.3194
R.PC	0.5339	**0.0084**	0.5315	0.3799	0.1269	0.2951	0.8744

HCs - Deg - Limbic FCN					
	Partial correlation				
	BIS	**DERS**	**ARS**	**SHI**	**RRS**
L.cAC	-0.0320	0.0584	0.0732	-0.1897	0.0504
L.ENTH	0.0776	0.2733	0.1760	**0.4136**	**0.3993**
L.PC	-0.1324	-0.0676	-0.0375	**-0.4081**	-0.1816
R.AMY	-0.1638	-0.0677	-0.0766	0.1319	0.0670
R.cAC	0.0716	0.0525	0.0810	-0.1796	0.0746
R.PC	-0.2193	0.1066	0.1888	-0.2587	0.0895
	p-Value				
	BIS	**DERS**	**ARS**	**SHI**	**RRS**
L.cAC	0.8766	0.7769	0.7222	0.3532	0.8070
L.ENTH	0.7064	0.1767	0.3898	**0.0357**	**0.0433**
L.PC	0.5192	0.7426	0.8557	**0.0385**	0.3745
R.AMY	0.4238	0.7425	0.7100	0.5206	0.7451
R.cAC	0.7281	0.7989	0.6942	0.3800	0.7171
R.PC	0.2819	0.6044	0.3556	0.2019	0.6637

Table 5.63: Partial correlation coefficients and corresponding p-Values of the nodal AUCs of the degree in the limbic FC network with the clinical scores, across patients and controls separately.

BPDs - Str - Limbic FCN							
	Partial correlation						
	BIS	**DERS**	**ARS**	**SHI**	**RRS**	**BDI**	**WSAS**
L.cAC	0.0125	0.0943	0.0718	0.3018	-0.2343	0.0125	0.0943
L.ENTH	-0.2054	-0.3502	-0.1109	-0.0416	0.0147	-0.2054	-0.3502
L.PC	-0.1565	0.3368	-0.2769	0.1543	0.2550	-0.1565	0.3368
R.AMY	-0.3039	0.0187	-0.2875	0.2605	-0.1367	-0.3039	0.0187
R.cAC	-0.0297	-0.0790	-0.0565	0.0676	-0.0869	-0.0297	-0.0790
R.PC	-0.3110	**0.4142**	-0.3143	0.2680	0.2307	-0.3110	0.4142
	p-Value						
	BIS	**DERS**	**ARS**	**SHI**	**RRS**	**BDI**	**WSAS**
L.cAC	0.9528	0.6538	0.7330	0.1425	0.2597	0.1976	0.6869
L.ENTH	0.3246	0.0861	0.5978	0.8436	0.9444	0.1808	0.4378
L.PC	0.4550	0.0997	0.1802	0.4614	0.2186	0.7012	0.5834
R.AMY	0.1396	0.9295	0.1635	0.2085	0.5145	0.4521	0.3638
R.cAC	0.8881	0.7073	0.7884	0.7481	0.6795	0.0832	0.8790
R.PC	0.1303	**0.0395**	0.1260	0.1953	0.2672	0.8052	0.6841

HCs - Str - Limbic FCN					
	Partial correlation				
	BIS	**DERS**	**ARS**	**SHI**	**RRS**
L.cAC	-0.0694	-0.0281	0.0892	-0.2060	-0.0193
L.ENTH	-0.0138	0.1870	0.1686	**0.3938**	0.3662
L.PC	-0.1657	-0.1499	0.0381	-0.3783	-0.1925
R.AMY	-0.2041	-0.1800	-0.0441	0.0880	-0.0032
R.cAC	-0.0105	-0.0286	0.0850	-0.2092	-0.0150
R.PC	-0.2215	-0.0459	0.2045	-0.2856	-0.0141
	p-Value				
	BIS	**DERS**	**ARS**	**SHI**	**RRS**
L.cAC	0.7364	0.8917	0.6646	0.3126	0.9253
L.ENTH	0.9468	0.3603	0.4103	**0.0465**	0.0658
L.PC	0.4185	0.4648	0.8533	0.0567	0.3461
R.AMY	0.3174	0.3789	0.8307	0.6690	0.9876
R.cAC	0.9595	0.8897	0.6796	0.3052	0.9421
R.PC	0.2768	0.8239	0.3163	0.1573	0.9455

Table 5.64: Partial correlation coefficients and corresponding p-Values of the nodal AUCs of the strength in the limbic FC network with the clinical scores, across patients and controls separately.

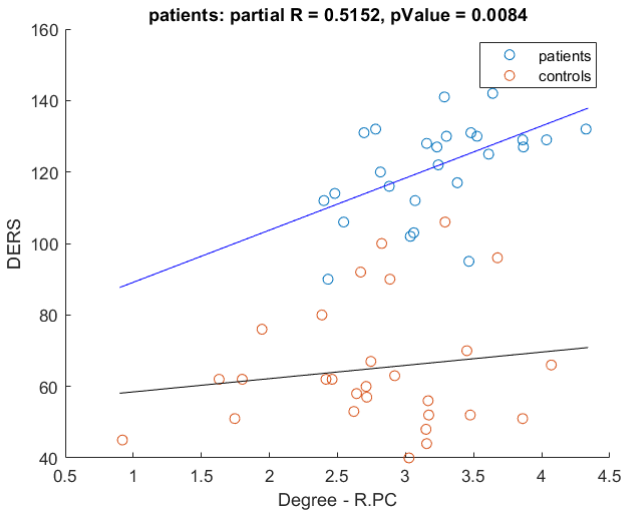

Figure 5.44: Correlation of DERS with the degree of the right posterior cingulate cortex in the limbic subnetwork, across patients and controls separately.

Scale 4 network

Global measures The scale 4 network, at global level, does not reflect the quite numerous results obtained within the full network: the only correlations found were in controls and mostly involving the SHI. The only exception, as it can be seen from Tab. 5.65, is between the small-worldness and the DERS, which did not emerge across all subjects. Even if the slopes are clearly not comparable, the correlation is positive also in patients.

Local measures

Degree The degree in the scale 4 network provided very few significant outcomes, especially if compared to the results obtained when performing the correlations across all subjects, as it can be seen fom Tab. 5.66. Note that in this case the right amygdala and pars orbitalis do not emerge above the other regions, and the same occurs for DERS which does not exhibit the significant outcomes that characterized it in the previous section.
Among the eight total significant correlations in patients and controls, the most interesting are those of the left inferior temporal gyrus with SHI in Fig. 5.45, which also passed the FDR and the right thalamus with DERS in Fig. 5.46, because they were found also across all subjects and they are both observed in patients. The other correlation found also in the previous case, i.e. the one in controls between the left temporal pole and SHI, suffers the same issue that affects all the other correlations involving such scale.
The correlation of the left temporal pole with SHI confirms, only for patients, the same negative trend that was observed across all subjects, whereas for controls the slope remains close to 0.
On the other hand, the same positive correlation seen in the previous section between the degree of the right thalamus and DERS is confirmed here for both patients and controls, even though it is statistically significant only for the firsts.

BPDs							
	Partial correlation						
	BIS	**DERS**	**ARS**	**SHI**	**RRS**	**BDI**	**WSAS**
E_{loc}	0.1569	0.0016	0.2395	-0.0730	0.0517	-0.1208	-0.0175
CC	0.1181	-0.0518	0.2481	-0.0819	-0.0015	-0.1179	0.0125
SW	0.1125	0.0912	0.1849	-0.0703	0.0025	-0.1058	-0.1014
$LCCsize$	0.3427	0.0340	0.2995	-0.0747	-0.1344	-0.1647	-0.1422
Q	0.0339	-0.1143	0.2470	-0.0763	-0.1292	-0.0948	0.0322
	p-Value						
	BIS	**DERS**	**ARS**	**SHI**	**RRS**	**BDI**	**WSAS**
E_{loc}	0.4540	0.9941	0.2489	0.7288	0.8061	0.5739	0.9337
CC	0.5740	0.8057	0.2318	0.6971	0.9942	0.5831	0.9529
SW	0.5924	0.6646	0.3763	0.7383	0.9905	0.6228	0.6296
$LCCsize$	0.0935	0.8718	0.1459	0.7226	0.5217	0.4418	0.4978
Q	0.8724	0.5864	0.2339	0.7170	0.5382	0.6595	0.8787

HCs					
	Partial correlation				
	BIS	**DERS**	**ARS**	**SHI**	**RRS**
E_{loc}	0.2722	0.3307	-0.0171	**0.4568**	0.3046
CC	0.1623	0.3235	-0.0157	0.4016	**0.3051**
SW	0.2231	**0.4078**	0.0622	**0.4711**	0.3773
$LCCsize$	0.1221	0.1931	-0.0658	**0.4418**	0.1051
Q	-0.0480	0.3309	0.0601	0.3283	0.3245
	p-Value				
	BIS	**DERS**	**ARS**	**SHI**	**RRS**
E_{loc}	0.1785	0.0989	0.9341	**0.0190**	0.1303
CC	0.4284	0.1069	0.9393	**0.0420**	0.1296
SW	0.2733	**0.0386**	0.7628	**0.0151**	0.0574
$LCCsize$	0.5524	0.3445	0.7494	**0.0238**	0.6094
Q	0.8157	0.0987	0.7706	0.1016	0.1058

Table 5.65: Partial correlation coefficients and corresponding p-Values of the AUCs of the global measures in the scale 4 network with the clinical scores, across patients and controls separately.

BPDs - Deg - Scale 4 FCN							
	Partial correlation						
	BIS	**DERS**	**ARS**	**SHI**	**RRS**	**BDI**	**WSAS**
L.FP (1)	0.2583	0.1437	0.3356	0.2056	-0.0607	0.0989	-0.1029
R.FP (1)	0.1652	-0.0615	0.1042	0.1522	-0.0202	0.0331	-0.2751
R.parsOR (1)	-0.1437	-0.1039	0.0276	-0.3422	-0.0171	-0.1156	0.1906
L.LING (3)	0.1169	0.0934	-0.2281	0.2271	0.2430	-0.1418	-0.1870
R.LING (3)	0.1528	0.0901	-0.2253	-0.0689	0.3674	-0.1820	-0.2050
L.IT (4)	-0.3274	-0.3373	-0.1834	***-0.5747***	0.1153	-0.0936	0.0862
L.MT (4)	-0.3467	-0.1648	0.1106	0.0781	-0.2236	-0.1494	-0.1603
L.TP (4)	-0.0006	-0.3365	0.1741	-0.0122	-0.1957	-0.2157	-0.1137
L.AMY (5)	0.1461	0.0827	0.0064	-0.0439	-0.2255	-0.0355	-0.1421
L.cAC (5)	0.0187	-0.1620	0.2390	-0.0056	-0.1645	-0.1822	0.0940
L.MoF (5)	0.1401	-0.1835	0.0897	-0.1594	-0.0167	-0.1280	0.0437
L.PC (5)	**-0.4226**	0.1658	-0.3105	0.2212	0.2465	-0.0058	**-0.4786**
R.AMY (5)	-0.1669	-0.0911	-0.2364	0.0433	-0.0678	-0.0728	0.0234
R.cAC (5)	0.0908	-0.2460	0.0218	-0.1409	-0.0657	-0.2039	0.3838
R.ENTH (5)	-0.0030	-0.1264	0.1549	0.0237	0.0543	0.0510	0.0459
R.INS (5)	0.0482	0.3737	0.0275	0.2336	0.1614	**0.4581**	0.1887
R.THA (6)	0.2095	**0.4003**	0.0801	0.0797	0.0123	0.1586	0.0686
	p-Value						
	BIS	**DERS**	**ARS**	**SHI**	**RRS**	**BDI**	**WSAS**
L.FP (1)	0.2125	0.4933	0.1010	0.3242	0.7731	0.6455	0.6246
R.FP (1)	0.4299	0.7704	0.6202	0.4677	0.9235	0.8781	0.1832
R.parsOR (1)	0.4932	0.6212	0.8958	0.0940	0.9355	0.5905	0.3613
L.LING (3)	0.5780	0.6571	0.2728	0.2749	0.2419	0.5086	0.3708
R.LING (3)	0.4658	0.6685	0.2789	0.7436	0.0708	0.3946	0.3255
L.IT (4)	0.1101	0.0992	0.3803	***0.0027***	0.5832	0.6635	0.6822
L.MT (4)	0.0895	0.4311	0.5987	0.7105	0.2826	0.4860	0.4441
L.TP (4)	0.9978	0.1001	0.4052	0.9539	0.3484	0.3113	0.5884
L.AMY (5)	0.4858	0.6943	0.9758	0.8349	0.2784	0.8692	0.4981
L.cAC (5)	0.9293	0.4391	0.2500	0.9787	0.4321	0.3940	0.6548
L.MoF (5)	0.5043	0.3800	0.6698	0.4465	0.9370	0.5513	0.8356
L.PC (5)	**0.0353**	0.4284	0.1309	0.2880	0.2348	0.9786	**0.0155**
R.AMY (5)	0.4252	0.6650	0.2553	0.8372	0.7474	0.7352	0.9118
R.cAC (5)	0.6661	0.2358	0.9176	0.5017	0.7551	0.3392	0.0582
R.ENTH (5)	0.9885	0.5471	0.4596	0.9104	0.7965	0.8130	0.8277
R.INS (5)	0.8191	0.0657	0.8961	0.2611	0.4410	**0.0244**	0.3663
R.THA (6)	0.3149	**0.0474**	0.7034	0.7049	0.9536	0.4592	0.7447

HCs - Deg - Scale 4 FCN					
	Partial correlation				
	BIS	**DERS**	**ARS**	**SHI**	**RRS**
L.FP (1)	-0.2051	0.1498	-0.0644	0.3089	0.0744
R.FP (1)	-0.0133	0.2959	-0.0524	0.2961	0.1038
R.parsOR (1)	-0.2770	-0.0234	-0.0621	-0.0488	-0.0725
L.LING (3)	-0.0319	-0.2834	-0.0188	-0.0975	-0.0066
R.LING (3)	0.0367	-0.1323	0.2342	-0.0557	0.0355
L.IT (4)	-0.0500	0.2372	**0.4060**	0.0196	**0.4402**
L.MT (4)	-0.2080	-0.1711	-0.0208	-0.2263	-0.0060
L.TP (4)	0.1604	0.2083	0.0902	**0.4784**	0.1808
L.AMY (5)	-0.1816	-0.1345	-0.2140	0.2399	-0.2274
L.cAC (5)	0.0385	0.1074	0.0632	-0.1988	0.0931
L.MoF (5)	-0.1702	0.1040	-0.1962	0.2494	-0.0658
L.PC (5)	0.3022	0.1333	-0.0035	-0.1650	0.1362
R.AMY (5)	-0.1103	-0.0150	0.1325	0.1677	-0.0371
R.cAC (5)	0.3559	0.1055	0.0641	-0.1504	0.0629
R.ENTH (5)	0.1111	0.0704	-0.0092	0.2414	-0.0543
R.INS (5)	0.0946	0.1246	0.3174	-0.0654	0.2581
R.THA (6)	0.1099	0.2521	0.0196	0.3019	0.1438
	p-Value				
	BIS	**DERS**	**ARS**	**SHI**	**RRS**
L.FP (1)	0.3149	0.4651	0.7547	0.1247	0.7179
R.FP (1)	0.9487	0.1422	0.7993	0.1419	0.6139
R.parsOR (1)	0.1707	0.9095	0.7632	0.8129	0.7248
L.LING (3)	0.8770	0.1606	0.9273	0.6357	0.9745
R.LING (3)	0.8587	0.5193	0.2495	0.7871	0.8634
L.IT (4)	0.8084	0.2432	**0.0396**	0.9241	**0.0244**
L.MT (4)	0.3080	0.4032	0.9197	0.2663	0.9766
L.TP (4)	0.4337	0.3072	0.6611	**0.0134**	0.3769
L.AMY (5)	0.3747	0.5125	0.2938	0.2379	0.2640
L.cAC (5)	0.8517	0.6015	0.7589	0.3304	0.6509
L.MoF (5)	0.4057	0.6131	0.3368	0.2192	0.7495
L.PC (5)	0.1336	0.5162	0.9865	0.4205	0.5069
R.AMY (5)	0.5918	0.9420	0.5188	0.4127	0.8571
R.cAC (5)	0.0744	0.6081	0.7557	0.4634	0.7603
R.ENTH (5)	0.5891	0.7325	0.9644	0.2349	0.7921
R.INS (5)	0.6459	0.5443	0.1141	0.7508	0.2030
R.THA (6)	0.5931	0.2141	0.9244	0.1338	0.4833

Table 5.66: Partial correlation coefficients and corresponding p-Values of the nodal AUCs of the degree in the scale 4 network with the clinical scores, across patients and controls separately.

Strength Tab. 5.67 resumes the results of the correlation analysis for strength in the scale 4 network. Again, it is evident that the significant outcomes are considerably reduced with respect to the regressions across all subjects.
The findings are similar to those of the degree. In controls, the only statistically significant result is the correlation between the strength of the left temporal pole and SHI; on the other hand, in patients some more results are found, but the only one that reproduces a result that emerged also across all subjects is the correlation between the strength of the right lingual gyrus and the RRS. The latter is shown in Fig. 5.47: the positive slope is confirmed in patients, with respect to the corresponding case in the previous section, whereas in controls the correlation is close to zero.

BPDs - Str - Scale 4 FCN							
	Partial correlation						
	BIS	**DERS**	**ARS**	**SHI**	**RRS**	**BDI**	**WSAS**
R.parsOR (1)	-0.1873	-0.0748	-0.0789	-0.3522	-0.0161	-0.0985	0.1850
L.LING (3)	0.0034	0.0923	-0.3398	0.2627	0.2908	-0.1174	-0.1572
R.LING (3)	0.0073	0.1014	-0.3583	-0.0328	**0.4132**	-0.1382	-0.1792
L.TP (4)	-0.0860	-0.2981	0.0958	0.0524	-0.1387	-0.2568	-0.1577
L.AMY (5)	0.0813	0.1300	-0.0461	0.0549	-0.1814	-0.0432	-0.1731
L.MoF (5)	0.0832	-0.1507	0.0312	-0.1299	0.0831	-0.1422	-0.0012
L.PC (5)	**-0.4378**	0.1677	-0.3786	0.2432	0.2039	-0.0293	**-0.4057**
R.AMY (5)	-0.1986	-0.0766	-0.2804	0.0712	-0.0455	-0.0816	0.0149
R.cAC (5)	-0.0565	-0.1452	-0.1501	-0.0280	-0.0387	-0.1848	0.2815
R.INS (5)	-0.0992	0.3932	-0.1631	0.2984	0.1795	**0.4199**	0.1330
R.THA (6)	0.1093	0.3796	-0.0675	0.1105	0.0095	0.1575	0.0403
	p-Value						
	BIS	**DERS**	**ARS**	**SHI**	**RRS**	**BDI**	**WSAS**
R.parsOR (1)	0.3699	0.7222	0.7078	0.0843	0.9393	0.6470	0.3761
L.LING (3)	0.9872	0.6609	0.0966	0.2045	0.1585	0.5850	0.4530
R.LING (3)	0.9724	0.6297	0.0786	0.8762	**0.0401**	0.5197	0.3913
L.TP (4)	0.6827	0.1478	0.6487	0.8036	0.5085	0.2257	0.4516
L.AMY (5)	0.6993	0.5355	0.8270	0.7944	0.3855	0.8410	0.4080
L.MoF (5)	0.6925	0.4721	0.8823	0.5360	0.6928	0.5074	0.9953
L.PC (5)	**0.0286**	0.4230	0.0620	0.2415	0.3283	0.8921	**0.0442**
R.AMY (5)	0.3411	0.7160	0.1746	0.7354	0.8291	0.7047	0.9435
R.cAC (5)	0.7884	0.4886	0.4740	0.8941	0.8544	0.3874	0.1728
R.INS (5)	0.6370	0.0518	0.4361	0.1474	0.3906	**0.0411**	0.5263
R.THA (6)	0.6029	0.0613	0.7484	0.5989	0.9640	0.4624	0.8485

HCs - Str - Scale 4 FCN					
	Partial correlation				
	BIS	**DERS**	**ARS**	**SHI**	**RRS**
L.AMY (5)	-0.1756	-0.1888	-0.1967	0.2231	-0.2424
L.LING (3)	-0.0173	-0.3039	0.0100	-0.1749	-0.0550
L.MoF (5)	-0.2084	0.0809	-0.1726	0.2525	-0.0676
L.PC (5)	0.2839	0.0485	0.0093	-0.2139	0.0609
L.TP (4)	0.1854	0.1774	0.1072	**0.4698**	0.1690
R.AMY (5)	-0.1298	-0.1203	0.1288	0.1364	-0.0913
R.THA (6)	0.1188	0.1493	0.0243	0.1812	0.0689
R.cAC (5)	0.3208	0.0467	0.0592	-0.2156	-0.0054
R.INS (5)	0.0783	0.0507	0.3117	-0.1910	0.1377
R.LING (3)	0.0434	-0.1961	0.2215	-0.1301	-0.0233
R.parsOR (1)	-0.3153	-0.0798	-0.0464	-0.0965	-0.1040
	p-Value				
	BIS	**DERS**	**ARS**	**SHI**	**RRS**
L.AMY (5)	0.3908	0.3557	0.3356	0.2732	0.2329
L.LING(39	0.9331	0.1313	0.9612	0.3927	0.7895
L.MoF (1)	0.3071	0.6943	0.3990	0.2133	0.7429
L.PC (5)	0.1599	0.8139	0.9639	0.2941	0.7675
L.TP (4)	0.3644	0.3861	0.6022	**0.0154**	0.4091
R.AMY (5)	0.5275	0.5581	0.5307	0.5066	0.6575
R.THA (6)	0.5632	0.4666	0.9062	0.3756	0.7381
R.cAC (5)	0.1100	0.8208	0.7740	0.2902	0.9791
R.INS (5)	0.7037	0.8058	0.1211	0.3501	0.5025
R.LING (3)	0.8331	0.3370	0.2768	0.5264	0.9101
R.parsOR (1)	0.1167	0.6984	0.8219	0.6390	0.6130

Table 5.67: Partial correlation coefficients and corresponding p-Values of the nodal AUCs of the strengths in the scale 4 with the clinical scores, across patients and controls separately.

The correlations concerning the other two local measures that presented ROIs passing the FDR, i.e. the betweenness centrality and the within-module strengths, did not provide any statistically significant results; therefore, for simplicity, the results are not reported here.

To summarize the findings of this section, the most evident result is that the correlations across patients and controls separately are definitely not as numerous as the ones found when merging the two groups into a unique one, therefore confirming that a considerable part of the relationships that emerged from section 5.3.1 are not reliable, but rather exhibited because of the considerable difference in terms of the neuro-psychological scores between BPDs and HCs. Nevertheless, also some confirmations were detected, which make more solid the inferences on the corresponding relationships.
Another aspect to underline is that the correlations evaluated on patients and controls separately never occur simultaneously, so that if a relationship is statistically significant in one group, it is not in the other. Note also that the only correlations that were found to be significant in both the cases studied always involve the correlations within patients,

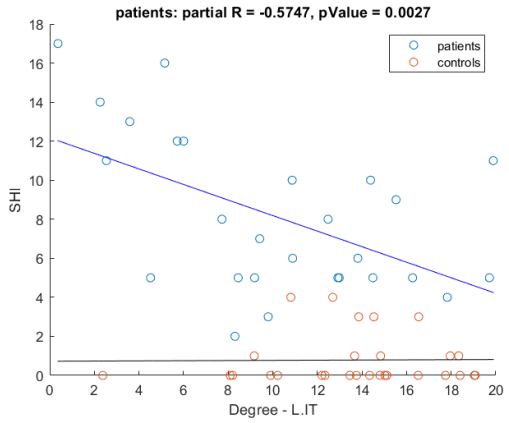

Figure 5.45: Correlation of SHI with the degree of the left inferior temporal gyrus in the scale 4 network across patients and controls separately.

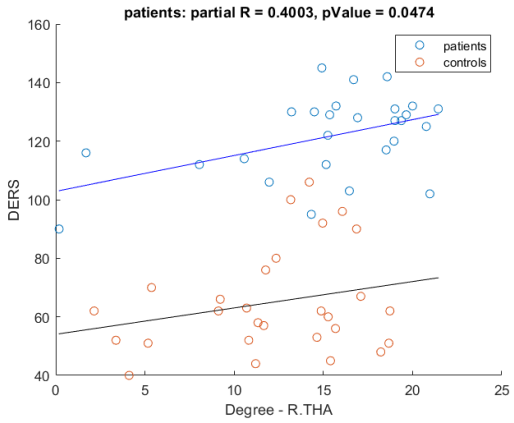

Figure 5.46: Correlation of DERS with the degree of the rigth thalamus in the scale 4 network, across patients and controls separately.

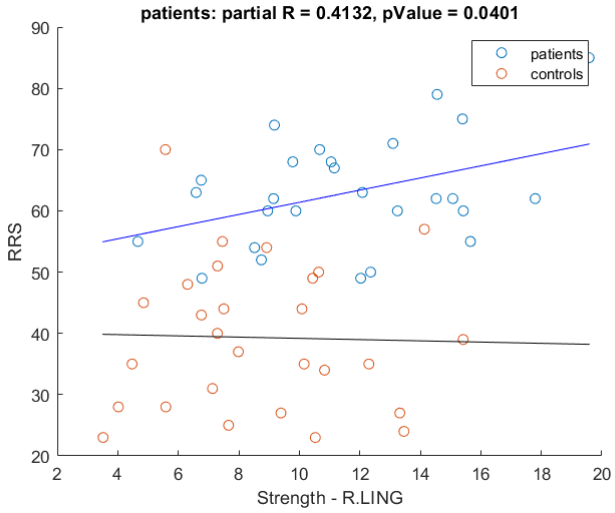

Figure 5.47: Correlation of RRS with the strength of the left lingual gyrus in the scale 4 network, across patients and controls separately.

rather than controls. These aspects will be deepened in the discussion in chapter 6.
In conclusion, the extended study of correlations has allowed to assess deeply the characteristics of networks related to the clinical scores, yet suggesting that some aspects could be developed by including the investigation of the presence of more than one effect in the differences between network measures.

Chapter 6

Discussion

6.1 Comparison with the random networks

The results of the comparison between the subjects' and the random networks provided the expected outcomes that are typically observed in brain graphs, both functional and structural. This was verified for each of the types of FC and SC networks studied.
As a preliminary step, the consistency of the strength distributions of subjects and randoms was verified, in order to ensure the comparability between the two. This, together with the degree distribution, also allowed to state that such shapes were compatible with the presence of hubs in the network, since they tended to present heavy tails or skewed shapes towards higher values, which indicate the presence of central nodes with many and strong connections within the network.
In particular, this was verified through two main aspects of the brain networks with respect to the random ones, which consist of the efficiency in information transfer at global and at local level. The first, in fact, was correctly found to be quantitatively comparable between subjects and randoms [10], as it was measured by the characteristic path length and the global efficiency; the slight penalization of the latter in subjects is likely attributable to the modular structure of brain networks, which makes it mandatory to pass through certain central nodes, in order to reach the peripheral ones. The only, mild, deviation from the behaviors otherwise observed was the characteristic path length in the SC networks, which was found to be slightly longer in subjects (patients in particular) with respect to randoms. Nevertheless, this discrepancy did not produce statistically significant result, as it was shown in section 5.2.2. On the other hand, the second was consistently and significantly higher in subject, as it was suggested by the great differences in terms of average local efficiency and clustering coefficient.
These information merge into the satisfaction of the criterion for the small-worldness property, which is the most characteristic feature of brain networks [10, 11, 62] and states their simultaneous good performances in terms of both global and, especially, local efficiency in information transfer.

6.2 Comparison between patients and controls

Several and significant differences in topological measures between patients and controls were detected, especially in the FC networks, and both at global and local level. On a

general line, this suggest that the Borderline Personality Disorder indeed affects functional brain networks in a measurable way.
The interpretation of the results obtained in this sense and exposed in the previous chapter are discussed in this section.

6.2.1 FC networks

A first comment should regard the trend inversion in the increment of certain global properties in patients or controls, in particular the average local efficiency and the average clustering coefficient, when they are normalized by the corresponding random outcomes. This can be explained by the fact that the BPDs' matrices, on average, present a structure that is closer to the corresponding random arrangement and weighting of links among nodes than HCs' ones, so that the quantities in patients are affected more by the normalization. This statement is actually supported by the fact that the modularity coefficient, which describes how likely it is that a network is subdivided into modules that maximize the ratio of intramodular to intermodular edges, is significantly higher in controls. Note, in fact, that the community configuration is a characteristic property of functional brain networks [10], which instead is not as clearly observed in random graphs.
The normalization of global properties is a standard procedure in the analysis of brain networks. Nonetheless, to verify their reliability in the case of weighted networks, which exhibited the inversion in increment just described, the same analysis of global properties within the full FC network was repeated after the binarization of the graphs. This analysis indeed revealed the same results as for weighted network, i.e. that in general the normalized global properties are significantly increased in controls. Nevertheless, in the binarized case, there was not an evident trend inversion as it was observed for the weighted networks, suggesting that the strength of links is actually at the base of this phenomenon.

The full and the wavelet-decomposed FC networks showed consistent variations between patients and controls at global level in terms of normalized average local efficiency, normalized average clustering coefficient, small-worldness, largest connected component size and modularity coefficient. In particular, all these quantities were decreased in BPDs. The decrement of the properties related to the efficiency in local information transfer, i.e. the first three among the ones just mentioned, implies the presence of a significantly less clustered structure within the functional brain networks of patients. Similar conclusions could be retrieved also from the information provided by the other two quantities, the modularity coefficient and the largest connected component size, which also provide information related to the cliquishness, at a higher hierarchical level. To further support this statement, it was also verified that there exists a positive correlation between the measures of local clustering and the LCC size and modularity, as it is shown in Fig. 6.1.

The greatest part of the local variations emerged from the limbic system, which was found to be the most affected in terms of topological properties by the disease. Within the FC networks, not only such aspect was observed in the full and in the scale 4 graphs, but it was also demonstrated by the numerous variations within the limbic network itself, when compared to the occipital one. Additionally, significant variations were detected also within the frontal system and the temporal poles. These findings are in accord with the results reported in literature, which describe a dysfunctional condition of the

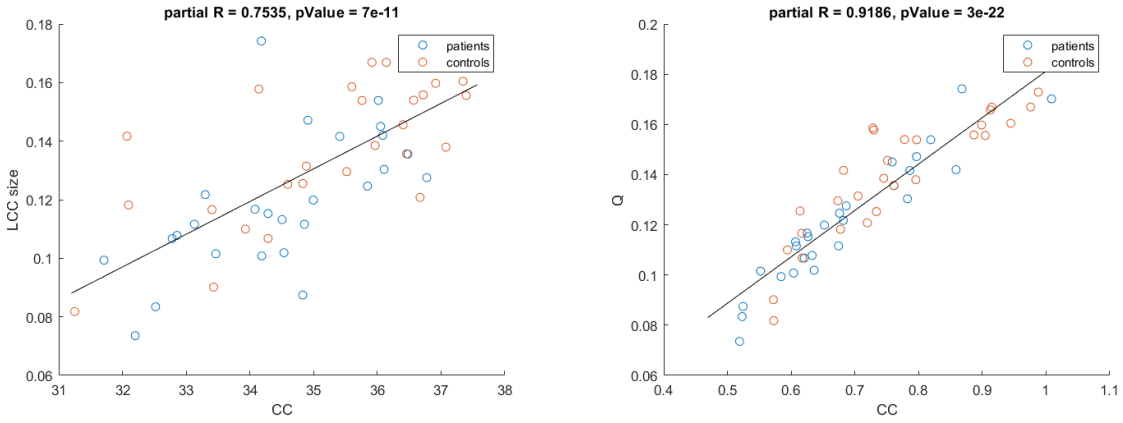

(a) *(b)*

Figure 6.1: Correlation of the largest connected component size and the modularity coefficient with the normalized clustering coefficient in the full FC network across all subjects.

frontolimbic system [21, 29, 63].
Among the regions that exhibited the most relevant variations, the bilateral amygdala, and the right one especially, emerged. Such area is acknowledged as characterized by dysfunctional activity in the borderline personality disorder, as it is reported by numerous papers on stimuli-based [21, 30] and resting-state [32, 64] studies of the disease. The amygdala has indeed a crucial function in terms of emotion regulation, as well as the entire frontolimbic system [65], therefore their frequent rise from researches on BPD should not surprise.
The results reported in the previous chapter, in general show a reduced connectivity of the amygdala in patients, which is exhibited both in terms of reduced centrality, in all the types of FC networks considered, and of efficiency in local information transfer, in the wavelet-decomposed one at low frequencies. Specifically, on the centrality condition of this region, it is interesting to note that its reduction is related both to its integration with the other modules of the network and of segregation within the module where it was assigned. In the full network, in fact, it is particularly significant the decrease in patients with respect to controls of the participation coefficient of the right amygdala, but also the within-module strength is affected by a relevant decrease in both hemisphere. The scale 4 of the wavelet-decomposed networks provide an additional information in this sense: in that case, the participation coefficient of the amygdala is not significantly varied, but the within-module strength does, suggesting that the reduced centrality is related to the connections within the module especially at low frequencies, and to connections with other communities at higher frequencies.
Similar considerations can be made for other frontolimbic regions, such as the bilateral entorhinal cortex, and the left in particular [32], the bilateral caudal anterior cingulate cortex and other medial and orbitofrontal regions [31, 66]. The left entorhinal cortex, for example, shows significantly reductions both in terms of centrality and local efficiency, which are consistent with its lower within-module strength; among the orbitofrontal ROIs, it is worth to mention the right pars orbitalis, which presents very significant variations, especially at low frequencies, in terms of centrality, which tends to be reduced, in particular concerning its integration within the network.
Outside of the frontal and limbic systems, the bilateral, and left in particular, temporal pole appears to be particularly relevant, especially in terms of local efficiency in

information transfer, even though, in the scale 4 network, it gains significance also for centrality; both the properties are reduced for this node. The dysfunction of this region is already reported in literature for borderline personality disorder [32, 67], and this is consistent with the fact that such area has an acknowledged role in emotion processing, being strongly connected to the limbic and paralimbic systems [68].
It is particularly interesting to note that recently Xu et al. [32], in the only paper (to our knowledge) on a network approach to the study of rs-fMRI data from BPD subjects, reported analogous but opposite results in terms of the comparison between patients and controls. In particular, they found variations in the same global properties of normalized average local efficiency, normalized average clustering coefficient, small-worldness and largest connected component size, but increased in BPDs instead of HCs; similarly the local efficiencies of the bilateral amygdala, the bilateral temporal poles and the left entorhinal cortex were reported by them to be higher in patients, in contrast to our findings. Even though they focused on binarized wavelet-decomposed networks, the procedure of the network construction can not explain the difference in terms of the comparison between patients and controls: to support this statement, recall that such approaches were attempted also for this study. The deviation, therefore must be traced back to the composition of the cohort of subjects involved in this study. In particular, the discrepancy might be related to a different average severity or stage of the disease affecting the patients: in fact, the age of the BPD patients investigated in that research, ranged from 20 to 45, with an average of 29 ± 7.3, against the 24.1 ± 3.5 of our case. Moreover they had a lower number of subjects in their cohort (20 BPDs and 10 HCs) with a ratio of males to females of 7 to 13 among BPDs and 4 to 6 among HCs, considerably more uniform with respect to the composition of our cohort of participants, which included 12 males over a total of 55 subjects.
Therefore, it would be particularly interesting to follow the participants to the present study, both from the clinical and the neuroimaging perspectives, in order to verify if the suggested changes would actually occur, and possibly investigate their origin.

Regarding the NBS analysis, from the point of view of the alterations of functional connectivity, those that emerged with a primary threshold of 2.9, at level of the mass univariate test, are not particularly informative, since they involve a set of nodes distributed across every system of the brain subdivision, even if showing a prevalence of the limbic network. Nevertheless, it is interesting to note that almost every altered link connects nodes belonging to different systems, suggesting that the intramodular structures are mostly preserved from this perspective.
It is significant, instead, to note the presence of the bilateral caudal anterior cingulate cortex when the primary threshold is increased to 4.0: this is consistent with the findings of dysfunctional activity reported for this region [31, 66].

More solid and reliable data could be obtained with the improvement of the quality of the latter, which could be achieved through the use of a 3 T scanner for the acquisition of the images, as it would ensure an upgrade of temporal resolution, allowing to reduce the repetition time (3 s in this case), so that more functional volumes could be collected within the same acquisition time: this would clearly enhance the accuracy of the analysis, since it would translate in additional data for the time series to correlate, when building the FC networks.

6.2.2 SC networks

From the SC networks, results as relevant as the ones obtained from a functional point of view did not emerge. In particular, the global topological properties did not reveal any significant variation between patients and controls and, at a local level, the outcomes were not as numerous nor significant as those exhibited from the functional perspective. Nevertheless, this could also be an interesting finding as well, since it may suggest that young BPD patients do not show many evident variations from a structural point of view, even though they do from a functional one. Nonetheless, it is also possible that effects on the anatomy of brain regions (volume in particular) are developed in later stages of the disease or in older age: observations of this type are indeed reported in literature [69].
Nonetheless, meaningful results could be retrieved also in this case: first of all, the statistically significant differences between patients and controls at nodal level, even if not numerous, were mostly detected within the limbic system, once again supporting the hypothesis of the pathological alteration of this system. Moreover, it is of particular interest to note that from the SC networks the hippocampus frequently emerged, even though it did not from the FC ones. This is consistent with the findings that often report structural abnormalities of the hippocampus in BPD subjects, together with the amygdala [33, 70], which, in this study, was associated to significant variations within the SC network mainly in the right hemisphere of females only.
Also from the point of view of altered connections among nodes, the results are not very informative, as only one connection, between the left and right caudate nucleus, passed the FDR through the z-score approach described in section 4.6.2.

In this case a greater accuracy of the results could be achieved by the inclusion of more subjects within the study: the main issue behind the construction of structural covariance networks is, in fact, that the series of data to correlate in order to build the matrices tend to be short. In this case, for example, for each ROI, they were constituted of 27 and 28 values for patients and controls respectively. It is evident that if such series included more data, also the correlation among each pair of ROIs would be more accurate, and this can only be achieved by increasing the dimension of the cohort of subjects.
It is also important to recall that the precision of this approach is also affected by the fact that the matrices or the outcomes of the measures can not be averaged across subjects, as it happens for the FC ones, since they do not originate from 4D images.

6.3 Correlation with the clinical scores

The correlations of the topological properties with the clinical scores provided some results that are worthy of further investigation. The main aspect to underline is that, even if the greatest part of the correlations across all subjects were statistically significant, so that many of them also passed the FDR correction, not all of them could be considered solid or reliable, since several originated from a well defined separation of the data of patients and controls, mostly due to the difference between their scores in the neuropsychological scales, rather than an intrinsic property of the data. Such observation was indeed confirmed by the linear regressions across BPDs and HCs independently, which reported only a small ratio of significant correlations over the total possible combinations, suggesting that most of the ones detected across all subjects were indeed biased.

Among patients and controls separately, statistically significant correlations were still found, but only two of those passed the FDR correction (the local efficiency of the left temporal pole in the full FC network with the BIS scores and the degree of the left inferior temporal gyrus in the scale 4 network with the SHI score). For these reasons, the regressions that we decided to focus on, were those that were observed in both the cases of study, as they are considered to be more solid throughout the analysis.
Nonetheless, the analysis under these two different conditions allowed us to deeply investigate the relationship between the topological characteristics of the functional brain networks and the clinical scores, definitely revealing the presence of a group effect that has a crucial role on the correlations. This suggest that further analyses on the data may be viable in order to highlight and explore such effect, for example through ANalysis Of VAriance (ANOVA).
It must also be noted that BPDs and HCs, not only did not present simultaneously a significant correlation for any combination, but in various cases they also showed inverted trends one with respect to the other. Nevertheless, all the combinations that emerged after the application of the criterion of reliability were found to be significant in patients rather than controls: this may suggest that there could exist a threshold effect within the neuro-psychological scales, so that after a certain value a relationship with specific topological properties may emerge, or, alternatively, that such conditions are exhibited only in specific mental disorders, such as the BPD.
Regarding the specific combinations that emerged from the analysis, the measures of centrality are the only ones that found a correspondence in both cases and they particularly correlate with DERS and RRS. The outcomes did not support a strong relationship with the limbic system in terms of correlations, as the only one that was detected across all subjects and in patients only was between the degree of the right posterior cingulate cortex and DERS. In particular neither the amygdala, nor the caudal anterior cingulate or any other region of the frontolimbic system satisfied the criterion of showing consistent correlations in both the cases examined. The remaining ROIs that are associated to significant correlations belong to all the other systems defined by the brain parcellation: the left superior parietal lobule within the parietal lobe, the left inferior temporal gyrus within the temporal pole, the right thalamus among the basal ganglia and the right lingual gyrus within the occipital lobe. Functional hyperactivation of the inferior temporal cortex is reported in literature during emotion discrimination tasks in BPD subjects [71], but it is not mentioned to be associated to self-harmful tendencies. The other regions just mentioned are not reported in literature to exhibit dysfunctional behaviors in borderline personality disorder, and they do not belong to areas typically affected by such disease, therefore they would need further verification, which could actually be accomplished through the analysis mentioned above.

Beside these comments, note that the correlations are not particularly strong in any combination: very few, in fact, overcome 0.5 and are in any case inferior to 0.6.
Obviously, a greater number of subjects would be crucial in improving the accuracy and the precision of the results of the correlations, in particular considering the variability that both the clinical scores and the topological measures can have for each individual.

Chapter 7

Conclusions

The network approach to the analysis of MR images of subjects affected by the Borderline Personality Disorder, compared to those of age- and sex-matched healthy controls, provided significant results, especially concerning the functional connectivity retrieved from the rs-fMRI data.
In particular, the study of the Functional Connectivity networks revealed reduced modular structure and efficiency in information transfer in patients, at both global and local levels when considering the graphs as a whole; in the node-specific analysis, alterations were predominantly found in the frontolimbic system. Such variations mainly involved the following regions: the amygdala, especially in the right hemisphere, whose centrality was reduced within and outside its module; the entorhinal cortex, left in particular, associated to decreased centrality and efficiency; the caudal anterior cingulate cortex, which instead presented an increment of these quantities; the right pars orbitalis, with a significantly decreased centrality at low frequencies; the temporal pole, which instead was associated to a reduction of efficiency.
On the other hand, the Structural Covariance networks, despite partly supporting an alteration of the limbic system, among which the hippocampus and the amygdala are of particular interest, did not provide as numerous nor significant outcomes. Nonetheless, considering the average young age of the participants, who were in an early stage of the disease, this could indicate an age- or condition-dependent evolution of BPD on anatomical structures.
The exploratory analysis concerning the correlations of the topological measures with the scores of the neuro-psychological scales provided some interesting results, that would be worthy to be deepened with further analysis. On one hand, the specific ROIs where the correlations were considered to be more markedly solid, i.e. those found when analyzing the relationships both across all subjects and across patients or controls separately, were not included among the ones found to be crucial in terms of characterization of the BPDs with respect to HCs. On the other hand, the correlations suggested the existence of a group effect, that appears to have a considerable weight in the evaluation of the relationships among topological and clinical features.

The limitations of this study mainly regarded the instrumentation, as a 3 T scanner, in place of the 1.5 T used, would ensure higher quality data, not only in terms of the spatial resolution of the images, but also of the accuracy of the FC networks. In fact, it

would allow to retrieve longer time series, which are at the basis of the construction of functional matrices, within the same acquisition time.
Another aspect of improvement is the dimension of the cohort of subjects, which particularly influence the accuracy of the SC networks, but also would ensure a higher precision of the outcomes of FC graphs.

A meaningful future direction for this study would be to further explore the topological data and their correlations with the clinical scores, using additional statistical methods, which may better assess the effect of the neuro-psychological conditions on network properties.
As a last note, an interesting long-term development for this work would be to perform a follow-up of the participants to the present study, by monitoring their neuro-psychological and psychiatric state and by repeating periodically the neuroimaging acquisitions. This procedure would allow to verify whether the changes, that our results suggest, based on the stage and the severity of the disease would actually occur, and explore their origin.

References

[1] Biswal B. et al. "Functional connectivity in the motor cortex of resting human brain using echo-planar mri". In: *Magnetic Resonance in Medicine* 34.4 (1995).

[2] Callaghan P.T. *Principles of nuclear magnetic resonance microscopy*. Clarendon Press, Oxford, 1991.

[3] Hornak J.P. *The basics of MRI*. URL: https://www.cis.rit.edu/htbooks/mri/index.html.

[4] Brown R.W. et al. *Magnetic Resonance Imaging: Physical Principles and Sequence Design, 2nd edition*. John Wiley & Sons, Inc., 2014.

[5] Huettel S.A. et al. *Functional Magnetic Resonance Imaging, 2nd edition*. Oxford Univeristy Press, 2009.

[6] Jezzard P., Matthews P.M., and Smith S. *Functional MRI: An Introduction to Methods*. Oxford Medical Publications, 2003.

[7] Jovicich J. "An investigation of the use of gradient and spin echo (GRASE) imaging for functional MRI of the human brain". PhD thesis. 1999.

[8] Margulies D.S. et al. "Resting developments: a review of fMRI post-processing methodologies for spontaneous brain activity". In: *Magn Reson Mater Phy* 23 (2010). DOI: https://doi.org/10.1007/s10334-010-0228-5.

[9] Bassett D.S. and Bullmore E.T. "Human Brain Networks in Health and Disease". In: *Curr Opin Neurol* 22.4 (2009), pp. 340–347. DOI: https://doi.org/10.1097/WCO.0b013e32832d93dd.

[10] E.T. Bullmore and D.S. Bassett. "Brain Graphs: Graphical Models of the Human Brain Connectome". In: *Annu. Rev. Clin. Psychol.* 7 (2011), pp. 113–140.

[11] Bullmore E. and Sporns O. "Complex brain networks: graph theoretical analysis of structural and functional systems". In: *Nat. Rev. Neurosci.* 10.3 (2009), pp. 186–198. DOI: https://doi.org/10.1038/nrn2575.

[12] Craddock R.C. et al. "Imaging human connectomes at the macroscale". In: *Nat Methods* 10.6 (2013), pp. 524–539. DOI: https://doi.org/10.1038/nmeth.2482.

[13] Sporns O. "Graph theory methods: applications in brain networks". In: *Dialogues Clin Neurosci* 20.2 (2018), pp. 111–121.

[14] Salvador R. et al. "A simple view of the brain through a frequency-specific functional connectivity measure". In: *NeuroImage* 39 (2008), pp. 279–289.

[15] Fischl B. et al. "Automatically parcellating the human cerebral cortex". In: *Cereb. Cortex.* 14 (2004), pp. 11–12.

[16] Tzouriomazoyer N. et al. "Automated anatomical labeling of activations in SPM using a macroscopic anatomical parcellation of the MNI MRI single-subject brain". In: *NeuroImage* 15.1 (2002), pp. 273–289.

[17] Power J.D. et al. "Functional network Organization of the Human Brain". In: *Neuron* 72.4 (2011), pp. 665–678.

[18] Wang J. et al. "Parcellation-dependent small-world brain functional networks: a resting-state fMRI study". In: *Hum. Brain Mapp* 30 (2009), pp. 1511–1523.

[19] Pervaiz U. et al. "Optimising network modelling methods for fMRI". In: *NeuroImage* 211 (2020).

[20] Xiang J. et al. "Graph-based network analysis of resting-state fMRI: test-retest reliability of binarized and weighted networks". In: *Brain Imaging and behavior* (2019).

[21] Leichsenring F. et al. "Borderline personality disorder". In: *Lancet* 377 (2011), pp. 74–84.

[22] Paris J. "Clinical Features of Borderline Personality Disorder". In: *Handbook of Personality Disorders. Second Edition. Theory, Research, and Treatment*. Ed. by Livesley W.J. and Larstone R. 2018. Chap. 23, pp. 419–424.

[23] Gunderson J.G. et al. "Borderline Personality Disorder". In: *Nature Reviews Disease Primers* 4.18029 (2018). DOI: https://doi.org/10.1038/nrdp.2018.29.

[24] First M. et al. "Structured Clinical Interview for DSM-IV Axis-II Personality Disorders (SCID II)". In: *Washington DC, American Psychiatric Press* (1997).

[25] Grant B.F. et al. "l. Prevalence, correlates, disability, and comorbidity of DSM-IV borderline personality disorder: results from the Wave 2 National Epidemiologic Survey on Alcohol and Related Conditions". In: *J Clin Psychiatry* 69 (2008), pp. 533–545.

[26] Gunderson J.G. et al. "Ten-year course of borderline personality disorder: psychopathology and function from the Collaborative Longitudinal Personality Disorders study". In: *Arch. Gen. Psychiatry* 68 (2011), pp. 827–837.

[27] Gabbard G.O. "Mind, brain, and personality disorders". In: *Am J Psychiatry* 162 (2005), pp. 648–655.

[28] Torgersen S. et al. "The Heritability of Cluster B Personality Disorders Assessed Both by Personal Interview and Questionnaire". In: *J Pers Disord* 26 (2012), pp. 848–866.

[29] Krause-Utz A. et al. "The latest neuroimaging findings in borderline personality disorder". In: *Curr. Psychiatry Rep.* 16.3 (2014), p. 438. DOI: https://doi.org/10.1007/s11920-014-0438-z.

[30] Schulze S. et al. "Neural Correlates of Disturbed Emotion Processing in Borderline Personality Disorder: A Multimodal Meta-Analysis". In: *Biological Psychiatry* 79.2 (2016), pp. 97–106. DOI: https://doi.org/10.1016/j.biopsych.2015.03.027.

[31] Koenigsberg H.W. et al. "Neural correlates of emotion processing in borderline personality disorder". In: *Psychiatry Res.* 172 (2009), pp. 192–199.

[32] Xu T. et al. "Network analysis of functional brain connectivity in borderline personality disorder using resting-state fMRI". In: *NeuroImage: Clinical* 11 (2016), pp. 302–315. DOI: https://doi.org/10.1016/j.nicl.2016.02.006.

[33] Nunes P.M. et al. "Volumes of the hippocampus and amygdala in patients with borderline personality disorder: a meta-analysis". In: *J Pers Disord* 23.4 (2009), pp. 333–345. DOI: https://doi.org/10.1521/pedi.2009.23.4.333.

[34] Patton J.H., Stanford M.S., and Barrat E.S. "Factor structure of the Barratt Impulsiveness Scale". In: *J. ClinPsychol.* (1995).

[35] Gratz K.L. and Roemer L. "Multidimensional assessment of emotion regulation and dysregulation: development, factor structure, and initial validation of the difficulties in emotion regulation scale". In: *J. Psychopathol. Behav. Assess.* 26 (2004), pp. 41–54.

[36] Sukhodolsk D.G., Golub A., and Cromwell E.N. "Development and validation of the anger rumination scale". In: *Personality and Individual Differences* 31 (2001), pp. 689–700.

[37] Sansone R.A., Wiederman M.W., and Sansone L.A. "The Self-Harm Inventory (SHI): development of a scale for identifying self-destructive behaviors and borderline personality disorder". In: *J. Clin. Psychol.* 54 (1998), pp. 973–983.

[38] Nolen-Hoeksema S. and Morrow J. "A prospective study of depression and posttraumatic stress symptoms following a natural disaster: The 1989 Loma Prieta Earthquake". In: *Journal of Personality and Social Psychology* 61.3 (1991), pp. 115–121.

[39] Beck A.T. et al. "An inventory for measuring depression". In: *Archives of General Psychiatry* 4 (1991), pp. 561–571.

[40] Mundt J.C. et al. "The Work and Social Adjustment Scale: a simple measure of impairment in functioning". In: *Br. J. Psychiatry* 180 (2002), pp. 401–464.

[41] Jenkinson M. et al. "FSL". In: *NeuroImage* 62.2 (2012), pp. 782–790. DOI: https://doi.org/10.1016/j.neuroimage.2011.09.015".

[42] Jenkinson M. et al. "Improved Optimisation for the Robust and Accurate Linear Registration and Motion Correction of Brain Images." In: *NeuroImage* 17.2 (2002), pp. 825–841. DOI: https://doi.org/10.1016/s1053-8119(02)91132-8.

[43] Smith S.M. "Fast Robust Automated Brain Extraction". In: *Human Brain Mapping* 17.3 (2002), pp. 143–155.

[44] Woolrich M.W. "Temporal Autocorrelation in Univariate Linear Modeling of FMRI Data". In: *NeuroImage* 14.6 (2001), pp. 1370–1386. DOI: https://doi.org/10.1006/nimg.2001.0931.

[45] Beckmann C.F. and Smith S.M. "Probabilistic Independent Component Analysis for Functional Magnetic Resonance Imaging". In: *IEEE Trans. Med. Imaging* 23.2 (2004), pp. 137–152.

[46] Griffanti L. et al. "Hand classification of fMRI ICA noise components". In: *NeuroImage* 154 (2017), pp. 188–205. DOI: https://doi.org/10.1016/j.neuroimage.2016.12.036.

[47] Jenkinson M. and Smith S.M. "A global optimisation method for robust affine registration of brain images". In: *Medical Image Analysis* 5.2 (2001), pp. 143–156. DOI: https://doi.org/10.1016/s1361-8415(01)00036-6.

[48] Anderrson J.L.R., Jenkinson M., and Smith S.M. *Non-linear registration aka Spatial normalisation.* FMRIB Centre. Oxford: FMRIB Technical Report TR07JA2, 2007.

[49] Buckner R.L. "Human functional connectivity: New tools, unresolved questions". In: *PNAS* 107 (2010), pp. 10769–10770.

[50] Rubinov M. and Sporns O. "Complex network measures of brain connectivity: Uses and interpretations". In: *NeuroImage* 52.3 (2010), pp. 1059–1069. DOI: http://doi.org/10.1016/j.neuroimage.2009.10.003.

[51] Achard S. et al. "A resilient, low-frequency, small-world human brain functional network with highly connected association cortical hubs". In: *J. Neurosci.* 26 (2006), pp. 63–72. DOI: https://doi.org/10.1523/JNEUROSCI.3874-05.2006.

[52] Skidmore F. et al. "Connectivity brain networks based on wavelet correlation analysis in Parkinson fMRI data". In: *Neurosci. Lett.* 499.1 (2011), pp. 47–51. DOI: https://doi.org/10.1016/j.neulet.2011.05.030.

[53] Fadili M.J. Bullmore E.T. "A comparative evaluation of wavelet-based methods for hypothesis testing of brain activation maps". In: *NeuroImage* 23.3 (2004), pp. 1112–1128. DOI: https://doi.org/10.1016/j.neuroimage.2004.07.034.

[54] Zhang Z. et al. "Choosing Wavelet Methods, Filters, and Lengths for Functional Brain Network Construction". In: *PLoS ONE* 11.6 (2016), pp. 1112–1128. DOI: https://doi.org/10.1371/journal.pone.0157243.

[55] Sanchis-Segura C. et al. "Sex differences in gray matter volume: how many and how large are they *really*?" In: *Biol Sex Differ* 10.32 (2019). DOI: https://doi.org/10.1186/s13293-019-0245-7.

[56] Power J.D. et al. "Evidence for Hubs in Human Functional Brain Networks". In: *Neuron* 79.4 (2013), pp. 798–813. DOI: https://doi.org/10.1016/j.neuron.2013.07.035.

[57] Xia M., Wang J., and He Y. "BrainNet Viewer: A Network Visualization Tool for Human Brain Connectomics". In: *PLoS ONE* 8.7 (2013). DOI: https://doi.org/10.1371/journal.pone.0068910.

[58] Winkler A.M. et al. "Permutation inference for the general linear model". In: *Neuroimage* 92 (2014), pp. 381–397. DOI: https://doi.org/10.1016/j.neuroimage.2014.01.060.

[59] Benjamini Y. and Hochberg Y. "Controlling the false discovery rate: A practical and powerful approach to multiple testing". In: *Journal of the Royal Statistical Society, Series B (Methodological)* 57.1 (1995), pp. 289–300.

[60] Groppe D. *fdr_bh*. url: https://www.mathworks.com/matlabcentral/fileexchange/27418-fdr_bh. MATLAB Central File Exchange, 2020.

[61] Zalesky A., Fornito A., and Bullmore E.T. "Network-based statistic: Identifying differences in brain networks". In: *NeuroImage* 53.4 (2010). DOI: https://doi.org/10.1016/j.neuroimage.2010.06.041.

[62] Rubinov M. and Sporns O. "Complex network measures of brain connectivity: uses and interpretations". In: *NeuroImage* 52.3 (2010), pp. 1059–1069. DOI: https://doi.org/10.1016/j.neuroimage.2009.10.003.

[63] Minzenberg M.J. et al. "Fronto-limbic dysfunction in response to facial emotion in borderline personality disorder: an event-related fMRI study". In: *Psychiatry Res.* 155.155 (2007), pp. 241–243.

[64] Krause-Utz A. et al. "Amygdala and anterior cingulate resting-state functional connectivity in borderline personality disorder patients with a history of interpersonal trauma". In: *Psychol. Med.* 44 (2014), pp. 2889–2901. DOI: https://doi.org/10.1017/S0033291714000324.

[65] Banks S.J. et al. "Amygdala–frontal connectivity during emotion regulation". In: *Social Cognitive and Affective Neuroscience* 2.4 (2007), pp. 303–312. DOI: https://doi.org/10.1093/scan/nsm029.

[66] Krause-Utz A. et al. "Influence of emotional distraction on working memory performance in borderline personality disorder". In: *Psychol. Med.* 42 (2012), pp. 2181–2192.

[67] Buchheim A. et al. "Neurobiology of borderline personality disorder (BPD) and antisocial personality disorder (APD)". In: *Schweizer Archiv fur Neurologie und Psychiatrie* 164 (2013), pp. 115–122.

[68] Olson I.R. et al. "The enigmatic temporal pole: a review of findings on social and emotional processing". In: *Brain* 130 (2007), pp. 1718–1731.

[69] Kimmel C.L. et al. “Age-related parieto-occipital and other gray matter changes in borderline personality disorder: A meta-analysis of cortical and subcortical structures”. In: *Psychiatry Research: Neuroimaging* 251 (2016), pp. 15–25. DOI: https://doi.org/10.1016/j.pscychresns.2016.04.005.

[70] Ruocco A.C. et al. “Amygdala and hippocampal volume reductions as candidate endophenotypes for borderline personality disorder: a meta-analysis of magnetic resonance imaging studies”. In: *Psychiatry Res.* 201.3 (2012), pp. 245–252. DOI: https://doi.org/10.1016/j.pscychresns.2012.02.012.

[71] Guitart-Masip M. et al. “Neural correlates of impaired emotional discrimination in borderline personality disorder: An fMRI study”. In: *Progress in Neuro-Psychopharmacology and Biological Psychiatry* 33.8 (2009), pp. 1537–1545. DOI: https://doi.org/10.1016/j.pnpbp.2009.08.022.

Appendices

Appendix A

Tables

ROI	ROI abbreviation	System ID
Brain Stem	BS	0
Left caudal middle frontal gyrus	L.cMF	1
Left frontal pole	L.FP	1
Left paracentral lobule	L.ParaC	1
Left pars opercularis	L.parsOP	1
Left pars orbitalis	L.parsOR	1
Left pars triangularis	L.parsTR	1
Left precentral gyrus	L.PreCG	1
Left rostral middle frontal gyrus	L.rMF	1
Left superior frontal gyrus	L.SF	1
Right caudal middle frontal gyrus	R.cMF	1
Right frontal pole	R.FP	1
Right paracentral lobule	R.paraC	1
Right pars opercularis	R.parsOP	1
Right pars orbitalis	R.parsOR	1
Right pars triangularis	R.parsTR	1
Right precentral gyrus	R.PreCG	1
Right rostral middle frontal gyrus	R.rMF	1
Right superior frontal gyrus	R.SF	1
Left inferior parietal lobule	L.IP	2
Left postcentral gyrus	L.PostCG	2
Left precuneus	L.PCUN	2
Left superior parietal lobule	L.SP	2
Left supramarginal gyrus	L.SM	2
Right inferior parietal lobule	R.IP	2
Right postcentral gyrus	R.PostCG	2
Right precuneus	R.PCUN	2
Right superior parietal lobule	R.SP	2
Right supramarginal gyrus	R.SM	2
Left cuneus	L.CUN	3
Left fusiform gyrus	L.FG	3
Left lateral occipital sulcus	L.LOC	3
Left lingual gyrus	L.LING	3

Left pericalcarine sulcus	L.PERIC	3
Right cuneus	R.CUN	3
Right fusiform gyrus	R.FG	3
Right lateraloccipital sulcus	R.LOC	3
Right lingual gyrus	R.LING	3
Right pericalcarine sulcus	R.PERIC	3
Left inferior temporal gyrus	L.IT	4
Left middle temporal gyrus	L.MT	4
Left superior temporal gyrus	L.ST	4
Left temporal pole	L.TP	4
Left transverse temporal gyrus	L.TT	4
Right inferior temporal gyrus	R.IT	4
Right middle temporal gyrus	R.MT	4
Right superior temporal gyrus	R.ST	4
Right temporal pole	R.TP	4
Right transverse temporal gyrus	R.TT	4
Left accumbens	L.ACC	5
Left amygdala	L.AMY	5
Left hippocampus	L.HIP	5
Right accumbens	R.ACC	5
Right amygdala	R.AMY	5
Right hippocampus	R.HIP	5
Left caudal anterior cingulate cortex	L.cAC	5
Left entorhinal cortex	L.ENTH	5
Left insular cortex	L.INS	5
Left isthmus of cingulate gyrus	L.iC	5
Left lateral orbitofrontal cortex	L.LoF	5
Left medial orbitofrontal cortex	L.MoF	5
Left parahippocampal gyrus	L.PHG	5
Left posterior cingulate cortex	L.PC	5
Left rostral anterior cingulate cortex	L.rAC	5
Right caudal anterior cingulate cortex	R.cAC	5
Right entorhinal cortex	R.ENTH	5
Right insular cortex	R.INS	5
Right isthmus of cingulate gyrus	R.iC	5
Right lateral orbitofrontal cortex	R.LoF	5
Right medial orbitofrontal cortex	R.MoF	5
Right parahippocampal gyrus	R.PHG	5
Right posterior cingulate cortex	R.PC	5
Right rostr alanterior cingulate cortex	R.rAC	5
Left caudate	L.CAU	6
Left pallidum	L.PAL	6
Left putamen	L.PUT	6
Left thalamus	L.THA	6
Left ventral DC	L.VEN	6
Right caudate	R.CAU	6
Right pallidum	R.PAL	6
Right putamen	R.PUT	6

Right thalamus	R.THA	6
Right ventralDC	R.VEN	6
Left cerebellum cortex	L.CER	7
Right cerebellum cortex	R.CER	7

Table A.1: List of anatomical cortical and sub-cortical ROIs identified with FreeSurfer. Systems: 0=brain stem, 1=frontal lobe, 2=parietal lobe, 3=occipital lobe, 4=temporal lobe, 5=limbic lobe, 6=basal ganglia, 7=cerebellum cortex.

Module 1		**Module 2**	
L.CUN (3)	R.CUN (3)	BS (0)	
L.FG (3)	R.FG (3)	L.ACC (5)	R.ACC (5)
L.LOC (3)	R.LOC (3)	L.AMY (5)	R.AMY (5)
L.LING (3)	R.LING (3)	L.HIP (5)	R.HIP (5)
L.PERIC (3)	R.PERIC (3)	L.VEN (6)	R.VEN (6)
L.SP (2)	R.SP (2)	L.FP (1)	R.FP (1)
L.TP (4)		L.iC	R.iC (5)
		L.MoF (5)	R.MoF (5)
		L.PHG (5)	R.PHG (5)
		L.PCUN (2)	R.PCUN (2)
		L.rAC (5)	R.rAC (5)
			R.TP (4)
Module 3		**Module 4**	
L.CAU (6)	R.CAU (6)	L.PAL (6)	R.PAL (6)
L.CER (7)	RCER (7)	L.PUT (6)	R.PUT (6)
L.cMF (1)	R.cMF (1)	L.THA (6)	R.THA (6)
L.ENTH (5)	R.ENTH (5)	L.cAC (5)	R.cAC (5)
L.IP (2)	R.IP (2)	L.INS (5)	R.INS (5)
L.IT (4)	R.IT (4)	L.paraC (1)	R.paraC (1)
L.LoF (5)	R.LoF (5)		R.parsOP (1)
L.MT (4)	R.MT (4)	L.PostCG (2)	R.PostCG (2)
L.parsOP (1)			R.PC (5)
L.parsOR (1)	R.parsOR (1)	L.PreCG (1)	R.PreCG (1)
L.parsTR (1)	R.parsTR (1)	L.ST (4)	R.ST (4)
L.PC (5)		L.SM (2)	R.SM (2)
L.rMF (1)	R.rMF (1)	L.TT	R.TT
L.SF (1)	R.SF (1)		

Table A.2: Modules found in a BPD patient by the community Louvain algorithm at a density of 32% in the full FC network.

Module 1		**Module 2**	
L.CAU (6)	R.CAU (6)		R.PAL (6)
L.CER (7)	RCER (7)		R.PUT (6)
L.PAL (6)		L.CUN (3)	R.CUN (3)
L.PUT (6)		L.FG (3)	R.FG (3)
L.THA (6)	R.THA (6)	L.IT (4)	R.IT (4)
L.cAC (5)	R.cAC (5)	L.INS (5)	R.INS (5)
L.cMF (1)	R.cMF (1)	L.LOC (3)	R.LOC (3)
L.LoF (5)		L.LING (3)	R.LING (3)
L.parsOP (1)	R.parsOP (1)	L.paraC (1)	R.paraC (1)
L.parsOR (1)	R.parsOR (1)	L.PERIC (3)	R.PERIC (3)
L.parsTR (1)	R.parsTR (1)	L.PostCG (2)	R.PostCG (2)
L.PC (5)	R.PC (5)	L.PreCG (1)	R.PreCG (1)
L.rMF (1)	R.rMF (1)	L.SP (2)	R.SP (2)
L.SF (1)	R.SF (1)	L.ST (4)	R.ST (4)
		L.SM (2)	R.SM (2)
			R.TP (4)
		L.TT	R.TT

Module 3	
BS (0)	
L.ACC (5)	R.ACC (5)
L.AMY (5)	R.AMY (5)
L.HIP (5)	R.HIP (5)
L.VEN (6)	R.VEN (6)
L.ENTH (5)	R.ENTH (5)
L.FP (1)	R.FP (1)
L.IP (2)	R.IP (2)
L.iC (5)	R.iC (5)
	R.LoF (5)
L.MoF (5)	R.MoF (5)
L.MT (4)	R.MT (4)
L.PHG (5)	R.PHG (5)
L.PCUN (2)	R.PCUN (2)
L.rAC (5)	R.rAC (5)
L.TP	

Table A.3: Modules found in a healthy control by the community Louvain algorithm at a density of 32% in the full FC network.

Module 1		**Module 2**	
BS (0)		L.ACC (5)	R.ACC (5)
L.AMY (5)	R.AMY (5)	L.CAU (6)	R.CAU (6)
L.CER (8)	R.CER (8)	L.PAL (6)	R.PAL (6)
L.HIP (5)	R.HIP (5)		R.cAC (5)
L.THA (6)	R.THA (6)	L.ENTH (5)	R.ENTH (5)
L.VEN (6)	R.VEN (6)	L.INS (5)	R.INS (5)
L.IT (4)		L.iC (5)	
L.PHG (5)		L.LOC (3)	
L.parsTR (1)			R.paraC (1)
L.PostCG (2)			R.parsOP (1)
L.TT (4)	R.TT (4)	L.PCUN (2)	R.PCUN (2)

Module 3		**Module 4**	
L.PUT (6)			R.PUT (6)
L.cAC (5)		L.cMF (1)	
	R.IP (2)		R.ENTH (5)
	R.IT (4)		R.FG (3)
L.MT (4)	R.MT (4)	L.IP (2)	
L.parsOP (1)			R.iC (5)
L.parsOR (1)		L.LoF (5)	R.LoF (5)
	R.parsTR (1)	L.MoF (5)	R.MoF (5)
	R.PostCG (2)	L.paraC (1)	
L.PreCG (1)			R.parsOR (1)
L.ST (4)		L.PC (5)	R.PC (5)
L.SM (2)			R.PreCG (1)
		L.rAC (5)	R.rAC (5)
		L.rMF (1)	R.rMF (1)
		L.SF (1)	R.SF (1)
			R.ST (4)
			R.SM (2)
		L.TP (4)	R.TP (4)

Module 5	
L.CUN (3)	R.CUN (3)
L.FP (1)	R.FP (1)
L.FG (3)	
	R.LOC (3)
L.LING (3)	R.LING (3)
	R.PHG (5)
L.periCG (3)	R.periCG (3)

Table A.4: Modules found in a BPD patient by the community Louvain algorithm at a density of 32% in the full SC network.

Module 1		**Module 2**	
	R.cAC (5)	BS (0)	

L.cMF (1)	R.cMF (1)	L.ACC (5)	R.ACC (5)
L.FP (1)	R.FP (1)	L.AMY (5)	R.AMY (5)
	R.INS (5)	L.CAU (6)	
L.LOC (3)		L.HIP (5)	R.HIP (5)
	R.LoF (5)	L.PAL (6)	R.PAL (6)
L.MoF (5)	R.MoF (5)	L.PUT (6)	R.PUT (6)
L.paraC (1)	R.paraC (1)	L.THA (6)	R.THA (6)
	R.parsOP (1)	L.VEN (6)	R.VEN (6)
L.parsOR (1)	R.parsOR (1)	L.IP (2)	
L.parsTR (1)	R.parsTR (1)	L.INS (5)	
L.PostCG (2)	R.PostCG (2)	L.iC (5)	
L.PC (5)	R.PC (5)	L.MT (4)	R.MT (4)
L.PreCG (1)	R.PreCG (1)		
L.PCUN (2)	R.PCUN (2)		
L.rAC (5)	R.rAC (5)		
L.rMF (1)			
L.SF (1)	R.SF (1)		
L.ST (4)	R.ST (4)		
L.SM (2)	R.SM (2)		
L.TT (4)	R.TT (4)		

Module 3		**Module 4**	
	R.CAU (6)	L.CER (7)	R.CER (7)
L.cAC (5)		L.CUN (3)	R.CUN (3)
L.ENTH (5)	R.ENTH (5)		R.iC (5)
L.FG (3)	R.FG (3)		R.LOC (3)
	R.IP (2)	L.LING (3)	R.LING (3)
L.IT (4)	R.IT (4)	L.periCG (3)	R.periCG (3)
L.LoF (5)		L.SP (2)	R.SP (2)
L.PHG (5)	R.PHG (5)		
L.parsOP (1)			
	R.rMF (1)		
L.TP (4)	R.TP (4)		

Table A.5: Modules found in a healthy control by the community Louvain algorithm at a density of 32% in the full SC network.

Appendix B

Codes

B.1 Harmonic characteristic path length

```
function lambda=charpath_harmonic(D)
%CHARPATH_HARMONIC
%
%    lambda=charpath_harmonic(D);
%
%    This function implements the harmonic mean version of the
%    characteristic path length to avoid the problem of
    disconnection
%    between nodes (distance between nodes is infinite)
%
%    Input:      D,        distance matrix
%
%    Output:     lambda, harmonic mean version of characteristic
     path length

Dv = D(D~=0);
lambda = harmmean(Dv);
end
```

B.2 Within-module strength

```
function Z=module_strength(W,Ci)
%MODULE_STRENGTH          Within-module strength
%
%    Z=module_strength(W,Ci);
%
%    The within-module strength is a within-module version of
    strength
%    centrality.
%
%    Inputs:     W,        weighted connection matrix
%                Ci,       community affiliation vector.
```

```
%
%    Output:      Z,        within-module strength.

n=length(W);                                %number of vertices
Z=zeros(n,1);
for  i=1:max(Ci)
     Koi=sum(W(Ci==i,Ci==i),2);
     Z(Ci==i)=Koi;
end

Z(isnan(Z))=0;
```

Ringraziamenti

I primi ringraziamenti sono dedicati alla professoressa Claudia Testa e alla dottoressa Stefania Evangelisti, che hanno reso possibile la stesura di questa tesi. Sono molto grato loro per avermi supportato ininterrottamente negli scorsi mesi e per i preziosi consigli e insegnamenti con cui mi hanno arricchito, nonostante la distanza fisica a cui siamo stati costretti. Ringrazio anche gli altri professori che, negli anni, hanno contribuito più di tutti alla mia crescita: Alessandra Manzini, grazie alla quale mi sono iscritto a Fisica, e Alain Goasduff, da cui ho appreso molto durante la preparazione della tesi triennale.

Ringrazio poi i miei magnifici amici: quelli di una vita, Matteo e Pietro, i miei punti di riferimento per definizione; quelle di una mezza vita, Michela, Serena ed Erika, le quali completano questa mia insostituibile famiglia allargata, che costituisce la costante delle migliori giornate; quelli recenti, Gianmarco e Matteo su tutti, che hanno avuto il grande merito di rendere piacevole il periodo padovano (e anche di aiutarmi a farlo finire); quelli nuovi, Elena in particolare, che è stata indispensabile in questi ultimi due anni.

Ringrazio tutti i miei parenti, che mi hanno sempre spronato nello studio, e principalmente mio cugino Lorenzo e i miei zii Grazia e Rinaldo, con cui ho un rapporto speciale. Ringrazio anche il mio gatto, che ha studiato con me ogni volta in cui ero a casa.

Ringrazio infine, ma soprattutto, la mia famiglia: mia sorella Francesca, che per me è sempre stata un esempio da seguire in (quasi) tutto, e i nostri genitori, che ogni giorno fanno tutto ciò che possono per supportarci in ogni modo.